Published in final edited form as:

*Nature*. 2025 May ; 641(8061): 222–231. doi:10.1038/s41586-025-08634-7.

# Brain-wide neuronal circuit connectome of human glioblastoma

**Yusha Sun**[1,25], **Xin Wang**[2,25], **Daniel Y. Zhang**[3], **Zhijian Zhang**[2], **Janardhan P. Bhattarai**[2], **Yingqi Wang**[2], **Kristen H. Park**[1], **Weifan Dong**[2], **Yun-Fen Hung**[4], **Qian Yang**[2], **Feng Zhang**[2], **Keerthi Rajamani**[5], **Shang Mu**[5], **Benjamin C. Kennedy**[3,6], **Yan Hong**[2], **Jamie Galanaugh**[1], **Abhijeet Sambangi**[7], **Sang Hoon Kim**[2], **Garrett Wheeler**[8], **Tiago Gonçalves**[8], **Qing Wang**[9], **Daniel Geschwind**[9], **Riki Kawaguchi**[9], **Angela N. Viaene**[10], **Ingo Helbig**[11,12,13,14], **Sudha K. Kessler**[11,14], **Ahmet Hoke**[15], **Huadong Wang**[16], **Fuqiang Xu**[16], **Zev A. Binder**[3,17], **H. Isaac Chen**[3,18,19], **Emily Ling-Lin Pai**[20], **Sara Stone**[20], **MacLean P. Nasrallah**[17,20], **Kimberly M. Christian**[2], **Marc Fuccillo**[2], **Nicolas Toni**[21], **Zhuhao Wu**[5], **Hwai-Jong Cheng**[4], **Donald M. O'Rourke**[3,17], **Minghong Ma**[2], **Guo-li Ming**[2,18,22,23,26], **Hongjun Song**[2,17,18,22,24,26]

[1]Neuroscience Graduate Group, Perelman School of Medicine, University of Pennsylvania, Philadelphia, PA, USA.

[2]Department of Neuroscience and Mahoney Institute for Neurosciences, Perelman School of Medicine, University of Pennsylvania, Philadelphia, PA, USA.

[3]Department of Neurosurgery, Perelman School of Medicine, University of Pennsylvania, Philadelphia, PA, USA.

[4]Institute of Molecular Biology, Academia Sinica, 115, Taipei, Taiwan.

[5]Helen & Robert Appel Alzheimer's Disease Research Institute, Weill Cornell Medicine, New York, NY, USA.

[6]Division of Neurosurgery, Children's Hospital of Philadelphia, Philadelphia, PA, USA.

[7]Sidney Kimmel Medical College, Thomas Jefferson University Hospital, Philadelphia, PA, USA.

[8]Department of Neuroscience and Gottesman Institute for Stem Cell Biology and Regenerative Medicine, Albert Einstein College of Medicine, Bronx, NY, USA.

[9]Program in Neurogenetics, Department of Neurology, David Geffen School of Medicine, University of California Los Angeles, Los Angeles, CA, USA.

[26]Corresponding authors: gming@pennmedicine.upenn.edu (G-l.M.) and shongjun@pennmedicine.upenn.edu (H.S.).

AUTHOR CONTRIBUTIONS

Y.S. led the study and performed most of the analyses. X.W., Y.S. and K.H.P. conducted *in vivo* transplantation experiments. X.W. and Z.Z. generated the relevant viral vectors. Z.Z. generated cortical organoids used for sequencing and assembloid generation. X.W. and Y.S. performed GBO generation and culture. Y.S., X.W., and D.Y.Z. contributed to library preparation and sequencing. Q.W., D.G., and R.K. performed sequencing. Q.Y. and Y.H. generated 2D neuronal cultures. F.Z. generated NPC cultures. K.R., S.M., Z.W. performed tissue clearing and whole-brain imaging and analysis. Y.S., X.W., D.Y.Z., and K.H.P. performed immunohistology and *in situ* analyses. J.P.B., Y.W., M.M., J.G., and M.F. contributed to electrophysiology experiments. Y.S., Y.W., J.P.B., and M.M. contributed to slice $Ca^{2+}$ imaging experiments. Y-F.H., H-J.C., and N.T. contributed to electron microscopy experiments. H.W. and F.X. provided HSV constructs. G.W. and T.G. provided the JRGECO1α construct. W.D., F.Z., A.S., A.H., S.H.K., and K.M.C. contributed to additional experiments and data collection. B.C.K., A.N.V., I.H., S.K.K., Z.A.B., H.I.C., E.L.P., S.S., M.P.N., and D.M.O. contributed to patient tissue collection. Y.S., X.W., G-l.M., and H.S. conceived the project, designed experiments, and wrote the manuscript with inputs from all authors.

CONFLICTS OF INTEREST

The authors declare no competing interests.

[10]Department of Pathology and Laboratory Medicine, Children's Hospital of Philadelphia, Philadelphia, PA, USA.

[11]Division of Neurology, Children's Hospital of Philadelphia, Philadelphia, PA, USA.

[12]The Epilepsy NeuroGenetics Initiative (ENGIN), Children's Hospital of Philadelphia, Philadelphia, PA, USA.

[13]Department of Biomedical and Health Informatics (DBHi), Children's Hospital of Philadelphia, Philadelphia, PA, USA.

[14]Department of Neurology, Perelman School of Medicine, University of Pennsylvania, Philadelphia, PA, USA.

[15]Department of Neurology, Johns Hopkins University School of Medicine, Baltimore, MD, USA.

[16]Shenzhen Key Laboratory of Viral Vectors for Biomedicine, Shenzhen-Hong Kong Institute of Brain Science, Shenzhen Institute of Advanced Technology, Chinese Academy of Sciences, Shenzhen, China.

[17]Glioblastoma Translational Center of Excellence, The Abramson Cancer Center, Perelman School of Medicine, University of Pennsylvania, Philadelphia, PA, USA.

[18]Institute for Regenerative Medicine, University of Pennsylvania, Philadelphia, PA, USA.

[19]Corporal Michael J. Crescenz Veterans Affairs Medical Center, Philadelphia PA, USA.

[20]Department of Pathology and Laboratory Medicine, Perelman School of Medicine, University of Pennsylvania, Philadelphia, PA, USA.

[21]Center for Psychiatric Neurosciences, Lausanne University Hospital, Lausanne, Switzerland.

[22]Department of Cell and Developmental Biology, Perelman School of Medicine, University of Pennsylvania, Philadelphia, PA, USA.

[23]Department of Psychiatry, Perelman School of Medicine, University of Pennsylvania, Philadelphia, PA, USA.

[24]The Epigenetics Institute, Perelman School of Medicine, University of Pennsylvania, Philadelphia, PA, USA.

[25]These authors contributed equally to this work.

## Abstract

Glioblastoma (GBM) infiltrates the brain and can be synaptically innervated by neurons, which drives tumor progression[1,2]. Synaptic inputs onto GBM cells identified so far are largely short-range and glutamatergic[3,4]. The extent of GBM integration into the brain-wide neuronal circuitry remains unclear. Here we applied rabies virus- and herpes simplex virus-mediated trans-monosynaptic tracing[5,6] to systematically investigate circuit integration of human GBM organoids transplanted into adult mice. We found that GBM cells from multiple patients rapidly integrate into diverse local and long-range neural circuits across the brain. Beyond glutamatergic inputs, we identified various neuromodulatory inputs, including synapses between basal forebrain cholinergic neurons and GBM cells. Acute acetylcholine stimulation induces long-lasting elevation of calcium

oscillations and transcriptional reprogramming of GBM cells into a more motile state via the metabotropic CHRM3 receptor. CHRM3 activation promotes GBM cell motility, whereas its downregulation suppresses GBM cell motility and prolongs mouse survival. Together, these results reveal the striking capacity for human GBM cells to rapidly and robustly integrate into anatomically diverse neuronal networks of different neurotransmitter systems. Our findings further support a model wherein rapid connectivity and transient activation of upstream neurons may lead to a long-lasting increase in tumor fitness.

GBM, a deadly primary brain cancer in adults, is characterized by its heterogeneity, complex tumor microenvironment, and invasiveness[7,8]. Growing evidence suggests that neuronal circuit integration of glioma drives tumor progression, invasion, and shorter patient survival[3,9–12]. Given that many GBM cells are highly infiltrative[7], synapses onto these migratory cells will inevitably be transient. Whether and how transient synapses exert long-lasting influences on GBM is unclear. Furthermore, synaptic inputs onto glioma cells identified so far have been largely limited to local glutamatergic projections[3,4], and the circuit architecture and neuronal subtype diversity of neuron-glioma interactions remain to be elucidated. Retrograde trans-monosynaptic tracing using modified rabies virus is a classic methodology to systematically map synaptic inputs onto defined targets, or starter cells[13]. Here we performed retrograde rabies virus trans-monosynaptic tracing of transplanted patient-derived GBM organoids (GBOs)[14,15] into the adult mouse brain to characterize the landscape of neuronal innervation of GBM cells *in vivo* and further investigated functional effects of neuromodulatory inputs onto GBM cells.

## Neurotransmitter receptor expression

To explore the potential for GBM to respond to distinct neurotransmitters, we first performed deep single-cell RNA sequencing (scRNAseq). To account for substantial intra- and inter-tumoral heterogeneity, we examined GBOs from genetically distinct, isocitrate dehydrogenase-wild type (IDH-wt) primary or recurrent GBM tumors resected from three patients (Fig. 1a, Extended Data Fig. 1a–c, Supplementary Tables 1 and 2). GBOs were cultured for an extended period to dilute nonmalignant cells from the tumor microenvironment[14]. Copy number aberration analysis identified all cells in these GBOs as malignant cells (Extended Data Fig. 1d–f), which were almost all $Nestin^{+}SOX2^{+}$ (Extended Data Fig. 1g–h, Supplementary Fig. 1). Human GBM cells express a variety of neurotransmitter receptors, including ionotropic and metabotropic glutamatergic, GABAergic, and cholinergic receptors as well as serotonergic, adrenergic, and dopaminergic receptors (Fig. 1a). Their expression levels were comparable to those in neural stem cells (NSCs) in human induced pluripotent stem cell (iPSC)-derived sliced neocortical organoids (SNOs)[16] we profiled in parallel (Fig. 1a, Extended Data Fig. 1i). Our analysis of published scRNAseq datasets of adult primary IDH-wt GBM[8,17] showed consistent results (Fig. 1a, Extended Data Fig. 1j). GBM cells abundantly expressed post-synaptic scaffold genes, such as *HOMER1* and *DLG4* (Fig. 1a). The levels of neurotransmitter receptor expression and enrichment scores for post-synaptic density genes were largely similar among IDH-wt GBM cells across cellular states[8] in all datasets and in NSCs from SNOs, with a slight enrichment in non-mesenchymal states and in peripheral infiltrating GBM cells compared to the tumor

core[18] (Extended Data Fig. 1k–n). These results reveal the capacity for GBM cells to receive and respond to inputs of diverse neurotransmitters.

## Rapid neuronal circuit integration

To map neuronal synaptic projections onto GBOs, we leveraged a rabies virus-based retrograde monosynaptically-restricted tracing approach[5,19]. Proliferating tumor cells in GBOs were retrovirally transduced to express a DsRed reporter (R), the EnvA receptor TVA (T), and rabies virus glycoprotein (G) (named RTG; Extended Data Fig. 2a). Starter GBO cells infected by G protein-deleted EnvA-pseudotyped rabies virus expressing a GFP reporter (ΔG rabies virus)[20], indicated by DsRed and GFP co-expression, can retrogradely transmit rabies virus to their presynaptic partner neurons, which exhibit GFP expression alone (Extended Data Fig. 2b). As these first-order presynaptic neurons do not express G protein, ΔG rabies virus is unable to further propagate, resulting in the monosynaptic nature of this approach[20]. GBOs that were transduced with RTG retrovirus (~20% transduction efficiency without cell sorting), but not control GBOs without RTG expression, were infected by ΔG rabies virus (Extended Data Fig. 2c). Around ~25% of $DsRed^+$ cells in GBOs were infected with rabies virus after 5 days *in vitro* (Extended Data Fig. 2d).

To test rabies virus transmission from GBOs, we pre-infected GBOs with ΔG rabies virus followed by fusion with 100-day old SNOs[16] to generate GBO-SNO assembloids (Supplementary Fig. 2a). $DsRed^+$ GBO cells rapidly and extensively infiltrated into the SNOs and many $NeuN^+GFP^+DsRed^-$ neurons were present at 10 days, indicative of retrograde rabies virus transmission from GBO starter cells to human neurons (Supplementary Fig. 2b–c).

To define GBO integration *in vivo*, we pre-infected GBOs derived from primary or recurrent GBM tumors resected from three patients with ΔG rabies virus and orthotopically transplanted them into the retrosplenial cortex (RSP) of adult immunodeficient mice (Fig. 1b). We observed GFP expression in both local (ipsilateral cortex, hippocampus) and long-range (ipsilateral thalamus, contralateral cortex, basal forebrain) projecting neurons beginning at 3 days post transplantation (dpt), with extensive labeling on the order of ~$10^3$–$10^4$ neurons by 10 dpt (Fig. 1c–e, Extended Data Fig. 2e). Light-sheet microscopy of whole cleared brains at 10 dpt revealed broad distributions of labeled neurons across the brain (Fig. 1e, Supplementary Video 1). As it takes at least 2 days for rabies virus to replicate, transmit retrogradely across synapses, and sufficiently label cells[20], the detection of $GFP^+$ neurons as early as 3 dpt suggests rapid neuronal circuit integration of GBM cells *in vivo*. To confirm the potential of GBOs for rapid circuit integration in an all human system, we explored an *ex vivo* anterograde polysynaptic tracing approach using herpes simplex virus (HSV)[21] and primary human tissue (Extended Data Fig. 2f–g). We treated freshly resected human hippocampal tissue with polysynaptic HSV to infect human neurons for 3 days, washed away residual virus, and then fused GBOs (Extended Data Fig. 2h–I, Supplementary Table 1). We confirmed no infection of GBOs treated with conditioned media from HSV-infected hippocampal slices (Extended Data Fig. 2j). Notably, we observed $GFP^+$ HSV-infected GBO cells by 3 days after co-culture (Extended Data Fig. 2k). Together, these results suggest rapid synapse formation onto GBM cells *in vivo* and *ex vivo*.

We also performed control experiments to ensure the fidelity of our approach. We engineered a control helper retroviral construct without the G protein gene (RTΔG) such that starter cells transduced by RTΔG retrovirus can be infected by rabies virus via the TVA receptor but cannot transmit rabies virus to upstream neurons (Extended Data Fig. 3a). Upon transplantation, we detected $DsRed^{+}GFP^{+}$ starter GBM cells, but no $GFP^{+}$ mouse neurons (Extended Data Fig. 3b). To rule out potential non-specific labeling due to rabies virus leakage from pre-infected GBM cells, we extracted infection-competent rabies virus from starter GBOs prior to transplantation and injected them into the brain. We found only very rare $GFP^{+}$ neurons during the same time window (159 ± 124 cells, $n = 4$ mice; Extended Data Fig. 3c). Immunostaining for the microglia marker IBA1, oligodendrocyte marker OLIG2, OPC marker NG2, astrocyte marker S100B, and neuronal marker NeuN showed nearly no co-labeling of non-neuronal markers with GFP either near or distant to the RSP transplantation site, consistent with the neuronal tropism of rabies virus transmission[5,19] (Extended Data Fig. 3d–e).

Together, this rabies virus trans-monosynaptic tracing approach uncovered rapid and robust neuronal connectivity of human GBM cells *in vivo*.

## Brain-wide anatomic projection atlas

We next systematically characterized the brain-wide distribution of rabies virus-labeled neurons after transplantation of pre-infected GBOs into four cortical and subcortical sites: primary somatosensory cortex (S1), primary motor cortex (M1), RSP, and hippocampus (HIP), which correspond to common anatomical regions where glioma appear in patients[22] (Fig. 2a–d). At 10 dpt, we observed broadly distributed $GFP^{+}$ cells across the brain for GBOs from all 3 patients (Fig. 2a–e, Extended Data Fig. 4 and 5a, Supplementary Video 1, and Supplementary Fig. 3), partially due to rapid infiltration of starter GBM cells (Fig. 2f). Transplantation of GBOs from different patients showed largely similar distributions of $GFP^{+}$ cells for each transplantation site, suggesting conserved neuron-GBM interaction patterns despite GBM heterogeneity (Fig. 2e). Quantification revealed that GBM cells in cortical areas received the highest proportion of inputs from the isocortex and secondarily from the thalamus (Fig. 2g). Cortical inputs onto GBM cells in both S1 and M1 were largely comprised of neurons in the sensory and motor cortex both ipsilaterally and contralaterally (Fig. 2a–b, e). Contralateral neurons accounted for nearly 20% of total $GFP^{+}$ cortical neurons (Fig. 2h), with L2/3 contralateral neurons as the dominant input subpopulation compared to those of L5 or L6 (Extended Data Fig. 5b), highlighting long-range cortical networks as substantial components of neuron-GBM circuitry[12]. Thalamic projections onto GBM cells, such as from ventral posteromedial and posterior complex thalamus upon S1 transplantation and from ventromedial thalamus upon M1/RSP transplantation (Fig. 2a–c, e), were almost entirely ipsilateral, consistent with known thalamo-cortical wiring[23]. For subcortical HIP transplantation, the most abundant inputs were in the hippocampal (dentate gyrus, CA1, CA3) and retrohippocampal (subiculum, entorhinal cortex) areas (Fig. 2d, e, g). We also found $GFP^{+}$ neurons in diverse subcortical regions, including the hypothalamus, claustrum, and midbrain, for all transplanted sites, and the diagonal band nucleus (NDB) and medial septal nucleus (MS) of the basal forebrain upon RSP and HIP transplantations (Fig. 2c–e, Extended Data Fig. 5c–e, Supplementary Video 1).

To assess the degree of connectivity of GBM cells, we quantified the input neuron to starter GBM cell ratios, which were 18:1 for cortical transplantation sites and 2.3:1 for HIP transplantations (Fig. 2i). As a comparison, we derived $SOX2^+$ neural progenitor cells (NPCs) from human iPSCs and transduced them with the RTG retrovirus (Extended Data Fig. 5f). Upon transplantation of ΔG rabies virus pre-infected NPCs into the RSP, we found a much lower input neuron to starter cell ratio (0.74:1 versus 16.6:1) and a lower number of total labeled neurons (2,300 versus 6,000) for NPCs compared to GBM cells transplanted in the same region at 10 dpt (Extended Data Fig. 5g–h). In addition, presynaptic inputs to NPCs were relatively limited in their anatomic diversity, and the degree of starter cell migration was much lower compared to GBM cells (Extended Data Fig. 5i–j). Together, these results indicate much higher neuronal connectivity of GBM cells in comparison to nonmalignant NPCs.

We also examined circuit integration of GBM cells following longer term engraftment. We injected ΔG rabies virus one month after transplantation of GBM cells expressing RTG into the RSP (Extended Data Fig. 6a–b). At 10 days post rabies virus injection, starter $DsRed^+GFP^+$ GBM cells were distributed in the corpus callosum, RSP, and CA1 hippocampus and other regions (estimated ~15,600 ± 7,500 starter cells with ~64 ± 5% $DsRed^+$ GBM cells infected by rabies virus near the injection site, $n = 3$ mice), whereas neuronal inputs included both ipsilateral and contralateral cortices, ipsilateral thalamus, and basal forebrain (Extended Data Fig. 6b–f), with largely similar though more extensive connection patterns to those found with pre-labeled GBOs (Fig. 2e). We also found no evidence of non-neuronal cell labeling (Extended Data Fig. 6d). To rule out the possibility that cell death might drive leakage of G protein-expressing rabies virus to directly infect neurons, we stained for cleaved caspase 3 (cCas3) and did not observe substantial apoptosis in $DsRed^+GFP^+$ GBM cells (Extended Data Fig. 6d).

Together, this systematic brain-wide connectome analysis revealed highly extensive and conserved integration of GBM cells from multiple patients into anatomically diverse neuronal circuitry, despite their inter-tumoral heterogeneity.

## Inputs of diverse neurotransmitters

Next, we characterized molecular identities of rabies virus-labeled neurons in diverse anatomical regions at 10 dpt. Simultaneous GFP immunostaining and *in situ* hybridization for *vGLUT1/2* and *GAD1* revealed inputs from both glutamatergic and GABAergic neurons in the cortical, subcortical, and hippocampal regions (Fig. 3a–c). We further found $GFP^+SATB2^+$ superficial layer neurons and $GFP^+CTIP2^+$ deep layer neurons in the cortex (Extended Data Fig. 7a), while $GFP^+$ GABAergic interneurons consisted of $PV^+$ and $SST^+$ subtypes (Extended Data Fig. 7b). Glutamatergic ($vGLUT1/2^+GAD1^-$) inputs were the most abundant, and GABAergic ($vGLUT1/2^-GAD1^+$) and other ($vGLUT1/2^-GAD1^-$) subtypes exhibited area-specific differences (Fig. 3d). To validate the preference for glutamatergic over GABAergic connectivity in an all-human model, we co-cultured pre-infected GBO starter cells with a 1:1 mixture of iPSC-derived glutamatergic and GABAergic neurons and observed a 25:1 input neuron to starter cell ratio (Extended Data Fig. 7c–e). Rabies virus is not known to be intrinsically selective for a particular neuronal subtype[24], yet we

found 98% glutamatergic neurons and 1.9% NKX2.1$^+$ GABAergic neurons among GFP$^+$ neurons, despite a 1:1 ratio of these two types in culture (Extended Data Fig. 7d, e). Notably, scRNAseq revealed lower expression levels of GABAergic versus glutamatergic receptors in GBM cells (Fig. 1a).

We also observed projections from MS/NDB basal forebrain areas upon transplantation in RSP or HIP for GBOs (Fig. 2e, Supplementary Video 1). Immunostaining for ChAT and/or VAChT in MS (Fig. 3e) and NDB (Fig. 3f, Extended Data Fig. 7g–h) revealed that about 40% of GFP$^+$ neurons in these areas were cholinergic (Fig. 3g). A subset of these GFP$^+$ cholinergic neurons also expressed *GAD1*, denoting potential co-release of acetylcholine (ACh) and GABA from these neurons[25] (Extended Data Fig. 7g–h). We additionally found cholinergic inputs onto GBM cells from the brainstem pedunculopontine nucleus[26] (Extended Data Fig. 7i). Several types of midbrain neuromodulatory neurons projected to GBM cells, including TPH2$^+$ serotonergic neurons in the raphe nuclei and TH$^+$ dopaminergic neurons in the ventral tegmental area (Fig. 3h, Extended Data Fig. 7j).

Together, our systematic analyses revealed long-range neuromodulatory projections of diverse neurotransmitter systems onto GBM cells, in addition to local and long-range glutamatergic and GABAergic inputs. With the expression of neurotransmitter receptors in GBM (Fig. 1a), our results suggest extensive crosstalk between different neurotransmitter systems and GBM cells in the adult brain.

## Metabotropic cholinergic-to-GBM inputs

We then focused on cholinergic inputs from the basal forebrain onto GBM cells for more detailed analyses. We first examined the potential for cholinergic innervation in patients and observed dense VAChT$^+$ or ChAT$^+$ puncta near EGFR$^+$ tumor cells in primary IDH-wt GBM and IDH-mutant tumor tissue (Extended Data Fig. 8a–c, Supplementary Table 1).

To confirm the connection *in vivo* between cholinergic neurons and GBM cells using an independent transsynaptic viral tracing approach, we leveraged Cre-dependent and thymidine kinase (TK)-deficient HSV (H129-LSL-ΔTK-tdTomato) for anterograde trans-monosynaptic tracing in starter cells co-expressing Cre and TK[6,27] (Fig. 4a). Co-injection of AAV-ChAT-Cre and AAV-DIO-TK-GFP into the basal forebrain resulted in expression of GFP in VAChT$^+$ChAT$^+$ cholinergic axon terminals at distant locations, such as the RSP (Extended Data Fig. 8d). We next injected a mixture of H129-LSL-ΔTK-tdTomato, AAV-ChAT-Cre, and AAV-DIO-TK-GFP into the basal forebrain and simultaneously transplanted GBO cells in the HIP or RSP (Fig. 4a). By 6 dpt, we found HSV infection of GFP$^+$ starter neurons with co-expression of GFP and tdTomato in the basal forebrain (Extended Data Fig. 8e). By 10 dpt, we found HSV infection of GBM cells with co-expression of tdTomato and human-specific STEM121 or human nuclear antigen in the HIP or RSP (Fig. 4b, Extended Data Fig. 8f–h). We detected HSV-infected postsynaptic GBM cells both within the tumor core and infiltrating margin (Extended Data Fig. 8g–h). High-resolution confocal microscopy showed localization of VAChT$^+$ cholinergic presynaptic boutons adjacent to HSV-infected, tdTomato$^+$ GBM cells in the RSP (Extended Data Fig. 8i). We also performed immuno-electron microscopy analysis of DsRed$^+$ GBM cells transplanted to the HIP (Fig.

4c). We injected a mixture of AAV-ChAT-Cre and AAV-Syn-DIO-Synaptophysin-EGFP into the NDB area to label synaptic vesicles with EGFP[28] in cholinergic neurons (Fig. 4c). After 3 weeks, synapses onto GBM cells were identified via a combination of silver-immunogold labeling for DsRed (tumor) and a DAB precipitate targeted toward EGFP. We observed cholinergic axonal terminals with synaptic vesicles at the axonal membrane immediately adjacent to GBM cells, revealing morphological cholinergic neuron-to-glioma synapses (Fig. 4d).

To verify functional cholinergic inputs onto GBM cells, we first performed calcium ($Ca^{2+}$) imaging. ACh exposure induced an immediate $Ca^{2+}$ rise in GBOs in culture, which was reduced by 4-DAMP, an M3 metabotropic receptor (CHRM3)-specific antagonist[29], but not by pan-nicotinic antagonist mecamylamine (Extended Data Fig. 9a–b). We next transplanted GBOs expressing red-shifted genetically encoded $Ca^{2+}$ indicator jRGECO1α[30] in the RSP and simultaneously injected a combination of AAV-ChAT-Cre and AAV-DIO-ChR2(H134R)-EYFP into the basal forebrain to label cholinergic neurons with ChR2 (Fig. 4e). In acute slices from animals 6 weeks after transplantation, optogenetic stimulation of $ChR2^{+}$ axon terminals induced immediate $Ca^{2+}$ transients in engrafted GBM cells, which were attenuated by 4-DAMP (Fig. 4f–g, Extended Data Fig. 9c). We employed sequential stimulations prior to blockade to rule out potential coincident spontaneous $Ca^{2+}$ transients[31] in this paradigm (Fig. 4f–g).

To further confirm functional cholinergic inputs onto GBM cells, we performed whole-cell patch-clamp electrophysiology. GBOs expressing DsRed were transplanted into the RSP while a combination of AAV-ChAT-Cre and AAV-DIO-ChR2(H134R)-EYFP was injected in the basal forebrain, and acute slices were prepared after 6 weeks for recording of $DsRed^{+}$ GBM cells (Fig. 4h, Extended Data Fig. 9d). The majority of GBM cells recorded exhibited singular action potential-like responses upon depolarizing current injection under current-clamp, as recently reported[32] (UP-10072; $n$ = 19 out of 28 cells, 68%, from 3 mice), and initial inward currents followed by outward currents with depolarizing pulses under voltage-clamp (UP-10072; input resistance: 1.04 ± 0.11 GΩ, $n$ = 34 cells, 4 mice; resting membrane potential: −55.2 ± 3.6 mV, $n$ = 28 cells, 5 mice; Extended Data Fig. 9e–h). Current-clamp recordings of GBM cells in the presence of the AMPA receptor blocker CNQX revealed membrane depolarizations upon light stimulation, which were attenuated in amplitude by 4-DAMP (Fig. 4i–j, Extended Data Fig. 9i–j). Overall, ~5% of recorded GBM cells exhibited robust light-induced responses ($n$ = 110 cells patched from 12 mice), with a response latency time of 148 ± 55.1 ms ($n$ = 5 cells from 3 mice; Fig. 4i), consistent with metabotropic GPCR-mediated synaptic responses[33,34].

Together, our results define a functional long-range cholinergic projection onto GBM cells mediated by the metabotropic CHRM3 receptor.

## Essential roles of CHRM3 for GBM biology

We further conducted $Ca^{2+}$ imaging on GBOs in an air-liquid interface culture with direct exposure to ACh. Consistent with prior reports[31], GBO cells displayed periodic $Ca^{2+}$ transients at a baseline mean frequency of 4.5 mHz (Fig. 5a–b, Extended Data Fig. 9k–l).

Brief (~5 min) exposure of GBOs to ACh led to an increase in the frequency of spontaneous transients 30 minutes later with a mean frequency of 18 mHz, which was reduced by 4-DAMP (Fig. 5a–b, Extended Data Fig. 9k–m, Supplementary Video 2). These results demonstrate that ACh has not only immediate but also prolonged influences on GBM cells.

We next examined ACh-induced transcriptional changes in GBM cells. We devised a time-resolved RNA sequencing paradigm to explore transcriptional dynamics upon continuous ACh stimulation or in response to varying pulse durations of ACh with sequencing at 1 hour (Extended Data Fig. 10a). Analysis of GBOs from three patients revealed ACh-induced upregulation of immediate early genes (e.g., AP-1 family transcription factors *FOS* and *FOSB*, *EGR1*), nuclear transcription factors associated with $Ca^{2+}$ oscillations (e.g., *NFATC2* at ~20 mHz[35]), epigenetic regulators (e.g., *GADD45B, DOT1L,* and *SETD1A*), and genes related to axon guidance and motility (e.g., *PLXNB3* and *MMP19*) (Fig. 5c, Supplementary Table 3). Many of these ACh-induced genes exhibited a time-dependent increase in expression levels over 1 hour (Extended Data Fig. 10b), whereas brief (5, 15, or 30 minute) pulses of ACh were sufficient to achieve maximal effects at 1 hour (Extended Data Fig. 10c), suggesting rapid induction of transcriptional reprogramming driven by acute ACh exposure. We defined genes with upregulated expression at 1 hour as fast-response genes, which were enriched in Gene Ontology (GO) terms related to semaphorin-plexin signaling, cellular migration, and post-synaptic density, while downregulated genes were generally associated with metabolic function (Fig. 5d, Supplementary Table 3). Gene signature enrichment showed upregulation of the AP-1 FOS family, migration, and axon guidance gene sets across GBOs from different patients at 1 hour (Extended Data Fig. 10d–f). scRNAseq analyses of these GBOs after 1-hour ACh treatment confirmed upregulation of the fast-response gene signature (Extended Data Fig. 10g–j, Supplementary Table 4). At the single-cell level, GBM cells more highly enriched in post-synaptic density genes tended to also be more enriched in ACh fast-response genes (Extended Data Fig. 10k). Higher expression of this fast response signature was correlated with worse patient prognosis in public GBM cohorts (Extended Data Fig. 10l).

To examine whether brief exposure of GBOs to ACh would be sufficient to induce long-lasting transcriptional changes, we performed RNA sequencing after various lengths of time following 1 hour ACh exposure (Extended Data Fig. 11a). We found expression changes of many genes after 1 day, which we defined as long-lasting response genes (Extended Data Fig. 11b, Supplementary Table 4). These genes were enriched in GO terms related to cellular adhesion, contractility, and migration (Extended Data Fig. 11c, Supplementary Table 5). Enrichment of the long-lasting response gene signature gradually decreased over time but remained elevated at day 5 (Fig. 5e–f). For example, *STC1, PLXNA4, MMP19, UNC5B, CEMIP*, and *P4HA3*, which promote tumor invasion[36,37] and progression[38] of glioma or other tumors[39–41], remained upregulated for 5 days following 1 hour ACh exposure (Fig. 5e). Enrichment of this long-lasting response signature was also associated with shorter patient survival time in public datasets (Extended Data Fig. 11d).

To examine the functional impact of ACh-induced transcriptional changes associated with cellular phenotypes such as migration, we performed cell motility and migration assays. We first applied a simple Matrigel-based assay to examine GBM cell migration across GBOs

derived from 5 patients in response to ACh treatment and subsequent inhibition with 4-DAMP (Fig. 5g–h, Extended Data Fig. 12a, Supplementary Table 1). Despite some patient-specific variability, 4-DAMP uniformly reduced migration compared to ACh stimulation in GBOs from all patients (Fig. 5g–h, Extended Data Fig. 12a). The heterogeneity in ACh-induced migration combined with the consistent inhibitory effect by 4-DAMP, even to levels below baseline in several GBOs, may be explained by cell-intrinsic constitutive activity of the CHRM3 G-protein coupled receptor (GPCR)[42] or activation of this receptor by other metabolites, such as choline present in the culture medium[43]. We additionally performed live imaging of acute mouse brain slices with GBOs transplanted for 2–3 weeks, which showed ACh-induced increases in tumor cell migration speed and displacement (Fig. 5i–k). To investigate tumor motility in an all-human model, we generated GBO-SNO assembloids and applied a single 1-hour pulse of ACh pretreatment before fusion. The pretreatment was sufficient to increase GBO cell migration into human neocortical organoids over 2 days (Extended Data Fig. 12b–c). Live imaging of GBO cells within the leading edge of both GBO-SNO assembloids and co-culture with adult human hippocampal slices confirmed increased tumor cell migration speed and displacement following ACh pretreatment (Extended Data Fig. 12d–f). To specifically assess whether membrane depolarization via CHRM3 may be sufficient to increase cell migration, we infected GBOs with lentivirus to express the designer receptor exclusively activated by a designer drug (DREADD) hM3Dq, which is a modified version of the human CHRM3 receptor. Chemogenetic activation of these GPCRs on GBO cells by clozapine *N*-oxide (CNO) induced $Ca^{2+}$ influx *in vitro* (Extended Data Fig. 12g–h) and increased the area of tumor cell distribution *in vitro* (Extended Data Fig. 12i) and after transplantation into the mouse brain *in vivo* (Fig. 5l–m).

To explore CHRM3 as a potential molecular target for GBM, we expressed a short-hairpin RNA (shRNA) targeting CHRM3 in GBOs via lentivirus (Extended Data Fig. 12j, Supplementary Table 2). CHRM3 knockdown in GBOs decreased the transcriptional response to ACh by RNA sequencing (Extended Data Fig. 12k) and inhibited GBO migration *in vitro* in the presence of ACh compared to a scrambled control shRNA (Extended Data Fig. 12l–m). At 7 days post transduction, we observed a decrease in GBO size and percentage of $Ki67^+$ cells and increased cCas3 expression, indicating a negative impact on GBM cell proliferation and increased apoptosis *in vitro* (Extended Data Fig. 12n–o). GBOs with CHRM3 knockdown also exhibited decreased migration into neocortical organoids in the GBO-SNO assembloid model with a 1-hour ACh pre-treatment (Extended Data Fig. 12p–q). Transplanted GBOs with CHRM3 knockdown exhibited decreased area of tumor distribution compared to GBOs expressing a scrambled control shRNA (Fig. 5n, Extended Data Fig. 12r), which could be due to a combined effect of reduced cell proliferation and migration and increased cell death upon CHRM3 knockdown as observed *in vitro*. GBM cells with CHRM3 knockdown also displayed decreased migration speed and displacement compared to scrambled control cells both in acute mouse brain slices after transplantation and in human hippocampal slices after co-culture (Extended Data Fig. 12s–t). Furthermore, mice transplanted with GBOs with CHRM3 knockdown exhibited increased overall survival compared to those with scrambled control GBOs from two patients (Fig. 5o).

Taken together, these results indicate that acute ACh stimulation can lead to a sustained impact on GBM cells by increasing tumor fitness through CHRM3.

## DISCUSSION

By applying viral transsynaptic tracing to systematically define malignant neuronal circuits, our study demonstrates rapid brain-wide connectivity of GBM cells. Beyond local glutamatergic synaptic inputs onto glioma cells signaling through ionotropic receptors[3,4,9], our study reveals strikingly extensive interactions between GBM cells and neurons that release diverse neurotransmitters and originate in different brain regions, including both bilateral cortices and subcortical areas, such as the basal forebrain, brainstem and thalamic nuclei, suggesting that GBM is a whole-brain disease. Given that rabies virus does not label all inputs onto starter cells, our observation may still represent an underestimate. These findings drastically expand the notion that tumor cells may be regulated by myriad neuronal subtypes[44], such as those comprising neuromodulatory systems[45,46] signaling through metabotropic neurotransmitter receptors. Therefore, physiological or environmental perturbations that affect these brain circuits may potentially impact tumor progression. Given the ability of glioma to bidirectionally interact with neuronal circuits[11,12] combined with established roles of diffuse neuromodulatory projections in memory and behavior[47], our discoveries also provide a foundation to investigate whether feedback to neurons that interact with GBM cells might explain generalized patient symptoms such as cognitive dysfunction, sleep disturbances, seizures, or behavioral deficits that affect quality of life[48], and to develop corresponding therapeutic interventions.

Here we also provided evidence of synapses from basal forebrain cholinergic neurons onto GBM cells via direct contact at the ultrastructural level and at the functional level mediated by CHRM3 with $Ca^{2+}$ imaging and electrophysiology analyses. Importantly, we discovered a long-lasting impact of acute ACh stimulation on GBM cells, defined by transcriptional reprogramming and enhanced migratory behavior. Our results collectively support a model wherein rapid formation and acute activation of inputs onto migratory GBM cells by upstream neurons may refuel tumor cells to enhance their migration and progression, analogous to gas stations refueling cars traveling along the highway.

The success in virus-based transsynaptic tracing for cancer offers a broader application of these approaches to study cancer-neuron interactions, such as mapping of connectomes of other brain tumors, brain metastases, or tumors innervated by neurons in the peripheral nervous system. This methodology may be further enhanced with the development of new generations of rabies virus with diminished toxicity[49] or direct coupling with scRNA-seq[24,50]. Together, our study reveals diverse and robust neuronal crosstalk with GBM cells from local and long-range projections by multiple neurotransmitters, and our findings may therefore serve as a framework to investigate the functional impact and therapeutic relevance of these complex interactions.

# METHODS

## Human specimens and animal models

De-identified human GBM surgical samples were collected at the Hospital of the University of Pennsylvania after informed patient consent under a protocol approved by the Institutional Review Board of the University of Pennsylvania. Sample distribution and collection were overseen by the University of Pennsylvania Tumor Tissue/Biospecimen Bank in accordance with ethical and technical guidelines on the use of human samples for biomedical research. Primary and recurrent GBM specimens were included in this study, and Supplementary Table 1 summarizes the epidemiological data for each subject and genomic data provided by the Neurosurgery Clinical Research Division (NCRD) at the University of Pennsylvania. Disease-relevant genomic alterations (Agilent Haploplex assay, Illumina HiSeq2500), fusion transcripts (Illumina HiSeq2500), and MGMT promoter methylation (PyroMark Q24, Qiagen) were performed by the University of Pennsylvania Center for Personalized Diagnostics. De-identified human hippocampal surgical specimens used for co-culture were collected at the Children's Hospital of Philadelphia after informed patient consent under a protocol approved by the Institutional Review Board of the Children's Hospital of Philadelphia (Supplementary Table 1).

All animal experiments in this study were conducted in accordance with institutional guidelines and protocols approved by the Institutional Animal Care and Use Committee (IACUC) at the University of Pennsylvania. Animals were housed on a 12-hour light/dark cycle with food and water *ad libitum*. We used 5–8-week-old female athymic nude mice (*Foxn1*$^{nu}$/*Foxn1*$^{nu}$, Jackson Laboratory, Strain #007850) for all experiments. Animals were monitored routinely for weight loss beyond 20% of the initial body weight and neurological abnormalities, which constituted an endpoint per IACUC guidelines. These limits were not exceeded in any experiments.

## GBM organoid culture

GBM cells were cultured as 3D GBM organoids (GBOs), which were generated directly from human GBM surgical specimens following our established protocols[14]. In brief, fresh surgically resected GBM tissue was placed in dissection medium consisting of Hibernate A (Thermo Fisher, A1247501), 1X GlutaMax (Thermo Fisher Scientific, 35050061), and 1X Antibiotic-Antimycotic (Thermo Fisher Scientific, 15240062) and kept at 4°C. Tissue was transported to the lab and subsequently dissected into ~1 mm$^3$ pieces with small spring scissors in a sterile petri dish. Dissected tumor pieces were washed in 1X Red Blood Cell (RBC) Lysis Buffer (Thermo Fisher Scientific, 00-4222-57) and then washed with DPBS (Thermo Fisher Scientific, 14040182). Samples were then transferred to an ultra-low attachment 6-well culture plate and cultured in GBO culture medium containing 50% Neurobasal (Thermo Fisher Scientific, 21103049), 50% DMEM:F12 (Thermo Fisher Scientific, 11320033), 1X NEAAs (Thermo Fisher Scientific, 11140050), 1X GlutaMax (Thermo Fisher Scientific, 35050061), 1X Penicillin-Streptomycin (Thermo Fisher Scientific, 15070063), 1X B27 without vitamin A supplement (Thermo Fisher Scientific, 12587010), 1X N2 supplement (Thermo Fisher Scientific, 17502048), 1X 2-mercaptoethanol (Thermo Fisher Scientific, 21985023), and 2.5 μg/ml human recombinant

insulin (Sigma, 19278). 6-well plates containing GBOs were cultured on an orbital shaker with continuous shaking speed (110 rpm) in a 37°C, 5% $CO_2$, and 85% humidity sterile culture incubator, and culture medium was replaced every 2 days. Generally, during the first 1–2 weeks of culture, cellular debris shed from tumor pieces could be observed; however, round GBOs typically formed after 2–3 weeks. GBOs were passaged by cutting larger (>1 $mm^3$) pieces to approximately 0.5 – 1 $mm^3$ pieces with dissection scissors. Biobanking and long-term storage of GBOs[14] were performed by transferring small GBO pieces (0.1 – 0.2 $mm^3$) to GBO culture medium containing 10% DMSO in cryogenic vials (Thermo Fisher Scientific, 13-700-504). Vials were stored in a foam Cell Freezing Container (Thermo Fisher Scientific, 07-210-002) at −80°C overnight and then transferred to liquid nitrogen for long-term storage. Because our culture medium contains no exogenous growth factors[14], tumor cells continue to divide, whereas non-tumor cells in the GBOs normally do not divide and gradually become depleted over long-term culture. For the current study, we employed GBOs that have been in culture for an extended period (>6–12 months) to generate sufficient cell numbers for all experiments and enrich malignant cells for viral transduction.

### Human iPSC-derived progenitor cell, neuron, and organoid culture

Human neural progenitor cells were derived from the dissociation of human iPSC-derived forebrain organoids generated following a protocol reported previously with minor modifications[51]. In brief, detached WTC-11[52] human iPSC cells were transferred to an ultra-low attachment U-bottom 96-well plate (20K cells/well) and cultured in mTeSR Plus media (StemCell Technologies, 5825) supplemented with 10 μM Y-27632 (StemCell Technologies, 72304) for 48 hours to achieve Embryoid Body (EB) aggregation. On days 3–7, EBs were cultured in F1 neural induction medium containing DMEM/F12 supplemented with 20% KnockOut Serum Replacement (Thermo Fisher Scientific, 10828028), 1X Penicillin-Streptomycin, 1X NEAAs, 1X GlutaMax, 0.1 mM 2-mercaptoethanol, 0.0002% heparin, 1 μM IWR-1-endo (StemCell Technologies, 72562), 5 μM SB-431542 (StemCell Technologies, 72234), and 1 μM LDN-193189 (StemCell Technologies, 72147). On day 7, organoids were embedded in Matrigel (Corning, 8774552) and cultured in F2 medium containing DMEM/F12 supplemented with 1X N2 supplement, 1X Penicillin-Streptomycin, 1X NEAAs, 1X GlutaMax, 0.1 mM 2-mercaptoethanol, 1 μM SB-431542, and 1 μM CHIR99021 (StemCell Technologies, 72054) for 7 days. On day 14, embedded organoids were dissociated from Matrigel and transferred to an ultra-low attachment 6-well plate, placed on an orbital shaker at 110 rpm, and cultured in F3 medium containing 50% DMEM/F12 and 50% Neurobasal supplemented with 1X B27 supplement (Thermo Fisher Scientific, 17504044), 1X N2 supplement, 1X Penicillin-Streptomycin, 1X NEAAs, 1X GlutaMax, 0.1 mM 2-mercaptoethanol, and 3 μg/ml human insulin. On day 20, forebrain organoids were digested with Accutase (Thermo Fisher Scientific, A1110501) at 37°C for 15 minutes and dissociated to single cells, which were later seeded on plates pre-coated with 1% Matrigel and cultured in F3 medium supplemented with 1 μM CHIR-99021, bFGF (20 ng/mL, PeproTech, 100–18B), and EGF (20 ng/mL, PeproTech, AF-100-15).

Human iPSC-derived sliced neocortical organoids (SNOs) were generated and maintained as described above for neural progenitor cells using either the WTC-11[52] or C1–2[51] iPSC lines but with the following modifications: organoids were not dissociated at day

20 but rather maintained in culture until day 70, at which point organoids were sliced as previously described[16] and cultured in F4 medium containing Neurobasal supplemented with 1X B27 supplement, 1X GlutaMax, 1X NEAAs, 1X 2-mercaptoethanol, 1X Penicillin-Streptomycin, 0.05 mM cAMP (STEMCELL Technologies, 73886), 0.2 mM ascorbic acid (Sigma, A0278), 20 ng/mL BDNF (PeproTech, 450-02), and 20 ng/mL GDNF (PeproTech, 450–10) thereafter.

Human iPSC-derived glutamatergic and GABAergic neurons were generated with modified protocols. In brief, WTC11 iPSCs were dissociated and aggregated into EBs and patterned toward a neural ectoderm fate in F1 neural induction medium for 6 days. To generate glutamatergic neurons, EBs were further cultured in modified F2 medium to promote progenitor cell expansion for 7 days. To generate GABAergic neurons, EBs were further cultured in F2 medium supplemented with 100 nM SAG (Cayman, 11914) and patterned to medial ganglionic eminence (MGE) fate for 7 days. After switching to F3 medium for 4 days, EBs were dissociated with Accutase into single cells and seeded on Matrigel-coated plates in F3 medium for neural progenitor culture. For mixed cultures, both types of neural progenitors were dissociated with Accutase and seeded at a 1:1 ratio on poly-D-lysine and laminin-coated coverslips in F4 medium for neuronal differentiation.

## Single-cell and bulk RNA sequencing

For single-cell RNA sequencing (scRNAseq) library preparation, we employed a plate-based scRNAseq method based on SMART-seq3[53,54] with minor modifications for increased throughput. GBOs were first dissociated into a single-cell suspension with a brain tumor dissociation kit (Miltenyi Biotech, 130-0950929). In brief, 5–10 GBOs were washed with DPBS and incubated in 1 mL of dissociation mix according to the manufacturer's protocol. GBOs were placed on a tube rotator in a 37°C incubator for 30 minutes to 1 hour with occasional pipetting to mechanically disrupt large tissue chunks. Cells were then strained through a 70 μm filter (Miltenyi Biotech, 130-110-916), centrifuged at 300 *g* for 5 minutes and resuspended in 1 mL of GBO culture medium. Cell viability and cell concentration were measured with an automated cell counter (Thermo Fisher Scientific, Countess 3 Automated Cell Counter) with trypan blue staining (Thermo Fisher Scientific, C10312). An ideal cell viability following dissociation is typically > 80%. Cells were then resuspended in FACS pre-sort buffer (BD, 563503) with 0.2 μg/mL DAPI (BD, 564907). For sliced neocortical organoid (SNO) scRNAseq, 100-day old SNOs cultured as described above were dissociated in a similar manner as GBOs but with the addition of 50 μL Enzyme P (Miltenyi, 130-107-677) per 1 mL of dissociation mix. Single cells were sorted on a BD Influx (100 μm nozzle) with FACSDiva software into low-profile 96-well PCR plates (USA Scientific, 1402-9500) containing 3 μL of SMART-seq3 lysis buffer (0.5 μL PEG 8000 (40% solution, Sigma Aldrich, P1458), 0.03 μL Triton X-100 (10% solution), 0.02 μL of 100 μM Oligo-dT30VN, 0.2 μL of 10 mM dNTPs (Roche, 50-196-5273), 0.02 μL Protector RNase inhibitor (Sigma Aldrich, 3335402001), 0.02 μL recombinant RNase inhibitor (Takara, 2313B) and 2.21 μL nuclease-free water per reaction (Thermo Fisher Scientific, AM9932)) and 3 μL Vapor-Lock (Qiagen, 981611). Plates after sorting were briefly centrifuged, frozen on dry ice, and stored at −80°C for later processing.

For library preparation, plates were thawed, heated to 72°C for 10 minutes, and subsequently kept at 4°C for cell lysis. 3 μL of RT mix, containing 0.1 μL of 1 M Tris-HCl pH 8.3 (Hampton Research, HR2-900-14), 0.024 μL of 5 M NaCl (Thermo Fisher Scientific, AM9759), 0.01 μL of 1 M $MgCl_2$ (Thermo Fisher Scientific, AM9530G), 0.04 μL of 1 mM GTP (Thermo Fisher Scientific, R1461), 0.32 μL of 100 mM DTT (Millipore Sigma, 3483-12-3), 0.016 μL of nuclease-free water, 0.025 μL Protector RNase inhibitor (Millipore Sigma, C852A14), 0.025 μL recombinant RNase inhibitor (Takara, 2313B), 0.04 μL reverse transcriptase (Thermo Fisher Scientific, EP0753), and 0.4 μL of 20 μM TSO, was added to each well of the 96-well plate. To enable multiplexing and enhance throughput, we designed 48 unique TSOs consisting of an additional 6-bp cell barcode directly adjacent to the 5'-end of the Smart-seq3 UMI (Supplementary Table 2). Reverse transcription was performed with the following thermocycling conditions: 42°C for 90 minutes, 10 cycles of 50°C for 2 minutes and 42°C for 2 minutes, 85°C for 5 minutes, and 4°C indefinitely. Next, for cDNA amplification, 6 μL of PCR mix, consisting of 2 μL 5X KAPA HiFi HotStart Buffer (Roche, KK2502), 0.3 μL of 10 mM dNTPs, 0.005 μL of 1 M $MgCl_2$, 0.01 μL of 1mM PCR forward primer, 0.01 μL of 100 μM PCR reverse primer, 3.475 μL of nuclease-free water, and 0.2 μL of KAPA HiFi HotStart polymerase (Roche, KK2502), was added to each well. cDNA amplification was performed with the following thermocycling conditions: 98°C for 3 minutes, 18 cycles of 98°C for 20 seconds then 65°C for 30 seconds then 72°C for 4 minutes, 72°C for 5 minutes, and 4°C indefinitely. cDNA from 48 wells was pooled together into one sample (2 samples per plate), and samples were then purified twice with 0.6X then 0.8X AMPure XP beads (Thermo Fisher Scientific, A63881) and eluted in 10 μL of nuclease-free water. cDNA was quantified using Qubit dsDNA HS assay kit (Life Technologies, Q32851).

Each sample was then tagmented by mixing 2 μL of 0.5 ng/μL cDNA, 4 μL of 2X TD buffer (20 mM Tris pH 8.0, 10 mM $MgCl_2$, 20% dimethylformamide (Sigma, D4551)), and 2 μL of Tn5 (Thermo Fisher Scientific, TNP92110) and incubating at 55°C for 20 minutes with reaction termination upon addition of 2 μL of 0.2% SDS (Invitrogen, 15553-035) at room temperature for 5 minutes. We chose to use i5-only Tn5 to enrich for the 5'-ends of mRNA, although full-length sequencing can be achieved using i5/i7 Tn5. Fragments were amplified by adding 1 μL of 10 μM Nextera i7 primer, 1 μL 10 μM Nextera i5 primer, 5 μL of 5X Phusion Plus Buffer (Thermo Fisher Scientific, F630L), 0.5 μL of 10 mM dNTPs, 0.5 μL of 1% Tween-20, 6.8 μL nuclease-free water, and 0.2 μL of Phusion Plus polymerase (Thermo Fisher Scientific, F630L). Tagmentation PCR was performed with the following thermocycling conditions: 98°C for 3 minutes, 8 cycles of 98°C for 10 seconds then 60°C for 30 seconds then 72°C for seconds, 72°C for 5 minutes, and then indefinitely at 4°C. Resulting DNA was purified twice with 0.8X then 1.0X AMPure XP beads and eluted in 10 μL of 10 mM Tris, pH 8.0. Samples were then quantified by qPCR with library sizes quantified by Bioanalyzer (Agilent). Samples were sequenced on either a NovaSeq 6000 (Illumina) or NextSeq 550 (Illumina) at a final depth of roughly 100K-200K reads/cell. All primer and TSO sequences are detailed in Supplementary Table 2.

For bulk RNA sequencing, GBOs were reaggregated into organoids of 2000 cells in 96-well U-bottom plates as described above. For ACh experiments, ACh (acetylcholine chloride, Sigma Aldrich, A6625) was applied to a final concentration of 1 mM for various durations

prior to removal of medium and sample lysis. If any condition required a waiting period prior to lysis, GBOs were washed once with GBO medium prior to complete replacement with fresh GBO medium. For sequencing of CHRM3 knockdown GBOs, GBO cells were directly infected with either scrambled or knockdown lentivirus prior to reaggregation as described above for retroviral infection, and cells were subjected to 1-hour ACh treatment 7 days following shRNA transduction. Library preparation was performed as described above for single-cell sequencing with minor modifications: all reactions were scaled up by 10X the volume (e.g., sample lysis in 30 μL of Smart-seq3 lysis buffer), cDNA amplification was performed with 16 cycles, and tagmentation PCR was performed with 10 cycles. Libraries were sequenced to roughly 12–15 M reads per sample.

## Sequencing pre-processing and analysis

To process single-cell RNA sequencing data, raw files were demultiplexed with bcl2fastq (Illumina) without adapter trimming and with the option for *--create-fastq-for-index-reads*. A combined fastq file consisting of a 22-bp cell barcode (composed of 8-bp index 1, 8-bp index 2, and 6-bp barcode) was then generated. Alignment was performed using STARsolo as part of STAR v2.7.10b[55,56] with GRCh38 as the reference genome and gencode v.41 GTF as the annotation file, and with the following additional parameters: *--alignIntronMax 1000000 --outFilterScoreMinOverLread 0.3 --outFilterMatchNminOverLread 0.3 --limitOutSJcollapsed 4000000 --soloType CB_UMI_Simple --soloCBstart 1 --soloCBlen 22 --soloUMIstart 23 --soloUMIlen 8 --soloBarcodeMate 1 --clip5pNbases 30 --soloCBmatchWLtype 1MM_multi --soloCellFilter EmptyDrops_CR --soloStrand Reverse*. A cell barcode text file was supplied, and multimapping alignments were discarded.

Count matrices via the “GeneFull” option including intronic counts from STARsolo were imported into R (v4.3.1) using Seurat (v4.3.0.1)[57]. Genes expressed in less than 10 cells were discarded, and cells that had less than 1000 UMIs or with a percentage of mitochondrial UMIs over 20% were discarded as well. Counts were normalized with SCTransform[58] with vst.flavor = “v2”, variable.features.n = 15000, and regression of percentage mitochondrial UMIs and number of UMIs. Copy number aberration (CNA) analysis was performed with the HoneyBADGER R package[59]. GBM cellular state was assigned as previously described[8] and implemented[60] in the function get.sig.scores. Relative enrichment scores of various gene signatures were computed via UCell[61] package as implemented in the function AddModuleScore_UCell, with genes for each signature detailed in Supplementary Table 4. To identify clusters in the SNO dataset, the FindAllMarkers function in Seurat was used with adjusted *P*-value < 0.05 (Wilcoxon rank-sum test with Bonferroni correction) and log fold-change threshold of 0.25. We also retrieved count matrices for various published datasets using either the Smart-seq2 platform[8,18] or 10X Genomics platform[17]. Annotated tumor cells from 6 patients (SF10108, SF11082, SF11780, SF12382, SF3391, SF9510) were merged from the Wang et al.[17] dataset. The Neftel et al.[8] dataset was first normalized by SCTransform[58] and then integrated using Harmony[62]. Dot plots in Fig. 1a and Extended Data Fig. 1n were plotted with the ‘RNA’ assay and ‘data’ slot following log-normalization with the dittoDotPlot function implemented in the dittoSeq package. scRNAseq data of GBOs at baseline conditions or treated with ACh were

first normalized with SCTransform[58] with method = 'glmGamPoi' and then integrated with rPCA in Seurat[57].

Bulk RNA sequencing data with UMIs were processed similarly but with an additional option of *--soloUMIdedup NoDedup* during alignment to account for increased UMI complexity of these samples. Samples with at least 10000 detected genes were included for further analysis. For the 1 hour ACh pulse experiments (fast response, Extended Data Fig. 10a–f, Fig. 5c–d), differential expression analysis was performed with DESeq2[63] using UMI counts as input and a model design of *~Tumor + Treatment* (where *Treatment* indicates whether ACh was applied and *Tumor* indicates patient GBO) to control for differences amongst patients, with effects size estimation performed with apeglm[64] (Supplementary Table 3). For the pulse experiments for long-lasting transcriptional changes (long-lasting response, Extended Data Fig. 11a–c, Fig. 5e–f), differential expression analysis was performed as above but with a model design of *~Tumor + Condition* (where *Condition* represents the duration prior to sample lysis). Differentially expressed genes between the control (no ACh) condition and each of the durations were obtained separately (adjusted *P*-value < 0.05) and visualized with the UpSetR package (Supplementary Table 5). GO analyses of differentially expressed genes were performed with an overrepresentation test as implemented in pantherdb.org[65] with sets of either upregulated or downregulated genes (defined as adjusted *P*-value < 0.05 and abs($\log_2$FC) > 0.25). The background genes for GO analysis were defined as genes that were detected with a low threshold (average of 0.25 – 0.5 UMIs per sample). The ACh fast response gene signature was defined as the top 100 genes upregulated from baseline after 1-hour ACh treatment ranked by adjusted *P*-value. The ACh long-lasting response gene signature was defined as the top 100 genes upregulated from baseline 1 day after 1-hour pulse of ACh ranked by adjusted *P*-value. Exemplary genes in Extended Data Fig. 10b–c were plotted as a fold-change from baseline using the DESeq2-normalized UMIs. Gene enrichment for various pathways (Supplementary Table 4) was obtained by importing the UMI count matrix into Seurat (with each 'cell' as a bulk sample), running SCTransform with vst.flavor = "v2", and using the AddModuleScore function with the 'SCT' assay as implemented in Seurat.

## Viral vector and plasmid generation

EnvA-pseudotyped G-deleted EGFP rabies virus was purchased from the Salk viral core (32635). Monosynaptic HSV (strain H129-LSL-ΔTK-tdTomato) was a kind gift from Lynn Enquist and expanded in-house. Polysynaptic HSV (strain H8, modified from H129) expressing GFP was generated as described previously[21]. AAV2/9-ChAT-Cre-WPRE-hGHpA (PT-0607), AAV2/8-EF1α-DIO-EGFP-2a-TK-WPRE-pA (PT-0087), and AAV2/9-hSyn-DIO-Synaptophysin-EGFP-WPRE-hGHpA (PT-4595) were purchased from BrainVTA. AAV9-EF1α-DIO-hChR2(H134R)-EYFP-WPRE-hGHpA was a gift from Karl Deisseroth (Addgene, viral prep 20298-AAV9). The retroviral CAG-DsRed-T2A-RabiesG-IRES-TVA (RTG helper plasmid) was a gift from Benedikt Berninger. To generate the control retroviral helper plasmid without G protein, we excised the G protein coding sequence and ligated the plasmid with an annealed duplex oligonucleotide (Supplementary Table 2). Plasmid sequences were confirmed by Sanger DNA sequencing (Penn Genomic and Sequencing Core) and whole plasmid sequencing (Plasmidsaurus). The lentiviral

construct for chemogenetic control of tumor cell depolarization was generated by excising the hM3D(Gq)-mCherry sequence from pAAV-GFAP-hM3D(Gq)-mCherry (Addgene, 50478) and inserting it in a lentiviral backbone under the CMV promoter.

ShRNA sequences for CHRM3 were designed using the Broad Institute RNAi Consortium (https://www.broadinstitute.org/rnai-consortium/rnai-consortium-shrna-library) (Supplementary Table 2). The backbone vector for shRNAs was purchased from Addgene (pLKO.1_mCherry, 128073). We followed the shRNA construction protocol from the Genetic Perturbation Platform web portal (https://portals.broadinstitute.org/gpp/public/resources/protocols). Plasmid sequences were confirmed by Sanger DNA sequencing.

Retroviruses were produced with HEK 293T cells. 293T packaging cells were prepared at 70–80% confluency in 15 cm tissue culture plates. For each plate, 6 μg pMD2.G (Addgene, 12259), 4 μg pUMVC (Addgene, 8449) and 18 μg transfer plasmid were mixed in 700 μL DMEM medium (Corning, 10-013-CV). Subsequently, 84 μL of LipoD293™ (SignaGen Laboratories, SL100668) was mixed with 700 μL DMEM medium. These two mixtures were then combined and incubated at room temperature for 10 minutes. The plate was then replenished with 15 mL of pre-warmed 293T culture medium (DMEM, 10% fetal bovine serum (Fisher Scientific, SH3007103) and 1X Penicillin-Streptomycin) and the combined mixture was added dropwise. Virus-containing medium was collected after 24, 48 and 72 hours and stored at 4°C. The 293T culture was replenished with 15 mL warm culture medium after each collection. After 72 hours, the virus-containing medium was pooled together and centrifuged at 500 *g* for 5 minutes to pellet cells. The supernatant was filtered through a 0.45 μm PES filter (Thermo Fisher Scientific, 566-0020). The filtered medium was then centrifuged with a high-speed centrifuge at 25,000 *g* and 4°C for 2 hours followed by resuspension in DPBS. Concentrated viruses were aliquoted and stored at −80°C. Viral titer was determined by serial dilution, infection in 293T cells, and counting of positive colonies. Lentiviruses were produced using a similar procedure with 293T cells using the psPAX2 plasmid (Addgene, 12260) instead of pUMVC.

### Assembloid generation with sliced neocortical organoids (SNO) and GBOs

To generate GBO-SNO assembloids, we used at least 100-day old SNOs[16] to provide a neuronal microenvironment for GBO integration. SNOs were sliced at a 300 μm thickness using a vibratome (Leica VT 1200S) at 0.1 mm/s speed and 1.2 mm vibration amplitude and immediately transferred to ALI cultures as described above. SNOs were maintained with the ALI system with 1.3 mL of culture medium (BrainPhys Neuronal Medium (STEMCELL Technologies, 5790), 1X NeuroCult SM1 Neuronal Supplement (STEMCELL Technologies, 05711), 1X N2 Supplement (Thermo Fisher Scientific, 17502048), and 1X Penicillin-Streptomycin (Thermo Fisher Scientific, 15070063)) in each well. Medium was replenished every two days, and SNOs were cultured on ALI for at least two days prior to GBO fusion. To generate assembloids, GBOs (~2000 – 10000 cells) were placed either directly adjacent to the SNOs such that they were physically in contact or on top of the SNOs using a P200 pipette.

For migration experiments, UP-10072 GBOs expressing RTG or expressing the shRNA construct marked by mCherry expression were used to generate assembloids to

easily distinguish tumor cells from the microenvironment by combined brightfield and fluorescence imaging on a confocal microscope (Zeiss LSM 710). For cholinergic stimulation, GBOs were treated with a 1-hour pulse of 1 mM ACh in GBO medium prior to assembloid generation. Images were exported from Zen 2 software and imported into ImageJ/FIJI to measure the extent of tumor migration at the specified timepoints. The area covered by GBO cells was measured by using the 'polygon' ROI function in ImageJ/FIJI to draw the largest bounding polygon that captured the invading cells.

### Viral tracing with human neurons *in vitro*

For monosynaptic rabies virus tracing with 2D iPSC-derived neurons, mixed glutamatergic and GABAergic neurons were generated as described above. Monosynaptic tracing experiments were conducted after a maturation period of 3–4 weeks following seeding. UP-10072 RTG-GBOs were pre-labeled overnight with ΔG rabies virus as described below and dissociated the following day for seeding onto the neuron culture at a 1:1000 tumor to neuron ratio. Coverslips were fixed for immunohistology after 10 days.

For polysynaptic HSV tracing with human hippocampal specimens, fresh surgical tissue was placed in ice-cold cutting solution (Ecocyte Bioscience, C748D56) pre-bubbled with carbogen (95% $O_2$, 5% $CO_2$) for at least an hour and sliced on a vibratome at 300 μm as described previously[66]. Tissues were cultured on top of 6-well cell culture plates containing a Millicell culture inset (0.4 μm pore size, 30 mm diameter, PICM03050). Slices were maintained using this air-liquid interface[66,67] (ALI) system with 1.3 mL of culture medium (BrainPhys Neuronal Medium (STEMCELL Technologies, 5790), 1X NeuroCult SM1 Neuronal Supplement (STEMCELL Technologies, 05711), 1X N2 Supplement (Thermo Fisher Scientific, 17502048), and 1X Penicillin-Streptomycin (Thermo Fisher Scientific, 15070063); 'brain-tissue medium') in each well such that slices were not submerged in liquid but rather open to air on one side. After 24 hours, pre-warmed HSV-containing medium was added to the top of the culture insert for 15 minutes prior to 3X washout with medium. 3 days following infection, medium underneath the ALI was completely refreshed prior to fusion with either UP-9121-RTG or UP-9096 GBOs. At 3 days after fusion, slices were fixed for immunohistology. For control experiments to rule out viral leakage, conditioned medium taken from underneath the ALI from parallel slice cultures after medium refresh (total of 4 days following infection) were added to GBOs in 6-well plates for 3 days prior to fixation for immunohistology.

### Stereotaxic GBO transplantation and virus injection

For all transplantation experiments, GBO cells were prepared in a single-cell suspension via the dissociation protocol as described above and kept in sterile Hibernate A prior to the surgical procedure. Transplantation was performed aseptically following IACUC guidelines for rodent survival surgery. The cranium was exposed following a midline scalp incision, and a hole was drilled through the cranium above the desired stereotaxic coordinates using a micromotor drill (Stoelting, 51449). Roughly 200,000 single GBM cells in 1–2 μL of Hibernate A were loaded into a 5 μL Hamilton syringe (Hamilton, 80016) with a 26-gauge needle (Hamilton, 7768–02). Injection stereotaxic coordinates used for monosynaptic tracing were as follows: M1 (1.2 mm anterior to bregma (A/P), 1.5 mm lateral to midline (M/L), and

1.5 mm deep to cranial surface (D/V)), S1 (A/P −0.9 mm, M/L +3.0 mm, D/V −1.5 mm), RSP (A/P −2.3 mm, M/L 0.4 mm, D/V −1.7 mm), ventral hippocampus (A/P −2.0 mm, M/L +1.6 mm, D/V −2.6 mm), and dorsal hippocampus (A/P −2.0 mm, M/L +1.6 mm, D/V −1.8 mm). Injection was performed with a flow rate of less than 0.2 μL/min. The needle was kept in place for a minimum of 5 minutes prior to slow withdrawal at a rate of less than 0.5 mm/min. The incision was sutured with 5–0 Vicryl (VWR, 95056–936) with application of topical bacitracin, and mice were transferred to a 37°C warming pad for recovery. Animals were monitored for at least 3 consecutive days following surgery and twice a week for dramatic weight loss or any physical abnormalities until the experimental endpoint.

For virus injections, similar procedures were employed but using a 1 μL Hamilton syringe (Hamilton, 80100). For injection of AAV into the basal forebrain, the following stereotaxic coordinates were used: A/P +1.2 mm, M/L 0 mm, and D/V −5.0 mm. Other GBO transplantation sites were chosen based on experimental necessity. For retrograde monosynaptic tracing, GBOs were transplanted into either M1, S1, RSP, or ventral hippocampus (all coordinates as described above), with transplantation into multiple sites for a subset of the experiments. For $Ca^{2+}$ imaging and electrophysiology experiments, GBOs were transplanted into the dorsal hippocampus. For monosynaptic anterograde tracing HSV experiments, GBOs were transplanted either in the RSP or the dorsal hippocampus. For transplantation of CHRM3 knockdown GBOs, the following stereotaxic coordinates were used: dorsal hippocampus (coordinates above) or striatum (A/P +1.0 mm, M/L +1.7 mm, D/V −3.5 mm).

### Trans-monosynaptic viral tracing with GBOs *in vivo*

Transsynaptic retrograde labeling with rabies virus requires expression of helper proteins including the rabies virus glycoprotein (G) and the TVA receptor in the starter (postsynaptic) GBO population[5,19,68]. To enhance viral transduction efficiency, GBOs were first dissociated into a single-cell suspension with the brain tumor dissociation kit as described above. Subsequently, a retrovirus encoding DsRedExpress, rabies glycoprotein (G), and the mammalian TVA receptor (CAG-DsRedExpress-T2A-Rabies G-IRES-TVA; RTG) was incubated with 10 μg/mL polybrene (Millipore Sigma, TR1003G) on ice for 1 hour and then added to the resuspended cells. 20,000 cells together with 10 μL retrovirus in 50–100 μL culture medium were added per well in low-attachment 96-well U-bottom plates (S-bio, MS-9096UZ) to reaggregate GBOs without orbital shaking. The next day, reaggregated GBOs were transferred to ultra-low attachment 6-well culture plates (Thermo Fisher Scientific, 07–200-601) and cultured on an orbital shaker as described above. DsRed signal could typically be detected via a fluorescence microscope 4–6 days post infection. We caution that for application of this method to other studies, care should be taken to ensure that non-tumoral cells are not infected with the helper retrovirus. Validation may be performed by immunostaining for tumor-specific markers, such as Nestin. However, we caution that Nestin may label some progenitor cells (Supplementary Figure 1), and other orthogonal markers should be considered for combined tumor cell identification such as SOX2 or EGFR. If infection rate of the retrovirus is relatively low (e.g., <10%), cell sorting for $DsRed^{+}$ cells may increase tracing efficiency. With the current protocol we cannot yet target GBM cells of specific cell states to map their connectome.

For ΔG rabies virus pre-infection retrograde tracing experiments, starter GBOs expressing RTG were incubated with EnvA-pseudotyped G-Deleted EGFP rabies virus (Salk, 32635) in low-attachment 96 well U-bottom plates. Around 2–3 GBOs (~50,000 cells) were incubated with 0.5 μL ΔG rabies virus in 50 μL GBO culture medium per well overnight. The next day, GBOs were washed three times with DPBS and dissociated into a single-cell suspension as described above. GBO cells were resuspended and kept in ice-cold Hibernate A before intracranial injection. For pre-infection experiments, mice were sacrificed at 3, 5, or 10 dpt. For long-term GBO transplantation and rabies virus tracing, starter GBOs expressing RTG were dissociated using the same procedure. At 1 month post transplantation, a second surgery was performed to inject 1 μL ΔG rabies virus into the same location as the initial transplantation. Mice were sacrificed 10 days following rabies virus injection.

For control experiments to rule out leakage of infection-competent rabies virus (Extended Data Fig. 3c), UP-10072 GBOs expressing RTG were pre-labeled with ΔG rabies virus as described above. At either 1 day or 5 days following pre-labeling, rabies virus was extracted from GBOs and injected into mice for analysis either 9 days or 5 days later, respectively. Viral extraction was accomplished by first resuspending cells in distilled $H_2O$. Cells were then snap frozen on dry ice for 2 minutes before thawing at room temperature, with freeze-thaw cycling repeated 5 times. Cells were then further lysed with a 26-gauge needle. Cell death and fragmentation were confirmed via trypan blue staining. 2 μL of cell lysate (from a total of 10 μL solution extracted from $9 \times 10^5$ cells) was then injected into the RSP per mouse as described above.

For anterograde tracing experiments with monosynaptic HSV, a mixture of 400 nL AAVs (composed of a mixture of 1:20 AAV2/9-ChAT-Cre-WPRE-hGHpA and Cre-dependent AAV2/8-EF1α-DIO-EGFP-2a-TK-WPRE-pA) and 600 nL H129-LSL-ΔTK-tdTomato were injected in the basal forebrain. During the same surgery, UP-10072 GBO cells were transplanted into either the RSP or the hippocampus as described above. Mice were sacrificed 10 days after the surgery and brains were harvested for immunohistology.

### Sample preparation, immunohistology, *in situ,* and confocal microscopy

To harvest brains of animals, mice were deeply anesthetized with ketamine/xylazine/acepromazine and perfused transcardially with 10 mL ice-cold DPBS followed by 10 mL of 4% paraformaldehyde (PFA). Brains were post-fixed in 4% PFA overnight at 4°C, washed with 10 mL DPBS, and transferred to 30% sucrose at 4°C for 24 hours for cryoprotection. Brains were then sectioned in the coronal plane (Leica SM 2010R) at 40 μm thickness for processing as floating sections and stored in anti-freeze medium (Bioennolife Sciences, 006799-1L) at −20°C. For each brain, every sixth section was collected into the same well of a 24-well plate. Floating mouse brain sections were washed with DPBS, incubated in DPBS with 0.3% Triton X-100 (Sigma-Aldrich, P1379) for 1 hour, and then incubated with blocking buffer (TBS with 0.1% Tween-20 (Sigma-Aldrich, T8787-50ML), 0.5% Triton X-100, 10% donkey serum (Millipore, S30), 1% BSA (Sigma-Aldrich, B6917), 22.52 mg/mL glycine (Sigma-Aldrich, 50046-50G), and 1% Mouse on Mouse Blocking Reagent (Vector Laboratories, MKB-2213-1)) for 30 minutes. Brain slices were then incubated in diluted primary antibodies in antibody buffer (TBS with 0.1% Tween-20, 0.5% Triton

X-100, and 5% donkey serum) at 4°C overnight on a horizontal shaker. The following day, slices were washed 3X in TBST (TBS with 0.1% Tween-20) for 5 minutes each and incubated with secondary antibodies diluted in antibody buffer as described above for 1–2 hours at room temperature. Unless otherwise indicated, DAPI (Thermo Fisher Scientific, D1306, 1:500) was incubated with slices simultaneously during the secondary antibody incubation. Slices were washed 3X in TBST for 5 minutes each and then mounted on a glass slide (Thermo Fisher Scientific, 1518848) in mounting medium (Vector Laboratories, H-1000-10), covered with glass coverslips, and sealed with nail polish. For SST staining, brain slices underwent an additional antigen retrieval step in 1X IHC Antigen Retrieval Solution (Invitrogen, 00-4956-58) for 15 minutes at 95°C prior to blocking.

The following primary antibodies were used: Goat anti-RFP (Biorbyt, orb11618, 1:500), rabbit anti-RFP (Rockland, 600-401-379, 1:500), chicken anti-GFP (Abcam, ab13970, 1:2000), goat anti-GFP (Rockland, 600-101-215, 1:500), mouse anti-Human Nuclei (Millipore, MAB1281, clone 235-1, 1:200), mouse anti-STEM121 (Takara, Y40410, clone STEM121, 1:250), goat anti-ChAT (Sigma-Aldrich, AB144P-200UL, 1:200), rabbit anti-VAChT (Synaptic Systems, 139103, 1:500), mouse anti-TPH2 (Thomas Scientific, AMAb91108, clone CL2990, 1:250), rabbit anti-TH (Novus Biologicals, NB300–109, 1:500), mouse anti-KI67 (BD Biosciences, 550609, clone B56, 1:500), rabbit anti-KI67 (Abcam, ab16667, clone SP6, 1:500), rabbit anti-cleaved caspase 3 (Cell Signaling, 9661, 1:500), mouse anti-GFAP (Millipore, MAB360, clone GA5, 1:500), goat anti-SOX2 (Thermo Fisher, AF2018, 1:500), mouse anti-SATB2 (Abcam, Ab51502, clone SATBA4B10, 1:500), rat anti-CTIP2 (Abcam, Ab18465, clone 25B6, 1:500), rabbit anti-PV (Abcam, Ab11427, 1:500), rabbit anti-SST (Thermo Fisher, PA-5-85759, 1:250), mouse anti-NeuN (Thermo Fisher Scientific, MA5-33103, clone 1B7, 1:500), rabbit anti-Nestin (Abcam, Ab105389, clone SP103, 1:500), mouse anti-EGFR (Novus Biologicals, NB200-206, clone EGFR1, 1:500), RFP-Booster Alexa Fluor 568 (ChromoTek, rb2af568, 1:500), GFP-Booster Alexa Fluor 488 (ChromoTek, gb2af488, 1:500), rabbit anti-TTF-1 (NKX2.1, Millipore, 07-601, 1:500), rabbit anti-S100 (Abcam, ab868, 1:500), rabbit anti-IBA1 (Wako Pure Chemical, 019-19741, 1:500), goat anti-OLIG2 (R&D Systems, AF2418, 1:500), rabbit anti-NG2 (Millipore, AB5320, 1:500), and mouse anti-O4 (R&D Systems, MAB1326, Clone O4, 1:250).. The following secondary antibodies were used: donkey anti-goat Alexa Fluor 488 (Thermo Fisher Scientific, A-11055, 1:500), donkey anti-goat Alexa Fluor 555 (Thermo Fisher Scientific, A-21432, 1:500), donkey anti-goat Alexa Fluor 647 (Thermo Fisher Scientific, A-21447, 1:500), donkey anti-rabbit Alexa Fluor 488 (Thermo Fisher Scientific, A-21206, 1:500), donkey anti-rabbit Alexa Fluor 555 (Thermo Fisher Scientific, A-31572, 1:500), donkey anti-rabbit Alexa Fluor 647 (Thermo Fisher Scientific, A-31573, 1:500), donkey anti-mouse Alexa Fluor 488 (Thermo Fisher Scientific, A-21202, 1:500), donkey anti-mouse Alexa Fluor 555 (Thermo Fisher Scientific, A-31570, 1:500), donkey anti-mouse Alexa Fluor 647 (Thermo Fisher Scientific, A-31571, 1:500), donkey anti-rat Alexa Fluor 647 (Thermo Fisher Scientific, A-48272, 1:500), and donkey anti-chicken Alexa Fluor 488 (Thermo Fisher Scientific, A-78948, 1:500). For a subset of the retrograde tracing experiments, RFP-Booster Alexa Fluor 568 (ChromoTek, rb2af568, 1:500) and GFP-Booster Alexa Fluor 488 (ChromoTek, gb2af488, 1:500) were used during the blocking step and sections were mounted immediately after blocking.

For assembloid, GBO and primary GBM tissue immunohistology, tissue pieces were transferred to 1.5 mL Eppendorf tubes using wide-bore P1000 pipette tips and washed with DPBS. Tissue was then fixed in 4% PFA at 4°C overnight, triple washed in DPBS, and cryoprotected in 30% sucrose at 4°C for at least 24 hours. Tissue pieces were then transferred to a plastic cryomold (Electron Microscopy Sciences), embedded in tissue freezing medium (TFM, General Data, 1518313), and stored at −80°C. Samples were sectioned at 16 μm (Leica, CM3050S) and mounted on glass slides stored at −20°C. For immunohistology, sectioned samples were warmed to room temperature, outlined with a hydrophobic pen, and washed with DPBS for 5 minutes to remove TFM. Samples were then taken for blocking as described above for brain slice sections. For smaller GBOs (e.g., 2000–5000 cells), organoids were directly taken for blocking following the 4% PFA fixation step in low-attachment 96-well plates without the need for cryosectioning. For 2D co-cultures, coverslips were fixed for 30 minutes in 4% PFA, triple washed in DPBS and taken for blocking as described above.

For *in situ* hybridization and concurrent immunostaining, cryopreserved floating mouse brain sections were mounted on (3-Aminopropyl)-triethoxysilane (Sigma Aldrich, A3648) coated glass slides using PBST (PBS with 0.1% Tween-20). Slides were then processed for *in situ* hybridization using the RNAscope Multiplex Fluorescent Reagent Kit v2 (ACD, 323270) according to the manufacturer's protocol with minor modifications. In brief, slides were washed with PBS and baked at 42°C for 30 minutes, followed by dehydration with ethanol, hydrogen peroxide treatment, and target retrieval, primary antibody incubation (chicken anti-GFP or rabbit anti-VAChT), and post-primary fixation according to the manufacturer's protocol (MK51–150, Rev B, Appendix D). Slides were then incubated with RNAscope Protease Plus at room temperature for 30 minutes. Next, slides were prepared for probe hybridization (ACD, UM-323100, Chapter 4) using probes for GAD1-C2 (ACD, 400951-C2), SLC17A7-C3 (ACD, 416631-C3), SLC17A6-C3 (ACD, 319171-C3), and/or GAD1-C3 (ACD, 400951-C3) and developed with TSA Vivid 570 (ACD, 323272, 1:1500) or TSA Vivid 650 (ACD, 323373, 1:1500). Following hybridization, slides were incubated with secondary antibody (donkey anti-chicken Alexa Fluor 488 and/or donkey anti-rabbit Alexa Fluor 555) with DAPI for 1 hour at room temperature before mounting slides as described above. For identification of glutamatergic neurons, we probed simultaneously for vGLUT1 (SLC17A7) and vGLUT2 (SLC17A6) with C3 probes.

Mouse brain slices, GBO (sections or whole mount), or primary tissue sections after immunohistology were imaged with a confocal microscope (Zeiss LSM 810 or Zeiss LSM 710) as *z*-stacks with either 5X, 10X, 20X, or 40X objectives. Images were pre-processed with Zen 2 software (Zeiss) for orthogonal projection and stitching and further processed with ImageJ/FIJI (v2.1.0) for exporting and quantification. 3D reconstruction of HSV-infected tumor cells was performed with Imaris (v9.0, Bitplane).

For neuron quantification after retrograde tracing, 40 μm coronal mouse brain slices consisting of every sixth slice from +2.5 mm to −4.5 mm A/P were imaged as *z*-stacks of approximately 15 μm and orthogonally projected for analysis. For each section, we annotated the number of cells in 'level 1' (e.g., thalamic nucleus or cortical area/layer) and 'level 2' regions (e.g., thalamus or isocortex) according to the coronal Allen Brain adult

mouse brain atlas (http://atlas.brain-map.org)[69] in either the ipsilateral or contralateral side to GBO or NPC injection. For each 'level 1' region, we identified the number of starter ($GFP^+DsRed^+$) cells and the number of input neurons ($GFP^+DsRed^-$). For starter cells in which cell number was too numerous to be quantified manually, we used an approach where we estimated the cell density (cell number per area) and then extrapolated the number of starter cells. Representative coronal sections in Fig. 2a–d were colored by $GFP^+DsRed^-$ cell proportion independently for contralateral versus ipsilateral regions. Schematic images (Fig. 2a–d) were obtained by querying the Allen Brain Atlas API (atlas ID: eq602630314)[69].

## Whole brain clearing, imaging and analysis

Whole brain clearing was performed on a subset of 10-day monosynaptic tracing experiments based on the pre-labeling paradigm. An optimized protocol (U.Clear, Wang et. al. manuscript in submission) based on the Adipo-Clear platform[70] was used to process the brains. PFA-fixed brains were washed with PBS and delipidated with several washes (1 hour, 2 hours, 4 hours, overnight, and 1 day × 5) of SBiP buffer (200 μM $Na_2HPO_4$, 0.08% sodium dodecyl sulfate, 16% 2-methyl-2-butanol, 8% 2-propanol in $H_2O$ (pH 7.4)) at room temperature. Brains were then transferred into B1n buffer (0.1% Triton X-100, 2% glycine, 0.01% 10N sodium hydroxide, 0.008% sodium azide in $H_2O$) under nutation at room temperature. The following day, the brains were washed with PTxwH buffer (0.1% Triton X-100, 0.05% Tween-20, 0.002% heparin (w/v), 0.02% sodium azide in PBS) (1 hour, 2 hours, 4 hours, and overnight). The next day, goat anti-GFP (Rockland, 601-101-215, 2 μg/brain) Syto24 green (ThermoFisher Scientific nuclear dye, S7559, 0.5 μl/brain) and rabbit anti-RFP (SICGEN, AB-1140-20, 1.25 μg/brain) diluted in PTxwH buffer were added to brains, and brains were kept at 37°C with gentle rocking for 20 days. Excess antibodies were washed off in 4 washes with PTxwH (1 hour, 2 hours, 4 hours, and overnight). Brains were then incubated with Alexa647-conjugated donkey anti-goat (Jackson Immunoresearch 705-607-003, 15 μg/brain) and Alexa594-conjugated donkey anti-rabbit secondary antibodies (Jackson Immunoresearch 711-587-003, 6.25 μg/brain) and diluted in PTxwH at room temperature with gentle rocking for 20 days and subsequently washed 4 times with PTxwH (1 hour, 2 hours, 4 hours, and overnight). Brains were then fixed (1% PFA) overnight at 4°C, rinsed in PTxwH (RT, 1 hour, 2 hours, 4 hours, and overnight followed by blocking with B1n at RT overnight). Samples were treated with 0.3% $H_2O_2$ (4°C, overnight) and washed in 20 mM PB (16 mM $Na_2HPO_4$, 4 mM $NaH_2PO_4$ in $H_2O$, RT, 2 hours). Additional delipidation was performed (SBiP, RT, 1 hour, 2 hours, 4 hours, overnight) followed by an extended delipidation (RT, 18 days). Subsequently, the brains were rinsed in 20 mM PB (RT, 2 hours, 4 hours) followed by washing with PTS solution (25% 2,2'-thiodiethanol/10 mM PB, RT, 3 hours, overnight). Brains were equilibrated with 75% Histodenz (Cosmo Bio USA AXS-1002424) and refractive index (RI – 1.53) matched using 2,2'-thiodiethanol. Samples were stored at −20°C until imaging. Imaging was performed using a light-sheet microscope (SmartSPIM, LifeCanvas Technologies). Syto24 nuclear dye, RFP and GFP immunohistochemistry were imaged using a 3.6x/0.2 detection lens and lasers at 514/561/639 nm. Lightsheet illumination was focused with a NA 0.2 lens, and axially scanned with an electrically tunable lens coupled to the camera (Hamamatsu Orca Back-Thin Fusion) in slit mode. Camera exposure was set at fast mode (2 ms) with 16b imaging. The *X*/*Y* sampling rate was 1.8 μm and *Z* step at 2 μm. The Maximum

Intensity Projection (MIP) images (Fig. 1e) were created by integrating the entire imaged 3D volume into a single 2D image on the XY plane. The serial MIP sections were produced by integrating a span of every 500μm in Z (250 Z optical planes) into a single 2D image (Extended Data Fig. 4i). Original image volumes at (1.8 × 1.8 × 2.0 $\mu m^3$/voxel resolution) were down sampled to 7.2 × 7.2 × 8.0 $\mu m^3$/voxel using the Igneous software (https://doi.org/10.3389/fncir.2022.977700, version 4.20.3, https://github.com/seung-lab/igneous) by averaging the original-resolution raw voxels ("average pooling"), and 3D renderings were produced using Imaris (v9.0, Bitplane) (Supplementary Video 1).

## Neural progenitor cell transplantation

To express the RTG helper proteins in NPCs, 200,000 cells were mixed with 100 μL of polybrene-treated retrovirus in 100 μL of F3 medium in an Eppendorf tube for 1 hour at 37°C. Cells were then seeded on six-well plates pre-coated with 1% Matrigel. After 24 hours, the medium was completely replaced with fresh F3 medium. DsRed expression could be observed under a fluorescence microscope by 5 days following retroviral infection. To pre-infect NPCs for monosynaptic tracing, 500,000 cells were infected overnight with 3 μL ΔG rabies virus in 1 mL medium in a 6-well plate. The next day, NPCs were detached with Accutase, washed 3X in DPBS, and resuspended in Hibernate-A for transplantation into the RSP as described above at 200,000 cells per mouse.

## GBO calcium imaging and analysis

To examine spontaneous $Ca^{2+}$ transient dynamics in GBOs, organoids were seeded on ALI cultures as described above for at least 24 hours before imaging. This allowed for the basal surface of the GBO to become relatively more flattened, making structures more amenable to live imaging in a single *z*-plane. Prior to imaging, 20 μL of 1 μM Fluo-4 AM (ThermoFisher Scientific, F14021) in GBO medium was added to each GBO at the ALI surface for at least 30 minutes. Live imaging was performed on a confocal microscope (Zeiss LSM 710) equipped with an enclosure maintaining samples at 37°C with 5% $CO_2$. Each organoid was imaged at 2 Hz with the 20X objective for either 5 or 10 minutes. Following baseline recordings, 20 μL of GBO medium containing 1 mM ACh with or without a combination of the M3 muscarinic receptor antagonist 4-DAMP (100 μM) and pan-nicotinic receptor antagonist mecamylamine (100 μM, Abcam, ab120459) was added to each GBO at the ALI surface 30 minutes prior to imaging with the same conditions. Liquid at the ALI surface typically dissipated by 5 minutes after addition.

Recordings were exported as .CZI files from Zen 2 software and imported to ImageJ/FIJI for further analysis. For each organoid recording, motion artifacts were corrected with the Linear Stack Alignment with SIFT function with default parameters as necessary. Cells were then segmented by first performing a *z*-projection with 'Average Intensity' settings and then drawing individual ROIs for all cells in a 200 $\mu m^2$ region for UP-10072 (and in a 300 $\mu m^2$ region for UP-9096 and UP-9121). Intensity traces over time for individual cells were exported as .xlsx files and imported into R for analysis. To generate dF/F traces, we used the same method as above for slice $Ca^{2+}$ imaging but with a 100-frame moving window. Traces were smoothed twice (triangular moving average) using a 5-frame window, and peaks were

called using the findpeaks function in R with nups = 5, ndowns = 5, and minpeakdistance = 5.

To evaluate the immediate $Ca^{2+}$ response of GBOs to ACh stimulation, GBOs were reaggregated into 2500 cells overnight as described above and seeded onto a Matrigel-coated 24-well plate (1:60 v/v in DMEM:F12) for at least 1 hour prior to imaging to ensure organoid adherence to the plate surface. 30 minutes before imaging, Fluo-4 AM was added to the medium to a final concentration of 1 μM. Each organoid was imaged at 2 Hz with the 20X objective on a confocal microscope as described above for 3 minutes, with ACh added to a final concentration of 1 mM at approximately the 1-minute timepoint. For antagonist experiments, either 4-DAMP or mecamylamine was added for at least 10 minutes to a final concentration of 100 μM before imaging and ACh stimulation. Like the $Ca^{2+}$ transient analyses, recordings were exported from Zen 2, imported to ImageJ/FIJI, and motion artifacts were corrected as necessary. Individual ROIs were drawn, and intensity traces were analyzed in R. To generate dF/F traces, we used the same method as above for slice $Ca^{2+}$ imaging, but the baseline intensity was computed as the mean intensity of 20 frames prior to ACh stimulation. Traces were smoothed twice (triangular moving average) using a 5-frame window, and $\Delta dF/F_{max}$ was defined as the change in dF/F between the maximum and minimum intensity values across the entire trace. For evaluation of responses of GBOs expressing hM3Dq-mCherry to CNO, calcium imaging was performed as above but with the addition of CNO (Tocris, 4639) to a final concentration of 20 μM or an equivalent volume of 0.9% normal saline (VWR, 76423–606).

### Immuno-electron microscopy

For electron microscopy experiments, a mixture of 600–800 nL AAVs (composed of a mix of 1:20 AAV2/9-ChAT-Cre-WPRE-hGHpA and Cre-dependent AAV2/9-hSyn-DIO-Synaptophysin-EGFP-WPRE-hGHpA) was injected in the basal forebrain. During the same surgery, UP-10072 GBO-RTG cells were transplanted into the dorsal hippocampus. At three weeks post-surgery, mice were perfused with 4% PFA and 0.5% glutaraldehyde (16210, Electron Microscopy Sciences) in PBS overnight. Brain sections were sliced via vibratome at 50 μm thickness. Sections were permeabilized and blocked in PBS with 0.5% BSA and 0.1% Triton-X 100 for 1 hour and subsequently incubated with anti-GFP (1:500; Abcam, ab5450) and anti-mCherry (1:500; Abcam, ab167453) at 4°C for two nights. After a PBS wash, sections were incubated with Nanogold-Fab' Goat anti-Rabbit antibody (1:200; Nanoprobes, #2004) for 2 hours and further fixed with 1% glutaraldehyde for 10 minutes. Immunogold-silver enhancement procedure was performed according to manufacturer's instructions (Nanoprobes, HQ Silver, #2012). Sections were washed in PBS and incubated with Goat-HRP secondary antibody (1:500; Abcam, ab6885) for 1.5 hours and then washed with PBS following by 3,3'-diaminobenzidine (DAB) precipitation for 10 minutes. After an $H_2O$ wash, the sections were further postfixed with 0.1% $OsO_4$ for 15 minutes and then with 0.2% uranyl acetate at 4°C overnight. They were then dehydrated in a graded alcohol series. Next, the sections were infiltrated with Epon (EMS, #14120) series from 10% to 100% for a total of two days, and then incubated in 100% Epon with catalyst in a 60°C oven for 48 hours. Finally, sections were cut into 70 nm thin sections via ultramicrotome for transmission electron microscopy (TEM) imaging (Thermo Scientific Talos L120C).

### Slice calcium imaging and analysis

UP-10072 GBOs expressing jRGECO1a were generated using lentiviruses with procedures as described above. A mixture of 600–800 nL AAVs (composed of a mix of 1:20 AAV2/9-ChAT-Cre-WPRE-hGHpA and Cre-dependent AAV9-EF1a-DIO-hChR2(H134R)-EYFP-WPRE-hGHpA) was injected in the basal forebrain. During the same surgery, UP-10072 GBO-jRGECO1a cells were transplanted into the dorsal hippocampus. At six weeks post-surgery, acute slices were prepared as described above for patch-clamp recordings. Live $Ca^{2+}$ imaging was performed with a confocal microscope (Zeiss LSM 710) on a 10X objective by acquiring images at 2 Hz in the 555 nm wavelength channel. Light pulses for optogenetic stimulation of local cholinergic axon terminals were delivered by a laser (LRD-0470-PFFD-00100-05) with 470 nm wavelength (~0.32 $mW/mm^2$ power) connected to a power supply (PSU-H-LED), with pulse length and frequency set by a programmable pulse generator (Master 8). Simultaneous $Ca^{2+}$ imaging and optogenetic stimulation (10 ms pulses at 20 Hz for 10 seconds) were performed with or without the presence of 100 μM 4-DAMP in oxygenated aCSF. For a given slice, an inter-stimulus interval of at least 5 minutes was maintained.

$Ca^{2+}$ imaging recordings were exported as .CZI files with Zen 2 software and imported to ImageJ/FIJI for quantification. Analysis was performed on GBM cells that consistently exhibited $Ca^{2+}$ transients in response to optogenetic stimulation. To generate the dF/F traces, we first generated the baseline intensity trace by computing the tenth percentile of a moving 50-frame window of each raw trace using the rollapply function in R. The dF/F trace was then defined as the (raw intensity – baseline intensity)/(baseline intensity) at each timepoint. The trace was then smoothed twice (triangular moving average) using a 7-frame window. We defined $\Delta dF/F_{max}$ as the maximum change in dF/F between the mean dF/F in a 10-second window prior to light stimulation compared to maximal dF/F.

### Patch-clamp electrophysiological recordings

For electrophysiology experiments, a mixture of 600–800 nL AAVs (composed of a mix of 1:20 AAV2/9-ChAT-Cre-WPRE-hGHpA and Cre-dependent AAV9-EF1a-DIO-hChR2(H134R)-EYFP-WPRE-hGHpA) was injected in the basal forebrain. During the same surgery, UP-10072 GBO-RTG cells were transplanted into the dorsal hippocampus. Acute slices were prepared from these animals six weeks later as previously described[71]. In brief, brains were harvested and placed immediately in ice-cold cutting solution (92 mM *N*-methyl-D-glucamine, 2.5 mM KCl, 1.2 mM $NaH_2PO_4$, 30 mM $NaHCO_3$, 20 mM HEPES, 25 mM glucose, 5 mM sodium L-ascorbate, 2 mM thiourea, 3 mM sodium pyruvate, 10 mM $MgSO_4$ and 0.5 mM $CaCl_2$) and continuously bubbled with 95% $O_2$ and 5% $CO_2$. 200 μm-thick coronal sections were cut with a vibratome (Leica VT 1200S) and placed in aCSF (126 mM NaCl, 2.5 mM KCl, 1.2 mM $MgSO_4$, 2.4 mM $CaCl_2$, 25 mM $NaHCO_3$, 1.4 mM $NaH_2PO_4$, 11 mM glucose and 0.6 mM sodium L-ascorbate) and continuously bubbled with 95% $O_2$ and 5% $CO_2$. Slices were incubated at 31°C for 30 minutes and then at room temperature for 30 minutes.

Brain slices were transferred into a recording chamber and perfused with oxygenated aCSF that additionally contained 200 μM 4-AP (Sigma Aldrich, A78403) and 25 μM CNQX

(Tocris, 0190). DsRed$^+$ GBM cells were located via a 40X water-immersion objective (Olympus BX61WI). Because of the diffusely infiltrative nature of the cells, at 6 weeks post transplantation, GBM cells could be observed in cortical, hippocampal, and subcortical regions. Recording pipettes were generated from borosilicate glass (Flaming-Brown puller, Sutter Instruments, P-97, tip resistance of 5–10 MΩ) and were filled with pipette solution consisting of 120 mM potassium gluconate, 10 mM NaCl, 1 mM $CaCl_2$, 10 mM EGTA, 10 mM HEPES, 5 mM Mg-ATP, 0.5 mM Na-GTP and 10 mM phosphocreatine. Whole-cell patch clamp recordings were controlled via an EPC-10 amplifier and Pulse v8.74 (HEKA Electronik). To generate the current-voltage curves, whole-cell patch clamp recordings were conducted in both current-clamp and voltage-clamp modes. In voltage-clamp mode, cells were held at −60/−70 mV, and a series of voltage pulses were applied in 10 mV steps for 50–100 milliseconds every 5 seconds. In current-clamp mode, current was injected to maintain the cell at a holding potential of −70 mV, and a series of current injections were applied for 1000 milliseconds in 10 pA steps (starting at −20 pA) every 5 seconds. The input resistance was calculated as the slope of the current-voltage (I-V) curve from a voltage-clamp recording (13 steps from −120 mV with 10 mV increments). The resting membrane potential was determined in current-clamp mode when no current was injected. For dye-filling experiments, Alexa Fluor 488 (10 μM, ThermoFisher Scientific, A10436) was included in the pipette solution, and slices were fixed with 4% PFA for 15 minutes prior to mounting and imaging on a confocal microscope (Zeiss LSM 810).

For optogenetic stimulation of cholinergic fibers, a train of 10 ms pulses at 20 Hz for 10 seconds was delivered via blue light stimulation (pE-300ultra, CoolLED) through the 40X objective. For current-clamp recordings, holding current was not adjusted during the experiment and was 0 pA. CHRM3 receptor blockade was achieved by bath perfusion of aCSF consisting additionally of 100 μM 4-DAMP (Santa Cruz, sc-200167). Data were exported as raw traces in ACS file format using PulseFit (HEKA Electronik) and imported into R (v4.3.1) for analysis. For analysis of maximum membrane depolarization from baseline for current-clamp traces, data were first smoothed twice using a 5-second window. Light-induced depolarization was quantified as the difference between the mean baseline voltage prior to stimulation and the maximum voltage value in the 20 seconds following the start of stimulation. Latency time between the beginning of stimulation and the beginning of the response was estimated by determining the first timepoint at which the membrane potential reached baseline + 2$\sigma$, where the standard deviation $\sigma$ is computed based on the values recorded in the 5 seconds prior to stimulation.

### GBO migration assays

GBOs were reaggregated as described above at 2000 cells per well in a U-bottom 96 well plate for at least 24 hours prior to the assay. 6-well plates were coated with Matrigel (1:60 v/v in DMEM:F12), and 6–8 reaggregated GBOs were seeded in 2 mL of GBO culture medium per well. Treatments (to a final concentration of 1 mM ACh and/or 100 μM 4-DAMP in GBO culture medium) were added to the wells 4 hours after seeding to ensure that GBO adhesion was not affected. For experiments with CHRM3 knockdown GBOs, only ACh was added. Images were collected using an inverted phase contrast microscope (Axiovert 40 CFL) and Zen 2 software. The area covered by GBO cells after 48 hours was

measured by using the 'oval' ROI function in ImageJ/FIJI to draw the largest bounding oval that captured the migrating cells. Organoids that landed too closely to each other in the 6-well plate were excluded from analyses. For migration assays with chemogenetic activation of tumor cells, a similar procedure was performed but with UP-10072 GBOs expressing hM3Dq-mCherry and a treatment of 20 μM CNO (or an equivalent volume of 0.9% normal saline).

For live imaging experiments with assembloids, GBOs expressing RTG were fused with SNOs, and a subset of GBOs were pre-treated for 1-hour with 1 mM ACh in GBO medium. At 12–24 hours post fusion, assembloids were taken for live imaging on a confocal microscope (Zeiss LSM 710) for 10–20 hours, with fluorescent images taken every 10 minutes. We focused on GBM cells at the leading edge of assembloids for migration analyses. Speed (in μm/hr) and displacement (in μm/hr from the original cell location) were obtained by the 'Manual Tracking' plugin in ImageJ/FIJI. Live imaging assays and analyses for adult human surgical brain slices and acute mouse brain slices with ACh activation or CHRM3 knockdown as described below were performed similarly. For mouse brain slices, GBOs were transplanted into the dorsal hippocampus for 2–3 weeks prior to slice generation as described above. For ACh stimulation, slices were transferred to ALI culture and directly treated with 1 mM ACh in brain-tissue medium prior to imaging.

### Chemogenetic activation of GBOs *in vivo*

To assess whether GPCR-mediated membrane depolarization could increase the GBM cell area of distribution *in vivo*, UP-10072 GBOs expressing hM3Dq-mCherry[72], generated via a reaggregation procedure as described above, were transplanted into the dorsal hippocampus (~200,000 cells per mouse). 5 days after transplantation, mice received CNO (40 μg/mL) or an equivalent volume of 0.9% normal saline via drinking water supplemented with 1% sucrose until 3 weeks post transplantation, at which point mice were sacrificed for immunohistology. To quantify relative area of distribution, the 'polygon' tool in ImageJ/FIJI was used to draw the largest bounding polygon that captured the $mCherry^+$ cells. For each mouse, 3–5 consecutive sections in a single stack (composed of every $6^{th}$ brain section) were quantified and averaged. If any sections included a clear needle track, care was taken that the portion within the cortex was not considered part of the tumor area.

### CHRM3 shRNA knockdown analyses

GBO cells were infected with lentivirus expressing mCherry and either CHRM3 shRNA or scrambled shRNA following a reaggregation procedure as described above. Knockdown was validated by qPCR after 72 hours. RNA was first extracted using Trizol reagent (Thermo Fisher Scientific, 15–596-026) and RNA microprep kits (Zymo Research, R2062) according to manufacturer's instructions. RNA concentration was quantified by Nanodrop (ThermoFisher Scientific, ND-2000), and 100 ng RNA was taken for reverse transcription and cDNA synthesis, which were performed using the Superscript IV First-Strand Synthesis System (ThermoFisher Scientific, 18091050) based on manufacturer's instructions. qPCR was performed with 2 μL of cDNA, 6.25 μL of SYBR Green Master Mix (ThermoFisher Scientific, 4385612), 0.5 μL of 10 μM forward primer, 0.5 μL of 10 μM reverse primer, and 3.25 μL of nuclease-free water with the following thermocycling conditions: 95°C for 30

seconds, and 40 cycles of 95°C for 15 seconds and then 60°C for 45 seconds. Expression of CHRM3 was normalized to GAPDH based on the mean of three technical replicates by the $\Delta C_t$ method. Primers used are detailed in Supplementary Table 2.

To determine the size of GBOs following CHRM3 knockdown, GBO cells were infected with CHRM3 shRNA or control scrambled shRNA lentiviruses and reaggregated as described above into organoids of 2000 cells each. After 7 days, GBOs were imaged using an inverted phase contrast microscope (Axiovert 40 CFL) and Zen 2 software, and the organoid area in a single *z*-plane was quantified using the 'polygon' ROI function in ImageJ/FIJI.

For quantification of Ki67 proportion and cCas3 intensity following CHRM3 knockdown, GBOs were collected after 7 days for whole-mount immunostaining as described above. To quantify the percentage of $Ki67^+$ cells, for each organoid, the number of $Ki67^+/DAPI^+$ nuclei was determined for 40–60 randomly chosen $DAPI^+$ nuclei. To quantify relative levels of cCas3, for each organoid, the DAPI channel image was first used to outline the perimeter of the organoid by setting a low manual threshold combined with the Analyze Particles function with size 5,000 to Infinity. Within the ROI marked by the DAPI perimeter, the mean grey value intensity for the cCas3 channel was then recorded.

For *in vivo* transplantation of GBOs with CHRM3 knockdown, we transplanted equivalent numbers (~100,000) of tumor cells into either the left or right hemispheres for each mouse, with shCHRM3 cells in the right and shScramble controls on the left, following procedures described above. Mice were sacrificed after 3 weeks, and brains were sectioned for immunostaining of mCherry and quantification of the area of distribution as described above.

For mouse survival analyses, either tumor cells expressing shRNA against CHRM3 or scrambled shRNA (~100,000 cells) were transplanted, and mice were continuously monitored for signs of symptoms denoting the IACUC approved endpoint. Mice were euthanized if any of the following criteria were met: a body condition score[73] (BCS) of 1; a BCS of 2 in addition to hunched posture, inactivity, ruffled haircoat, or dehydration; weight loss of > 20%; or severe neurologic dysfunction such as an inability to ambulate. Dates of death were recorded for Kaplan-Meier statistical analyses.

### Analysis of patient survival from public databases

We queried the public GBM database GlioVis[74] (http://gliovis.bioinfo.cnio.es) to access both gene expression and patient phenotypic data for The Cancer Genome Atlas (TCGA) GBM[75] (HG-UG133A) and Chinese Glioma Genome Atlas (CGGA)[76] datasets. The CGGA dataset was filtered to only include histology consistent with GBM. A gene signature score for ACh response (either fast or long-lasting, Supplementary Table 5) was calculated with the GSVA[77] package in R with method = 'gsva', and the score was used as an input to the function surv_cutpoint as implemented in the survminer package in R to determine the optimal cutoff for high versus low expression using maximally selected rank statistics.

## Statistics

Statistical analyses were performed in R (v4.3.1) via base R or with the rstatix package, with specific tests, sample sizes, and *P*-values indicated in figure legends or within figures. For quantifications of multiple cells across different organoids, a linear mixed-effects model (LMM) fit was performed by maximum likelihood with organoid number as a random variable as described in[78]. All data are shown as mean ± s.e.m., including for bar plots and for numerical values in the main text. In all box plots, unless otherwise indicated in the legends, the center line represents median, the box edges show the 25$^{th}$ and 75$^{th}$ percentiles, and whiskers extend to maximum and minimum values. No statistical methods were used to predetermine sample sizes. Quantifications of migration areas and organoid immunohistology were performed blinded by two independent investigators. $P < 0.05$ was considered to be statistically significant.

## Reporting Summary

Further information on research design is available in the Nature Research Reporting Summary linked to this paper.

## Extended Data

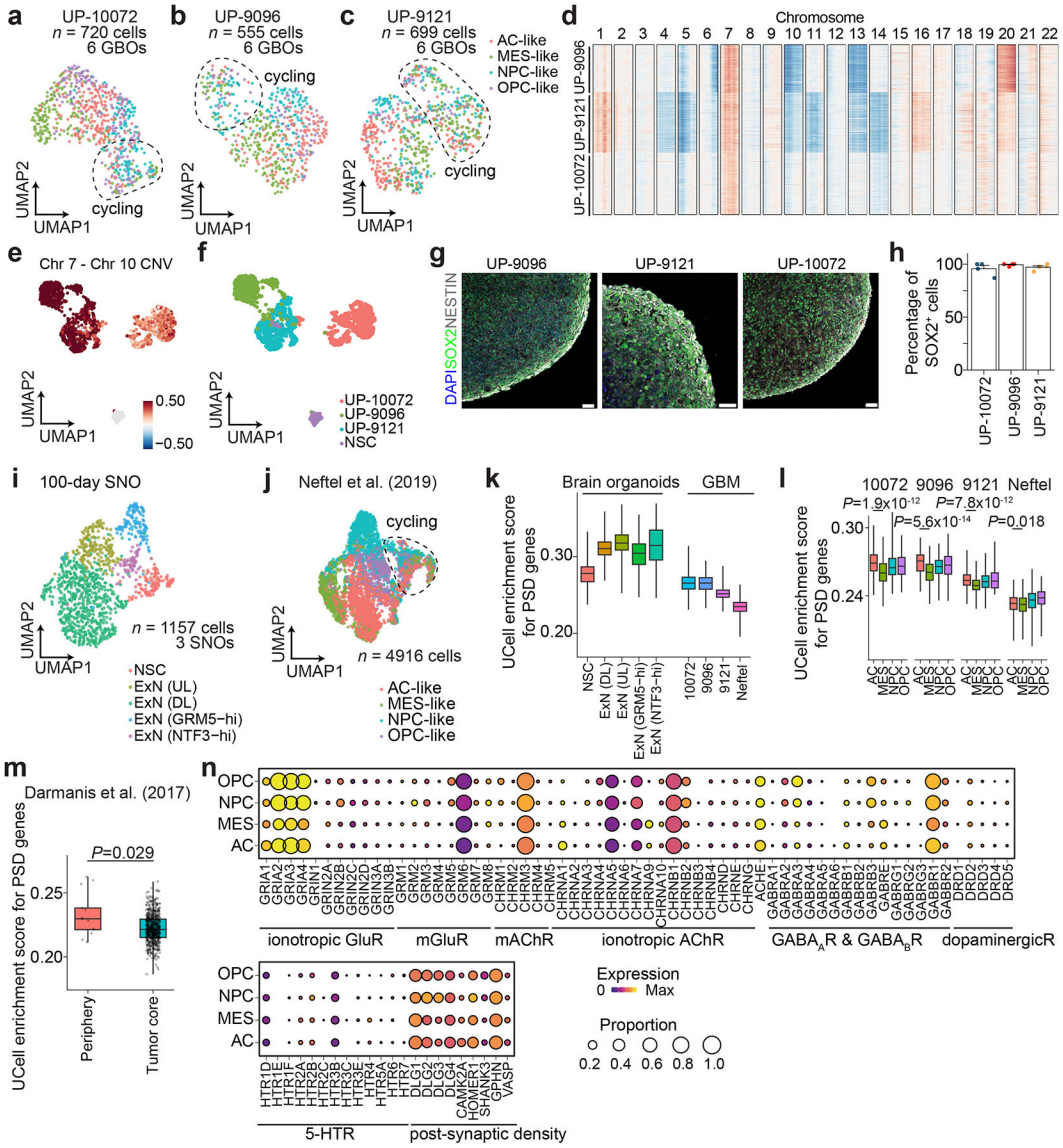


**Extended Data Fig. 1. Synaptic gene enrichment in IDH-wt GBM and GBOs.**

**a-c**, Uniform manifold approximation and projection (UMAP) plots of scRNAseq data from UP-10072 GBOs (**a**, mean 5,525 genes per cell), UP-9096 GBOs (**b**, mean 6,153 genes per cell), and UP-9121 GBOs (**c**, mean 6,937 genes per cell). Cells are colored by assigned cell state via marker genes defined by Neftel et al[8]. Circled clusters represent cycling cells as determined by MKI67 expression. AC, astrocyte; MES, mesenchymal; NPC, neural progenitor cell; OPC, oligodendrocyte progenitor cell. **d**, Copy number aberration (CNA) analysis of UP-10072, UP-9121, and UP-9096 scRNAseq data from **a – c**. **e – f**, UMAP plots of UP-10072, UP-9121, UP-9096, and neural stem cells (NSC, **i**), colored by either Chr7 minus Chr10 CNV level (**e**) or cell identity (**f**). **g**, Representative confocal images of UP-9096 GBOs, UP-9121 GBOs, and UP-10072 GBOs. Scale bars, 50 μm. **h**, Quantification of percentages of DAPI$^+$ cells that were SOX2$^+$ ($n$ = 3 patients, $n$ = 4 GBOs per patient).

**i**, UMAP plot of 100-day human SNOs, colored by cluster identity. ExN, excitatory neuron; UL, upper layer; DL, deeper layer. **j**, Same as **a-c** but for Neftel et al.[8] adult primary GBM. **k**, Plot of enrichment scores of post-synaptic density genes (GO: 0014069)[24] across SNO-derived nonmalignant clusters versus glioma. **l**, Same as **k** but for glioma datasets split by cell state. **m**, Same as **k** but for enrichment by location (periphery versus tumor core) with the Darmanis et al.[18] dataset ($n$ = 665 cells). **n**, Gene expression dot plot as in Fig. 1a, but comparing between states for the Neftel et al.[8] dataset. Comparisons in **l**, **m** with two-tailed Mann-Whitney tests.

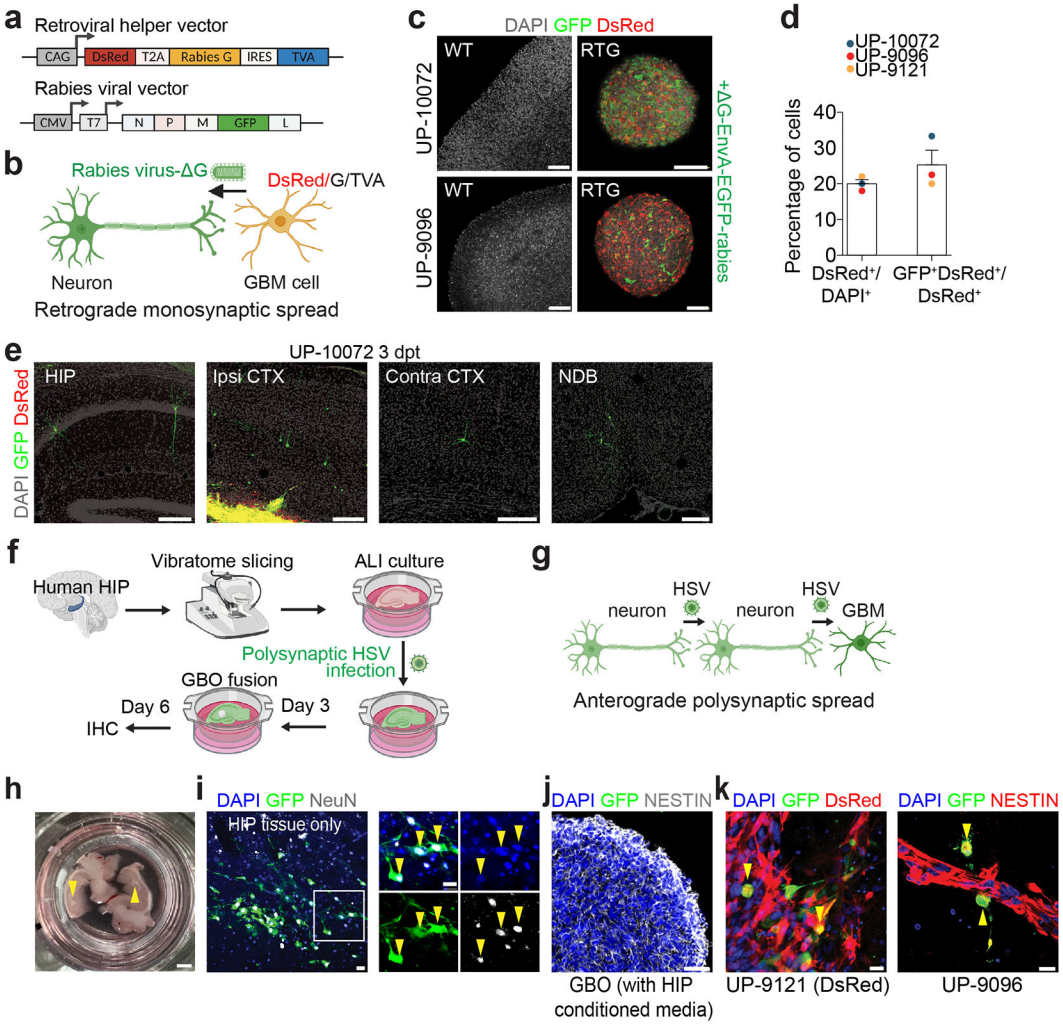


**Extended Data Fig. 2. Virus-based trans-monosynaptic tracing with GBOs.**

**a**, Schematic illustrations of the retroviral helper and EnvA-pseudotyped ΔG rabies virus vector. **b**, Principle of rabies virus spread. **c**, Control experiments to establish specificity of rabies virus towards infecting GBO cells expressing TVA. Nontransduced (WT, wild-type) GBOs and GBOs expressing DsRed-G-TVA were infected with ΔG rabies virus for 5 days. Nontransduced GBOs were unable to be infected by ΔG rabies virus. Scale bars, 50 μm. **d**, Quantification of percentages of cells infected by the helper retrovirus ($DsRed^+$/$DAPI^+$) and percentages of $DsRed^+$ tumor cells infected by ΔG rabies virus after 5 days

(GFP$^+$DsRed$^+$/DsRed$^+$) ($n$ = 3 GBOs from $n$ = 3 patients). **e**, Representative confocal images of monosynaptic labeling of neurons 3 dpt of pre-labeled UP-10072 GBM cells (representative of $n$ = 3 mice). Scale bars, 200 μm. **f – g,** Schematic illustrations of paradigm (**f**) to perform HSV-based polysynaptic anterograde tracing (**g**) with GBOs and freshly resected human hippocampal tissue in culture. **h**, Representative image of the fusion of GBOs with hippocampal tissues. Yellow arrow denotes fused GBO. Scale bar, 4 mm. **i**, Representative confocal image showing infection of NeuN$^+$ neurons in human hippocampal tissue by HSV, resulting in GFP expression. Yellow arrow denotes infected neuron (representative of hippocampal tissue from $n$ = 3 patients). Scale bar, 20 μm. **j**, Control experiments showing no direct infection of GBM cells by HSV from culture medium of infected slices. Conditioned media from slices 24 hours after medium refresh (4 days since initial infection) were added to UP-10072 GBOs for 3 days, then fixed for immunohistology and confocal imaging ($n$ = 6 GBOs). Scale bars, 50 μm. **k**, Representative images of tumor cells infected by HSV 3 days after fusion with human hippocampal tissues ($n$ = 2 samples). Scale bars, 20 μm.

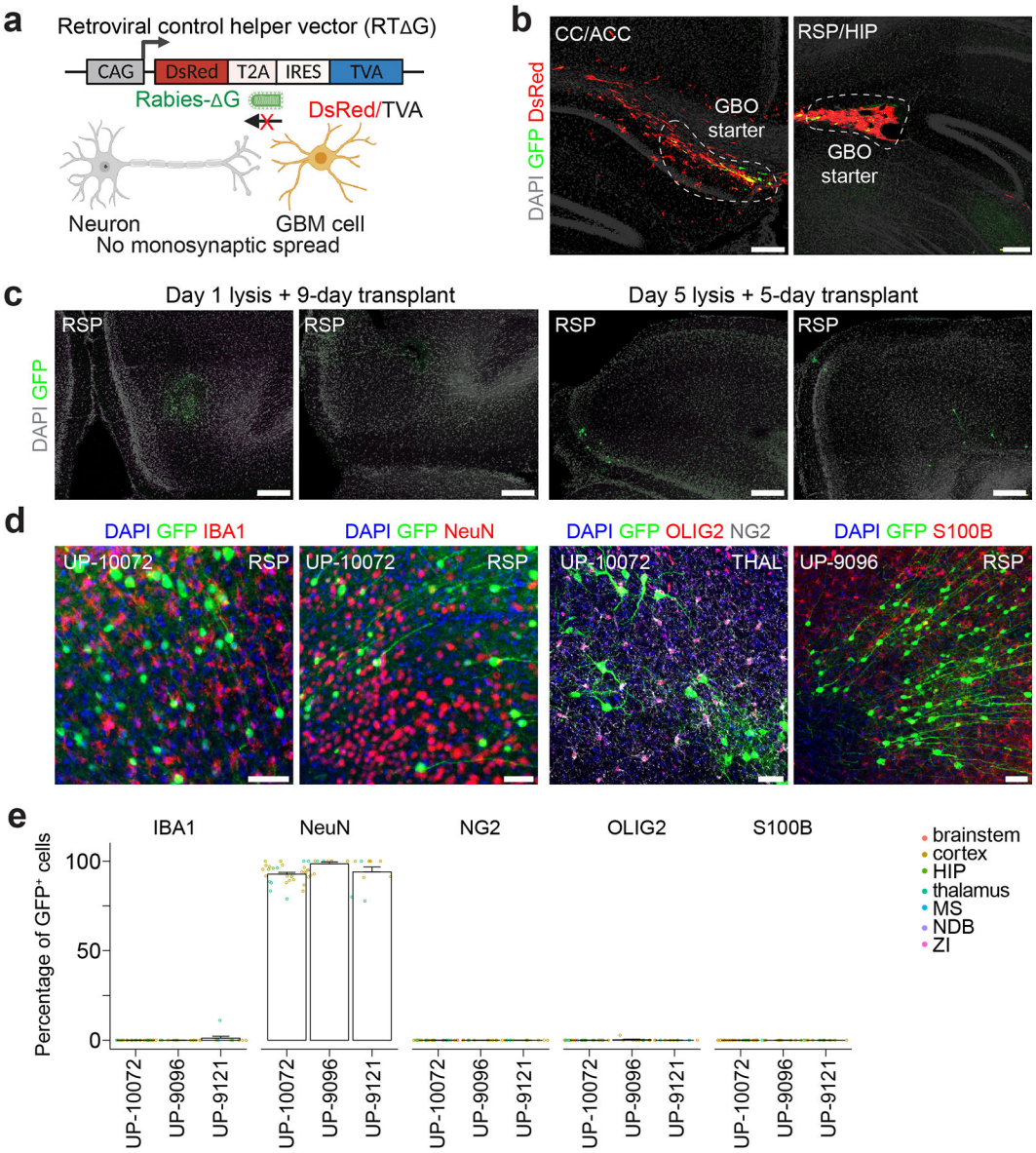


**Extended Data Fig. 3. Selectivity and specificity of rabies virus transmission in GBOs.**

**a** – **b**, Schematic (**a**) and representative confocal images (**b**) of a control helper vector with deletion of the G protein, thus preventing G protein-mediated transsynaptic rabies virus transmission. UP-10072 GBO cells expressing DsRed-TVA were pre-infected with ΔG rabies and transplanted into the RSP for 10 days, with no evidence of $GFP^+$ neurons ($n = 4$ mice) (**b**). Scale bars, 200 μm. **c**, Representative confocal images from control experiments showing that release of rabies virus from infected GBO cells is not a mechanism of mouse neuronal labeling ($n = 2$ mice). UP-10072 GBOs ($n = 3$ organoids) expressing DsRed-G-TVA were pre-infected with ΔG rabies virus, lysed after 1 day and subsequently injected into the RSP for 9 days (Day 1 lysis + 9-day transplant). To allow for maximal viral load within GBOs prior to transplantation, the same experiment was repeated with lysis after 5 days and injected into the RSP for 5 days (Day 5 lysis + 5-day transplant). Low numbers of $GFP^+$ mouse neurons were observed in the latter condition, suggesting

successful extraction of infection-competent rabies virus. Scale bars, 200 μm. **d – e**, Sample confocal immunostaining images for IBA1 (microglia), NeuN (neurons), OLIG2 (oligodendrocytes), NG2 (oligodendrocyte precursor cells), and S100B (astrocytes) (**d**) and quantification of proportions of these cells co-labeled with GFP (**e**) to establish selectivity of viral transmission to neurons *in vivo.* Scale bars, 50 μm. Each dot represents a separate section from $n = 4$ mice including $n = 3$ pre-labeling experiments with $n = 3$ patients and $n = 1$ long-term experiment with UP-10072.

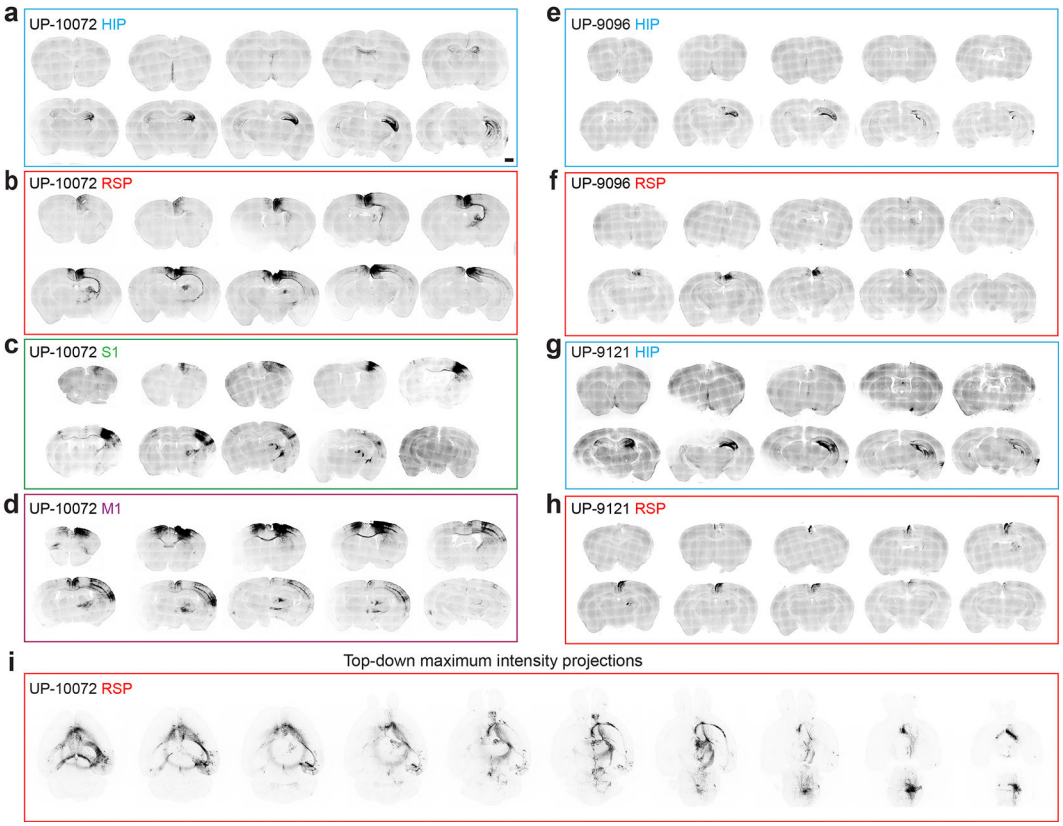


**Extended Data Fig. 4. Representative brain sections across GBO transplantation sites.**

**a – h**, Confocal brain section images of $GFP^+$ cells following transplantation of ΔG rabies virus pre-infected GBOs expressing RTG for 10 days. Images are coronal sections and are arranged from anterior to posterior. Sections are arranged by GBO patients: UP-10072 (**a – d**), UP-9096 (**e, f**), UP-9121 (**g, h**). Location of transplantations include hippocampus (HIP) (**a, e, g**), retrosplenial cortex (RSP) (**b, f, h**), primary somatosensory cortex (S1) (**c**), and primary motor cortex (M1) (**d**). Scale bar, 1 mm. **i**, Representative images from whole-brain clearing and light-sheet microscopy of a pre-labeling experiment with injection of UP-10072 into the RSP at 10 dpt for one mouse. Images are presented as top-down maximum intensity projections obtained by collapsing a span of every 500 μm in the *z*-direction in the rostral to caudal direction. Scale bar, 4 mm. See Supplementary Video 1.

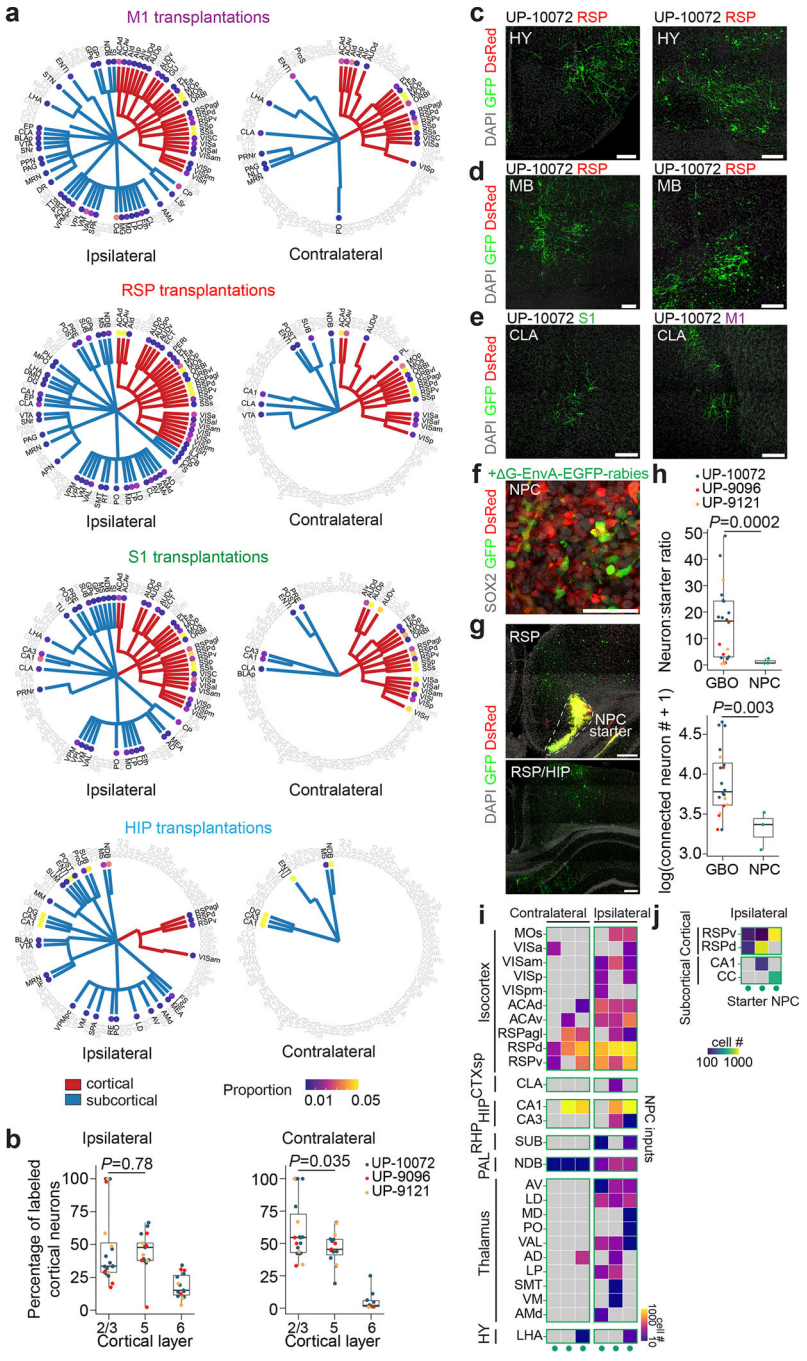


**Extended Data Fig. 5. Additional characterization of monosynaptic projections onto GBM cells and human iPSC-derived NPCs.**

**a**, Dendrogram plots showing relative proportions of input projections across cortical (red) and subcortical (blue) for ipsilateral and contralateral sites averaged across all experiments ($n$ = 20 mice as described in Fig. 2e). **b**, Percentages of input cortical neurons distributed across layers for ipsilateral and contralateral neurons. Each dot represents data from one mouse ($n$ = 20 mice across $n$ = 3 GBOs), and data were plotted only if neurons from that cortical layer were detected. Two-tailed Student's $t$-tests. **c – e**, Representative confocal

images of $GFP^+$ projections onto GBM cells from the hypothalamus (**c**), midbrain (**d**), and claustrum (**e**), each representative of $n = 3$ sections. Scale bars, 200 μm. **f**, Representative confocal images of $SOX2^+$ human iPSC-derived NPCs expressing DsRed-G-TVA infected with ΔG rabies virus for 5 days, representative of $n = 4$ coverslips. Scale bar, 50 μm. **g**, Representative confocal images of monosynaptic tracing with ΔG rabies virus pre-infected NPCs transplanted into the RSP ($n = 3$ mice). Starter cells are circled (left), and images show projections either near (left) or distal (right) to the transplantation site. Scale bars, 200 μm. **h**, Comparison of neuron to starter cell ratio and total labeled neuron number for GBO transplantation ($n = 20$ mice) and NPC transplantation ($n = 3$ mice). Two-tailed Student's *t*-tests with Welch's correction. **i**, Quantification as in Fig. 2e but for the $n = 3$ NPC transplantation experiments across brain regions. **j**, Quantification as in Fig. 2f but for the starter NPC cells from the NPC transplantation experiments.

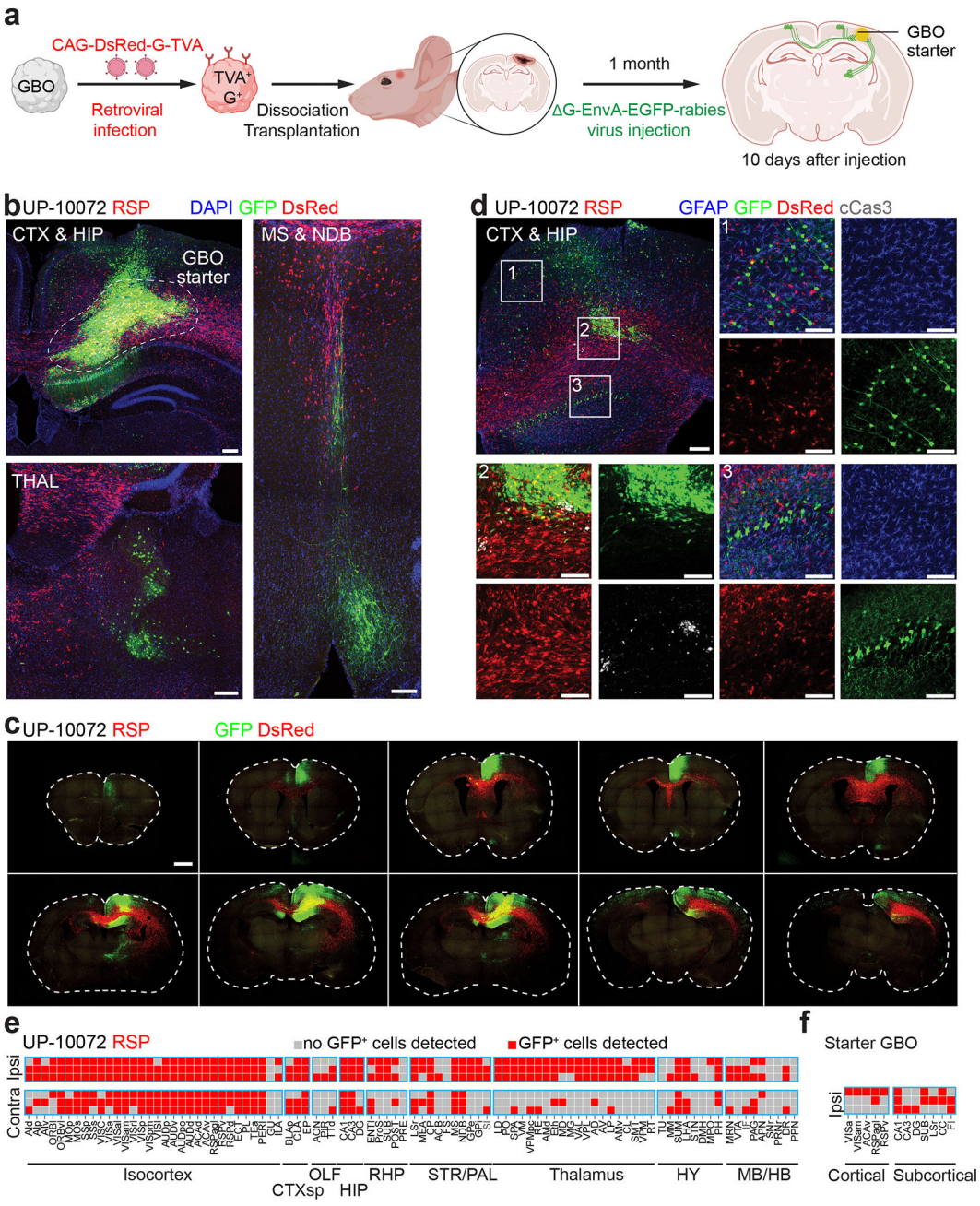


**Extended Data Fig. 6. Trans-monosynaptic tracing following long-term engraftment of GBO cells.**

**a**, Schematic illustration of two-step GBO retrograde trans-monosynaptic tracing. GBOs expressing DsRed-G-TVA were transplanted into the RSP, and ΔG rabies virus was injected one month following engraftment. Mice were examined 10 days following ΔG rabies virus injection ($n$ = 5 mice). **b**, Representative confocal images after trans-monosynaptic tracing, with $GFP^+DsRed^+$ GBM starter cells (circled), $GFP^-DsRed^+$ GBM cells that were unable to transmit rabies virus, and $GFP^+DsRed^-$ upstream neuronal inputs ($n$ = 3 mice). Scale bars, 200 μm. **c**, Representative coronal sections from anterior to posterior. Scale bar, 500 μm. **d**, Sample confocal immunostaining images for glial marker GFAP and apoptosis marker

cleaved caspase 3 (cCas3), with no evidence of glial labeling by rabies virus either proximal (inset 3) or distal (inset 1) to the starter cell site and no evidence of massive cell death of GFP$^+$ GBM cells at this timescale (inset 2). Representative of $n$ = 3 mice. Scale bars, 200 μm (low magnification images) and 50 μm (high magnification images). **e – f,** Qualitative analysis of input neuron (**e**) and starter cell (**f**) locations from the areas in Fig. 2e for $n$ = 3 mice.

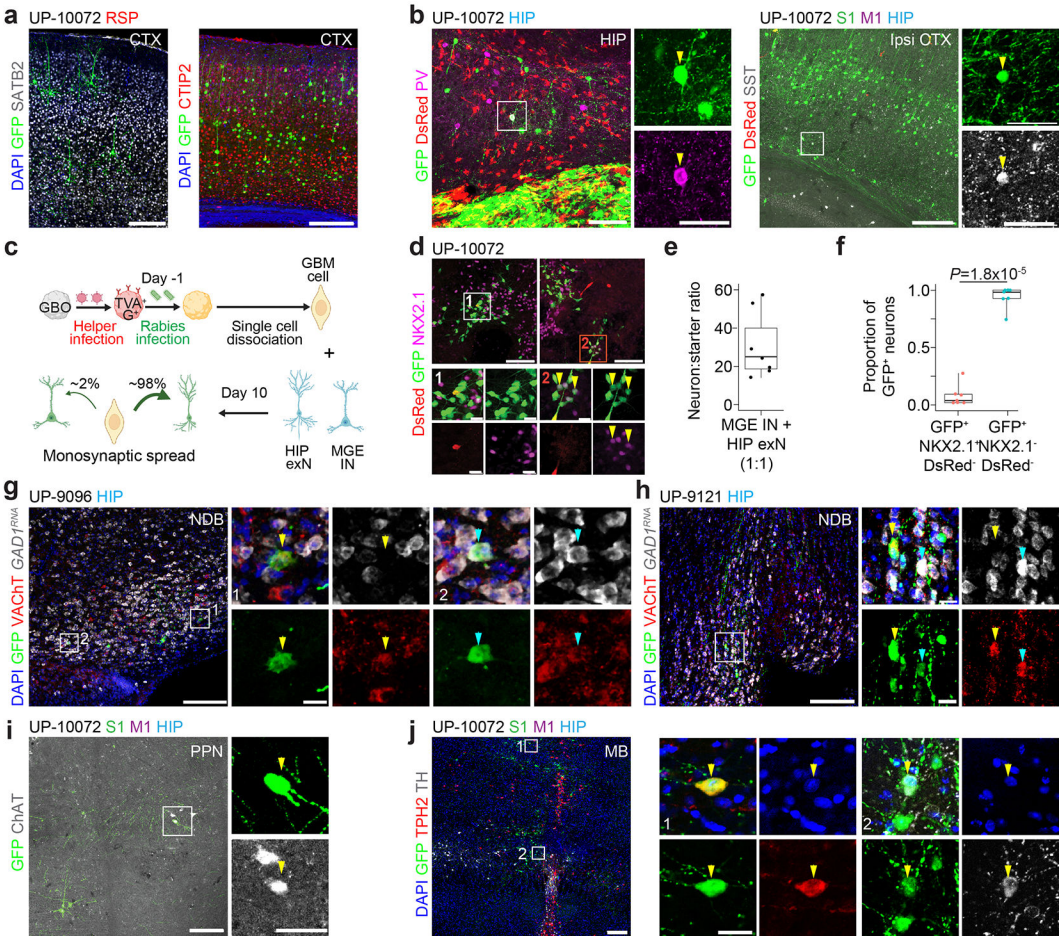


**Extended Data Fig. 7. Additional characterization of input neuron subtype identities upon GBO cell transplantation.**

**a**, Sample confocal images of SATB2$^+$GFP$^+$ and CTIP2$^+$GFP$^+$ cortical glutamatergic neurons that project to GBM cells. **b**, Sample confocal images showing PV$^+$GFP$^+$ (left, hippocampus/HIP) or SST$^+$GFP$^+$ (right, ipsilateral cortex/ipsi CTX) GABAergic neurons. Arrowheads indicate GABAergic neurons. **c**, Schematic illustration of paradigm to perform trans-monosynaptic tracing with 3-week-old 2D iPSC-derived 1:1 mixed glutamatergic and GABAergic neuron-tumor co-culture. **d**, Representative confocal images of 2D co-culture 10 days after seeding of GBM cells. GFP$^+$NKX2.1$^-$ cells denote glutamatergic neurons infected by ΔG rabies, GFP$^+$NKX2.1$^+$ cells denote GABAergic neurons infected by ΔG rabies, and GFP$^+$DsRed$^+$ cells indicate starter GBM cells. Scale bars, 200 μm (large images) and 20 μm (insets). **e**, Quantification of the proportion of GFP$^+$DsRed$^-$ cells in 2D co-culture that were either GABAergic or glutamatergic ($n$ = 7 cultures). IN, interneuron;

MGE, median ganglionic eminence. **f**, Quantification of neuron-starter cell ratio for 2D co-culture ($n$ = 7 cultures). Two-tailed paired $t$-test. **g – i**, Sample confocal images of either VAChT$^+$GFP$^+$ or ChAT$^+$GFP$^+$ cholinergic neurons that projected to GBM cells from either the diagonal band nucleus (NDB) (**g – h**) or pedunculopontine nucleus (PPN) (**i**). For NDB images, RNA *in situ* hybridization for *GAD1* (white) and immunostaining for VAChT and GFP were performed. Arrowheads indicate either VAChT$^+$GAD1$^-$GFP$^+$ or VAChT$^+$GAD1$^+$GFP$^+$ cholinergic neurons of interest. **j**, Sample confocal images showing TPH2$^+$GFP$^+$ serotonergic neurons (inset 1) and TH$^+$GFP$^+$ dopaminergic neurons (inset 2) in the midbrain (MB). For all images, GBOs and corresponding transplantation sites are as indicated. For all scale bars in this figure, 200 μm (low magnification images) and 20 μm (high magnification images). Images in **a – b, g – j** are representative of at least $n$ = 3 mice.

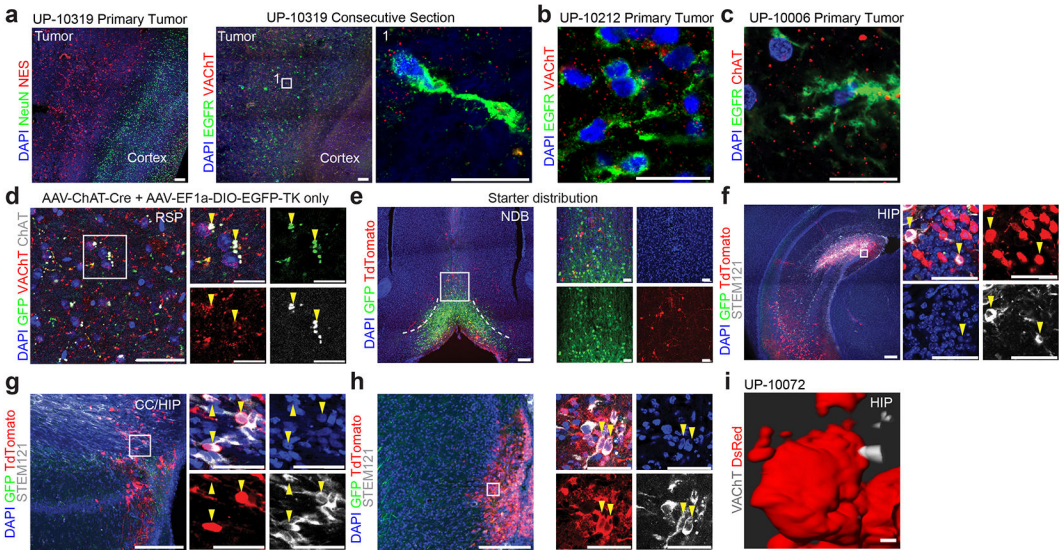


**Extended Data Fig. 8. Additional validation of neuromodulatory cholinergic projections onto GBM cells.**

**a**, Left, confocal images of a primary human GBM sample (UP-10319) immunostained for NeuN$^+$ cortical neurons and NESTIN$^+$ tumor cells, revealing a distinct tumor-cortical boundary. Right, confocal images of a consecutive section with VAChT$^+$ puncta near EGFR$^+$ tumor cells. Scale bars, 200 μm (low magnification) and 20 μm (high magnification). **b – c**, Confocal immunostaining images of human GBM samples (**b**, UP-10212; **c**, UP-10006) with enrichment of either VAChT$^+$ (**b**) or ChAT$^+$ (**c**) puncta near EGFR$^+$ tumor cells. Scale bars, 20 μm. **d**, Representative images of cholinergic axon terminals in the RSP (by VAChT$^+$ and/or ChAT$^+$ expression) 7 days after viral injection to BF. GFP$^+$ puncta co-express VAChT and/or ChAT, confirming Cre-dependent GFP expression of long-range cholinergic neurons. Arrowheads indicate examples GFP$^+$ cholinergic puncta. Scale bars, 50 μm (low magnification) and 20 μm (high magnification). BF: basal forebrain. **e**, Representative images to confirm monosynaptic HSV infection of starter neurons in BF. A mixture of H129-LSL-ΔTK-tdTomato, AAV-ChAT-Cre and AAV-EF1a-DIO-EGFP-TK was injected into the BF, and immunostaining 6 days post infection revealed GFP$^+$tdTomato$^+$ starter cells. Scale bars, 200 μm (low magnification) and 20 μm (high magnification). **f – h**, Representative images of postsynaptic GBM cells infected by monosynaptic HSV

(tdTomato) in the HIP (**f**), the CC/HIP boundary (**g**), and the RSP (**h**). Arrowheads indicate tdTomato$^{+}$STEM121$^{+}$ GBM cells. Scale bars, 200 μm (low magnification) and 20 μm (high magnification). **i**, Confocal image of a 3D-reconstructed, tdTomato$^{+}$ GBM cell in the HIP with VAChT$^{+}$ cholinergic presynaptic boutons in proximity from experiments in **f**. Scale bar, 1 μm. Representative images in **a – c** are derived from primary tissue from $n = 1$ patient each; images from **d – e** are from $n = 3$ mice; images from **f – h** represent $n = 3$ mice.

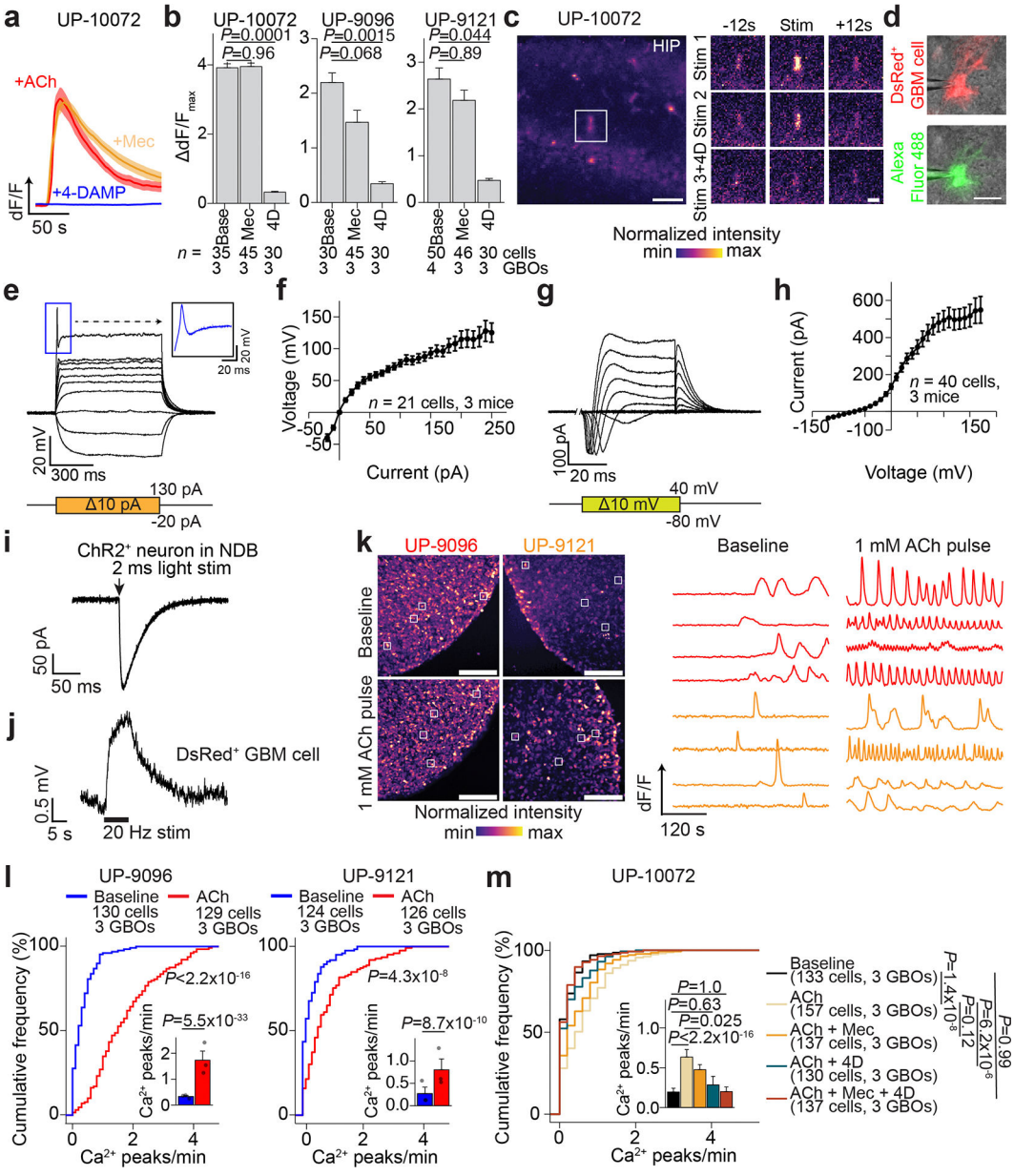


**Extended Data Fig. 9. ACh-driven responses in GBM cells.**

**a**, Representative traces of $Ca^{2+}$ response of UP-10072 GBOs to 1 mM ACh (Base; red), 1 mM ACh with 100 μM 4-DAMP (4D; blue), and 1 mM ACh with 100 μM mecamylamine (Mec; yellow). Data are plotted for $n = 10$ cells from one representative organoid for each condition with shaded s.e.m. **b**, Quantification of the maximal $Ca^{2+}$

response to ACh normalized to baseline intensity. *P*-values by LMM (see Methods); multiple comparisons adjustment with Tukey's method. **c**, Representative $Ca^{2+}$ imaging confocal images of acute brain slices with transplanted jRGECO1α-expressing GBM cells and optogenetic stimulation following the paradigm in Fig. 4e. Inset, GBM cell showing an increase in $Ca^{2+}$ levels upon first and second stimulations but not after the addition of 4D. Representative of $n = 9$ cells from 3 mice. Scale bars, 50 μm (low magnification) and 20 μm (high magnification). **d**, Dye-filling of patched UP-10072 GBM cells (arrowheads) after transplantation, showing representative $DsRed^{+}$Alexa Fluor $488^{+}$ cells. Representative of $n = 3$ patched and filled cells. Scale bar, 10 μm. **e**, Representative membrane potential changes to injected current steps in a GBM cell under current clamp. Inset, magnification of the box area showing a current injection-induced action potential-like response in the recorded cell. **f**, Relationship of membrane potential change (measured at the end of the step) and injected current. **g**, Representative current responses to voltage steps in a GBM cell under voltage clamp (holding potential −60 mV). Depolarizing voltage steps induced inward current followed by outward current. **h**, Relationship of induced current (measured at the end of the step) and voltage step. **i**, Blue (470 nm) light-induced inward current in an NDB $ChR2^{+}$ neuron following the paradigm in Fig. 4h, with $V_m = -70$ mV. **j**, Representative trace showing change in $V_m$ of a $DsRed^{+}$ GBM cell after 470 nm light stimulation (I = 0 pA; resting $V_m = -77$ mV). **k**, Representative $Ca^{2+}$ imaging GBOs *in vitro* at baseline or 30 minutes after a pulse of ACh, similar to Fig. 5a. Insets (white squares) correspond to example cells with traces shown. Scale bars, 50 μm. **l**, Cumulative distribution plots of the number of spontaneous $Ca^{2+}$ peaks per minute in UP-9096 or UP-9121 GBOs either under baseline conditions (blue) or 30 minutes after a pulse of 1 mM ACh (red), similar to Fig. 5b, *P*-values using Kolmogorov-Smirnov tests. Inset, bar plot of $Ca^{2+}$ peaks per minute, LMM. **m**, Same as **l** but for UP-10072 GBOs with various receptor antagonist treatments, *P*-values by Kolmogorov-Smirnov tests. Inset, bar plot of calcium peaks per minute, *P*-values by LMM, *P*-value adjustment for multiple comparisons with Tukey's method.

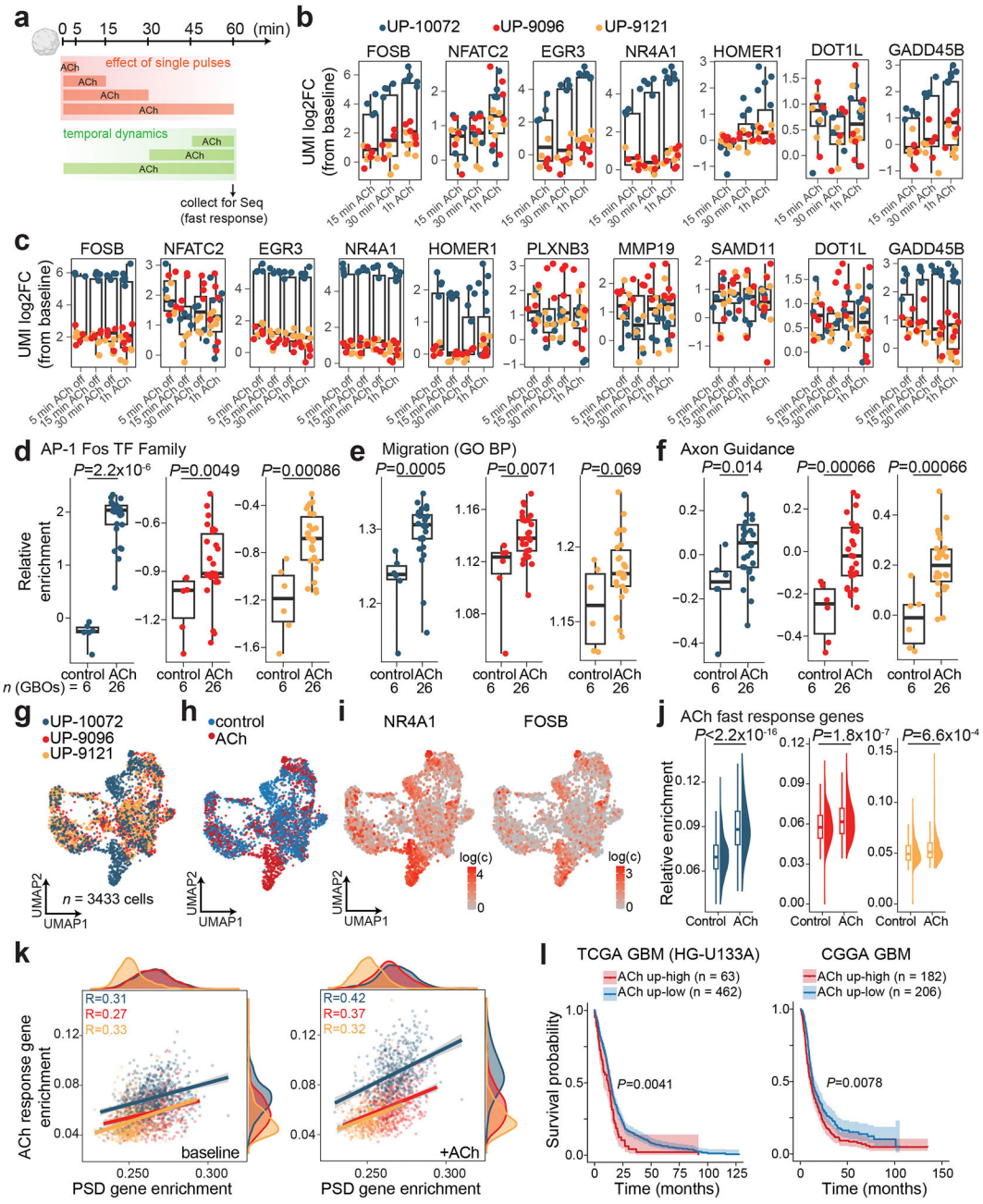


**Extended Data Fig. 10. ACh-induced fast transcriptional reprogramming of GBM cells.**

**a**, Schematic illustration of massively parallel RNA sequencing paradigm in GBOs to investigate the transcriptional effects of short pulses of ACh or the temporal dynamics of continuous ACh treatment for various lengths of time. **b**, Plots of exemplary differentially expressed genes that vary across treatment time. Genes are plotted as log2 fold change from baseline (no ACh) values using UMI counts normalized with DeSeq2[63]. The *x*-axis represents the length of time for which GBOs were treated with ACh prior to library preparation. Each dot represents a distinct bulk sample ($n = 4$ samples per condition per patient, $n = 3$ patients). **c**, Same as **b** but for a set of differentially expressed genes that demonstrate long-lasting effects of an ACh pulse. The *x* axis represents the length of

time for which GBOs were treated with ACh, with samples taken for library preparation uniformly at 1 hour. **d – f**, Plots of module enrichment scores for the FOS transcription factor family (**d**), cell migration gene set (**e**), and axon guidance gene set (**f**) at baseline conditions or after treatment with ACh. Note that all ACh-exposed GBO samples were aggregated for the ACh condition for this analysis. *P*-values by two-tailed Mann-Whitney tests. **g – h**, UMAP plots of integrated scRNAseq data of GBOs (**g**, colored by patient) under either baseline or 1 mM ACh treatment conditions (**h**, colored by condition). **i**, UMAP plots of exemplary upregulated genes in response to ACh. **j**, Plots of module enrichment scores of the ACh response gene signature derived from bulk RNA sequencing experiments (**a**). *P*-values by two-tailed Mann-Whitney tests. Half violin plots extend to maximum and minimum values. **k**, Scatter plots of single-cell post-synaptic density (PSD) enrichment (as described in Extended Data Fig. 1k) vs. ACh response gene enrichment in both baseline (left, no ACh) and ACh (right) conditions. Pearson correlation values are displayed and color-coded by patient. **l**, Kaplan-Meier plots of GBM patients from TCGA GBM (HG-U133A, left), and CGGA (right) datasets from GlioVis[74]. Patient profiles were grouped by GSVA score of the ACh fast response gene set, and cutoffs between high and low expression were selected using maximally selected rank statistics. Shaded areas represent the two-sided 95% confidence intervals. *P*-values by log-rank test. For box plots in **b**, **c**, **j**, the center line represents the median, the box edges show the $25^{th}$ and $75^{th}$ percentiles, and whiskers extend to ±1.5*IQR values.

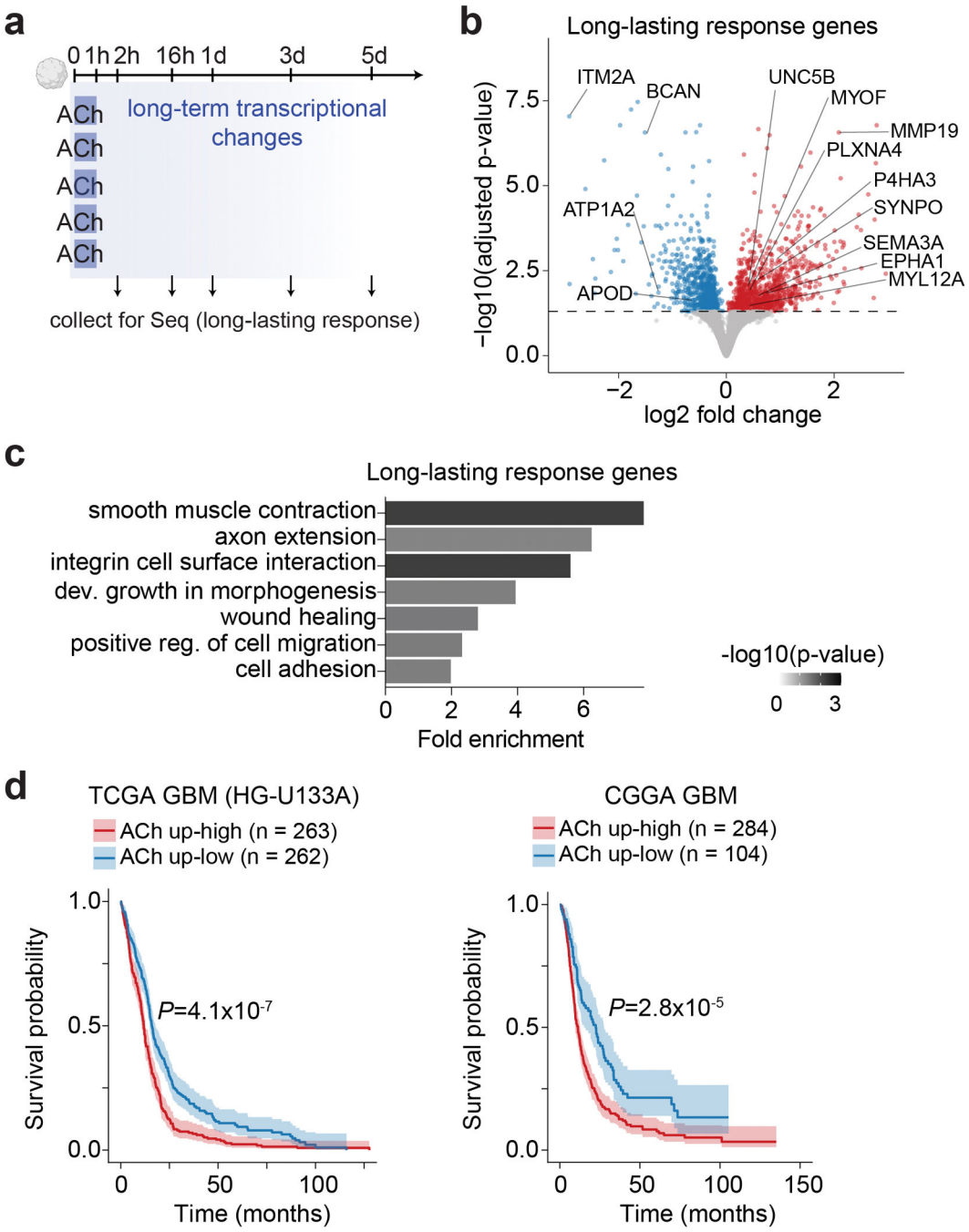


**Extended Data Fig. 11. ACh-induced long-lasting transcriptional reprogramming of GBM cells.**

**a**, Schematic illustration of massively parallel bulk RNA sequencing paradigm in GBOs to investigate the long-term transcriptional effects of a single 1-hour pulse of ACh. **b**, Volcano plot of differentially expressed genes across UP-10072, UP-9096, and UP-9121 GBOs at 1 day following a 1-hour treatment of 1 mM ACh, defined as the long-lasting response genes. Exemplary upregulated (red) and downregulated (blue) genes are indicated. Horizontal dashed line, adjusted *P*-value cutoff of 0.05 with effect size estimation by apeglm[64]. **c**, Representative GO terms for upregulated differentially expressed genes at 1 day, with the

x axis indicating fold enrichment of observed genes over expected. *P*-values, Fisher's exact test, FDR $P < 0.05$. Reg., regulation; dev., developmental. **d**, Kaplan-Meier plots of GBM patients from TCGA GBM (HG-U133A, left), and CGGA (right) datasets from GlioVis[74]. Patient profiles were grouped by GSVA score of the ACh long-lasting response gene set, and cutoffs between high and low expression were selected using maximally selected rank statistics. Shaded areas represent the two-sided 95% confidence intervals. *P*-values by log-rank test.

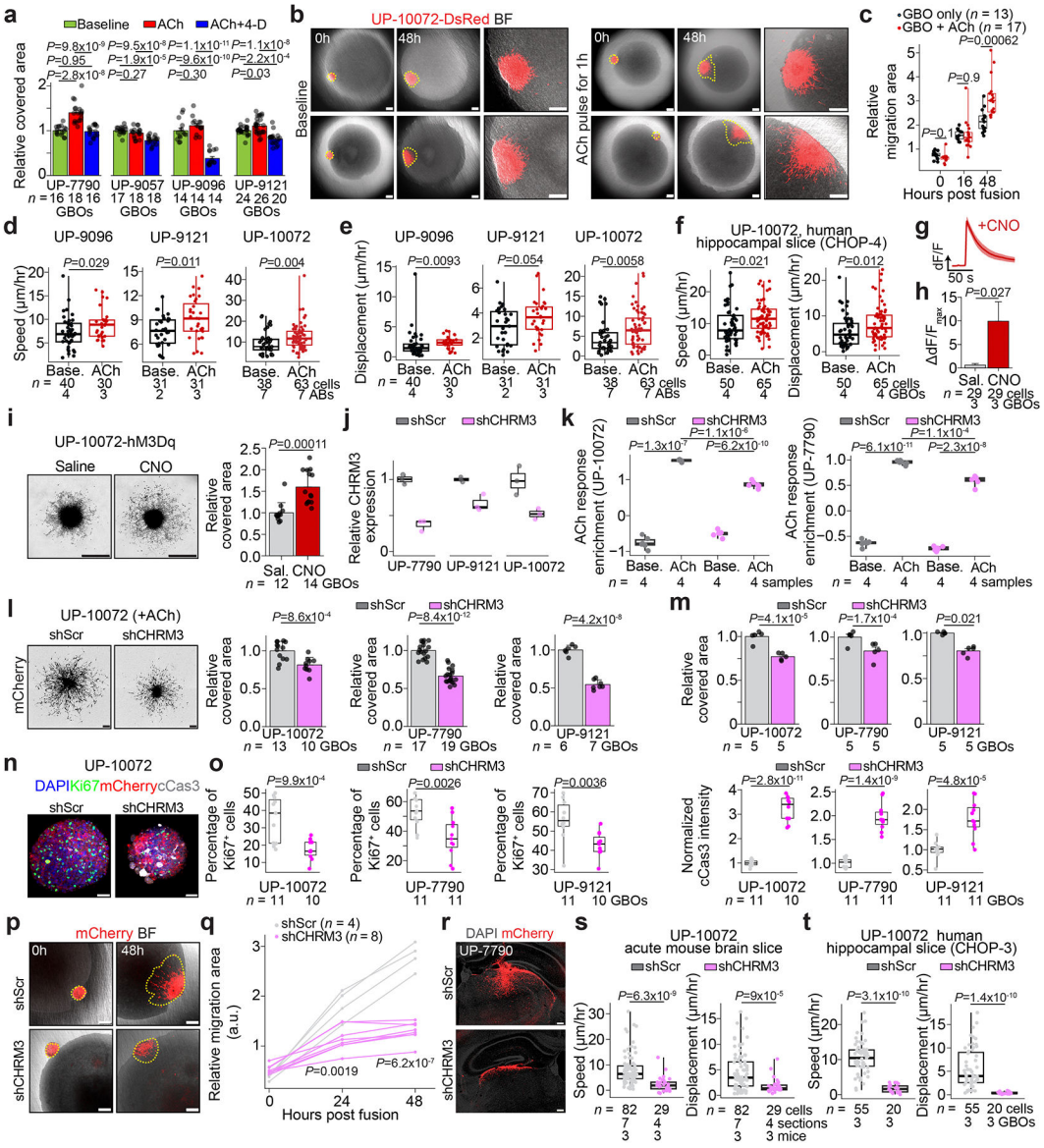


**Extended Data Fig. 12. ACh-induced enhanced migration of GBM cells via CHRM3.**
**a**, Quantification of Matrigel-based migration assay from 4 patients. **b**, Representative confocal images of the assembloid model with GBOs (red) and SNOs. GBOs were fused with SNOs under baseline conditions or after a 1-hour pulse of 1 mM ACh. Insets are zoomed-in images of the 48-hour timepoint. BF, brightfield. Scale bars, 200 μm. **c**,

Quantification of relative migration area of GBOs up to 48 hours post fusion. **d – e**, Quantification of GBM cell speed (**d**, in μm/hr) and displacement (**e**, in μm/hr from original cell location) at baseline and ACh pre-treated conditions. AB, assembloid. **f**, Quantification of GBM cell speed and displacement as in **d, e** but for GBO fusion with human hippocampal slices. GBOs were fused with slices either under baseline conditions or after a 1-hour pulse of 1 mM ACh and imaged 1 day later. **g**, Representative traces of the $Ca^{2+}$ response of UP-10072-hM3Dq-mCherry GBOs in culture to 20 μM CNO. Data are plotted as mean ± s.e.m. of $n = 10$ cells from one representative organoid. **h**, Quantification of the maximal $Ca^{2+}$ response to 20 μM CNO normalized to baseline intensity. Sal., saline. **i**, Representative images (left) and migration area quantification (right) of UP-10072-hM3Dq-mCherry GBOs with saline versus CNO stimulation. **j**, Relative efficacy of CHRM3 knockdown via shRNA normalized to GAPDH expression assayed by qPCR. Each dot represents RNA from GBOs from an independent lentiviral transduction ($n = 3$ biological replicates). **k**, Plots of module enrichment scores of the top ACh response genes as defined by RNA sequencing of shScramble and shCHRM3 GBOs. Each dot represents a bulk RNA sequencing sample under either baseline conditions or after a 1-hour pulse of ACh. **l**, Representative images (left) and migration area quantification (right) of GBOs with CHRM3 knockdown versus scrambled shRNA. Assays were performed in the presence of ACh and images were taken after 48 hours. Scale bars, 200 μm. **m**, Quantification of GBO size in culture 7 days following shRNA infection. **n**, Representative confocal immunostaining images of GBOs expressing either shScramble or shCHRM3 shRNA 7 days after transduction, with mCherry representing shRNA expression. Scale bars, 50 μm. **o**, Quantification of the percentages of $Ki67^{+}$ cells and normalized cCas3 intensity in shScramble vs shCHRM3 GBOs. **p**, Representative confocal images of assembloid model with shCHRM3 or shScramble UP-10072 GBOs (red) and SNOs (brightfield) at 0- or 48-hours post-fusion. GBOs were treated with a pulse of ACh for 1 hour and washed prior to assembloid generation. Scale bars, 200 μm. **q**, Quantification of relative migration area of shCHRM3 or shScramble over time. **r**, Representative confocal images of UP-7790 GBOs expressing shScramble or shCHRM3 3 weeks post transplantation into HIP (immediate paradigm as described in Fig. 5n). Scale bars, 200 μm. **s – t**, Quantification of speed and displacement as in **f** for GBM cells either expressing shScramble or shCHRM3 after transplantation into mice (**s**) or after fusion with human hippocampal slices (**t**). One-way ANOVA with Tukey's post hoc test was used in **a**. Two-tailed Student's *t*-tests were used for **c**, **f**, **i**, **l**, **m**, **o**, **q**, **s**, **t.** Two-tailed Mann-Whitney tests were used for **d – e**. LMM with *P*-value adjustment for multiple comparisons with Tukey's method was used for **h**. Multiple Student's *t*-tests with FDR correction were used for **k**.

## Supplementary Material

Refer to Web version on PubMed Central for supplementary material.

## ACKNOWLEDGMENTS

We thank the patients and their families for the generous donations of tissue specimens; other members of the Song & Ming laboratories for discussion and suggestions for this study; Brian Temsamrit, Emma LaNoce, Angelina Angelucci, and Giana Alepa for laboratory support; Andrew Morschauser and the Penn Cytomics and Cell Sorting Shared Resource Laboratory at the University of Pennsylvania for help with single-cell sorting;

Dr. Benedikt Berninger at University College of London for providing the retroviral helper plasmid; Dr. Lynn Enquist at Princeton University for providing trans-monosynaptic HSV; and the EM Core at the Institute of Molecular Biology, Academia Sinica for assistance with ultrastructural microscopy. Several schematic illustrations were created or modified from Biorender.com. This work was supported by the National Institutes of Health (R35NS116843 to H.S., R35NS097370 and R35NS137480 to G-l.M., and F31NS137664 to Y.S.), Dr. Miriam and Sheldon G. Adelson Medical Research Foundation (to G-l.M., D.G., R.K. and A.H.), the Pennsylvania Department of Health (to G-l.M.), the National Science Foundation (1949735 to G.W.), the Abramson Cancer Center Glioblastoma Translational Center of Excellence (to H.S., Z.A.B. and D.M.O.), The Institute for Regenerative Medicine and Department of Neurosurgery at University of Pennsylvania (to H.S., D.M.O., M.P.N.), the Templeton Family Initiative in Neuro-Oncology (to Z.A.B. and D.M.O.), and the Maria and Gabriele Troiano Brain Cancer Immunotherapy Fund (to Z.A.B. and D.M.O.).

## DATA AVAILABILITY

Raw and processed single-cell and bulk RNA sequencing data reported in this study are available at the NCBI Gene Expression Omnibus under accession numbers GSE274460 and GSE274633. Patient sample information is listed in Supplementary Table 1 and primer sequences are listed in Supplementary Table 2. The human reference genome (GRCh38 v.41) is available at https://www.gencodegenes.org/human/release_41.html. The scRNAseq data in Fig. 1 and Extended Data Fig. 1 are available from https://singlecell.broadinstitute.org/single_cell/study/SCP393/single-cell-rna-seq-of-adult-and-pediatric-glioblastoma#study-download, GSE174554, and GSE84465. Source data are provided with this paper.

## MAIN TEXT REFERENCES

1. Monje M et al. Roadmap for the Emerging Field of Cancer Neuroscience. Cell 181, 219–222 (2020). [PubMed: 32302564]
2. Shi DD et al. Therapeutic avenues for cancer neuroscience: translational frontiers and clinical opportunities. Lancet Oncol. 23, e62–e74 (2022). [PubMed: 35114133]
3. Venkataramani V et al. Glutamatergic synaptic input to glioma cells drives brain tumour progression. Nature 573, 532–538 (2019). [PubMed: 31534219]
4. Venkatesh HS et al. Electrical and synaptic integration of glioma into neural circuits. Nature 573, 539–545 (2019). [PubMed: 31534222]
5. Luo L, Callaway EM & Svoboda K Genetic Dissection of Neural Circuits: A Decade of Progress. Neuron 98, 256–281 (2018). [PubMed: 29673479]
6. Zeng W-B et al. Anterograde monosynaptic transneuronal tracers derived from herpes simplex virus 1 strain H129. Mol. Neurodegener. 12, 38 (2017). [PubMed: 28499404]
7. Mathur R et al. Glioblastoma evolution and heterogeneity from a 3D whole-tumor perspective. Cell 187, 446–463.e16 (2024). [PubMed: 38242087]
8. Neftel C et al. An Integrative Model of Cellular States, Plasticity, and Genetics for Glioblastoma. Cell 178, 835–849.e21 (2019). [PubMed: 31327527]
9. Venkataramani V et al. Glioblastoma hijacks neuronal mechanisms for brain invasion. Cell 185, 2899–2917.e31 (2022). [PubMed: 35914528]
10. Chen P et al. Olfactory sensory experience regulates gliomagenesis via neuronal IGF1. Nature 606, 550–556 (2022). [PubMed: 35545672]
11. Krishna S et al. Glioblastoma remodelling of human neural circuits decreases survival. Nature 1–9 (2023) doi:10.1038/s41586-023-06036-1.
12. Huang-Hobbs E et al. Remote neuronal activity drives glioma progression through SEMA4F. Nature 1–7 (2023) doi:10.1038/s41586-023-06267-2.
13. Miyamichi K et al. Cortical representations of olfactory input by trans-synaptic tracing. Nature 472, 191–199 (2011). [PubMed: 21179085]

14. Jacob F et al. A Patient-Derived Glioblastoma Organoid Model and Biobank Recapitulates Inter- and Intra-tumoral Heterogeneity. Cell 180, 188–204.e22 (2020). [PubMed: 31883794]
15. Wang X, Sun Y, Zhang DY, Ming G & Song H Glioblastoma modeling with 3D organoids: progress and challenges. Oxf. Open Neurosci. kvad008 (2023) doi:10.1093/oons/kvad008. [PubMed: 38596241]
16. Qian X et al. Sliced Human Cortical Organoids for Modeling Distinct Cortical Layer Formation. Cell Stem Cell 26, 766–781.e9 (2020). [PubMed: 32142682]
17. Wang L et al. A single-cell atlas of glioblastoma evolution under therapy reveals cell-intrinsic and cell-extrinsic therapeutic targets. Nat. Cancer 3, 1534–1552 (2022). [PubMed: 36539501]
18. Darmanis S et al. Single-Cell RNA-Seq Analysis of Infiltrating Neoplastic Cells at the Migrating Front of Human Glioblastoma. Cell Rep. 21, 1399–1410 (2017). [PubMed: 29091775]
19. Xu X et al. Viral Vectors for Neural Circuit Mapping and Recent Advances in Trans-synaptic Anterograde Tracers. Neuron 107, 1029–1047 (2020). [PubMed: 32755550]
20. Wickersham IR, Finke S, Conzelmann K-K & Callaway EM Retrograde neuronal tracing with a deletion-mutant rabies virus. Nat. Methods 4, 47–49 (2007). [PubMed: 17179932]
21. Su P et al. High-brightness anterograde transneuronal HSV1 H129 tracer modified using a Trojan horse-like strategy. Mol. Brain 13, 5 (2020). [PubMed: 31931837]
22. Larjavaara S et al. Incidence of gliomas by anatomic location. Neuro-Oncol. 9, 319–325 (2007). [PubMed: 17522333]
23. Oh SW et al. A mesoscale connectome of the mouse brain. Nature 508, 207–214 (2014). [PubMed: 24695228]
24. Saunders A et al. Ascertaining cells' synaptic connections and RNA expression simultaneously with barcoded rabies virus libraries. Nat. Commun. 13, 6993 (2022). [PubMed: 36384944]
25. Saunders A, Granger AJ & Sabatini BL Corelease of acetylcholine and GABA from cholinergic forebrain neurons. eLife 4, e06412 (2015). [PubMed: 25723967]
26. Mena-Segovia J & Bolam JP Rethinking the Pedunculopontine Nucleus: From Cellular Organization to Function. Neuron 94, 7–18 (2017). [PubMed: 28384477]
27. Li X et al. Serotonin receptor 2c-expressing cells in the ventral CA1 control attention via innervation of the Edinger–Westphal nucleus. Nat. Neurosci. 21, 1239–1250 (2018). [PubMed: 30104733]
28. Sürmeli G et al. Molecularly Defined Circuitry Reveals Input-Output Segregation in Deep Layers of the Medial Entorhinal Cortex. Neuron 88, 1040–1053 (2015). [PubMed: 26606996]
29. Thomas EA et al. Conversion of N-(2-chloroethyl)-4-piperidinyl diphenylacetate (4-DAMP mustard) to an aziridinium ion and its interaction with muscarinic receptors in various tissues. Mol. Pharmacol. 41, 718–726 (1992). [PubMed: 1569923]
30. Dana H et al. Sensitive red protein calcium indicators for imaging neural activity. eLife 5, e12727 (2016). [PubMed: 27011354]
31. Hausmann D et al. Autonomous rhythmic activity in glioma networks drives brain tumour growth. Nature 1–8 (2022) doi:10.1038/s41586-022-05520-4.
32. Tong T et al. Glioblastoma Cells Imitate Neuronal Excitability in Humans. http://biorxiv.org/lookup/doi/10.1101/2024.01.08.574637 (2024) doi:10.1101/2024.01.08.574637.
33. Özçete ÖD, Banerjee A & Kaeser PS Mechanisms of neuromodulatory volume transmission. Mol. Psychiatry (2024) doi:10.1038/s41380-024-02608-3.
34. Silbering AF & Benton R Ionotropic and metabotropic mechanisms in chemoreception: 'chance or design'? EMBO Rep. 11, 173–179 (2010). [PubMed: 20111052]
35. Smedler E & Uhlén P Frequency decoding of calcium oscillations. Biochim. Biophys. Acta BBA - Gen. Subj. 1840, 964–969 (2014).
36. Xiong Y & Wang Q STC1 regulates glioblastoma migration and invasion via the TGF-β/SMAD4 signaling pathway. Mol. Med. Rep. 20, 3055–3064 (2019). [PubMed: 31432189]
37. Lettau I et al. Matrix Metalloproteinase-19 is Highly Expressed in Astroglial Tumors and Promotes Invasion of Glioma Cells. J. Neuropathol. Exp. Neurol. 69, 215–223 (2010). [PubMed: 20142769]

38. Kigel B, Rabinowicz N, Varshavsky A, Kessler O & Neufeld G Plexin-A4 promotes tumor progression and tumor angiogenesis by enhancement of VEGF and bFGF signaling. Blood 118, 4285–4296 (2011). [PubMed: 21832283]
39. Chen Y et al. The role of CEMIP in tumors: An update based on cellular and molecular insights. Biomed. Pharmacother. 146, 112504 (2022). [PubMed: 34922110]
40. Wu S et al. High expression of UNC5B enhances tumor proliferation, increases metastasis, and worsens prognosis in breast cancer. Aging 12, 17079–17098 (2020). [PubMed: 32902412]
41. Wang T, Wang Y-X, Dong Y-Q, Yu Y-L & Ma K Prolyl 4-hydroxylase subunit alpha 3 presents a cancer promotive function in head and neck squamous cell carcinoma via regulating epithelial-mesenchymal transition. Arch. Oral Biol. 113, 104711 (2020). [PubMed: 32220804]
42. Casarosa P, Kiechle T, Sieger P, Pieper M & Gantner F The Constitutive Activity of the Human Muscarinic M3 Receptor Unmasks Differences in the Pharmacology of Anticholinergics. J. Pharmacol. Exp. Ther. 333, 201–209 (2010). [PubMed: 20035022]
43. Costa LG & Murphy SD Interaction of choline with nicotinic and muscarinic cholinergic receptors in the rat brain in vitro. Clin. Exp. Pharmacol. Physiol. 11, 649–654 (1984). [PubMed: 6536422]
44. Balood M et al. Nociceptor neurons affect cancer immunosurveillance. Nature 1–8 (2022) doi:10.1038/s41586-022-05374-w.
45. Thompson EG & Sontheimer H Acetylcholine Receptor Activation as a Modulator of Glioblastoma Invasion. Cells 8, 1203 (2019). [PubMed: 31590360]
46. Chen H-C et al. Histone serotonylation regulates ependymoma tumorigenesis. Nature 632, 903–910 (2024). [PubMed: 39085609]
47. González-Burgos I & Feria-Velasco A Serotonin/dopamine interaction in memory formation. in Progress in Brain Research (eds. Di Giovann G, Di Matteo V & Esposito E) vol. 172 603–623 (Elsevier, 2008). [PubMed: 18772052]
48. van Kessel E et al. Tumor-related neurocognitive dysfunction in patients with diffuse glioma: a retrospective cohort study prior to antitumor treatment. Neuro-Oncol. Pract. 6, 463–472 (2019).
49. Reardon TR et al. Rabies Virus CVS-N2c ΔG Strain Enhances Retrograde Synaptic Transfer and Neuronal Viability. Neuron 89, 711–724 (2016). [PubMed: 26804990]
50. Clark IC et al. Barcoded viral tracing of single-cell interactions in central nervous system inflammation. Science 372, (2021).

## ADDITIONAL REFERENCES (METHODS)

51. Zhang F et al. Epitranscriptomic regulation of cortical neurogenesis via Mettl8-dependent mitochondrial tRNA m3C modification. Cell Stem Cell 30, 300–311.e11 (2023). [PubMed: 36764294]
52. Jacob F et al. Human Pluripotent Stem Cell-Derived Neural Cells and Brain Organoids Reveal SARS-CoV-2 Neurotropism Predominates in Choroid Plexus Epithelium. Cell Stem Cell 27, 937–950.e9 (2020). [PubMed: 33010822]
53. Hagemann-Jensen M et al. Single-cell RNA counting at allele and isoform resolution using Smart-seq3. Nat. Biotechnol. 38, 708–714 (2020). [PubMed: 32518404]
54. Hagemann-Jensen M, Ziegenhain C & Sandberg R Scalable single-cell RNA sequencing from full transcripts with Smart-seq3xpress. Nat. Biotechnol. 1–6 (2022) doi:10.1038/s41587-022-01311-4. [PubMed: 34980916]
55. Kaminow B, Yunusov D & Dobin A STARsolo: accurate, fast and versatile mapping/quantification of single-cell and single-nucleus RNA-seq data. 2021.05.05.442755 Preprint at 10.1101/2021.05.05.442755 (2021).
56. Dobin A et al. STAR: ultrafast universal RNA-seq aligner. Bioinformatics 29, 15–21 (2013). [PubMed: 23104886]
57. Hao Y et al. Integrated analysis of multimodal single-cell data. Cell 184, 3573–3587.e29 (2021). [PubMed: 34062119]
58. Hafemeister C & Satija R Normalization and variance stabilization of single-cell RNA-seq data using regularized negative binomial regression. Genome Biol. 20, 296 (2019). [PubMed: 31870423]

59. Fan J et al. Linking transcriptional and genetic tumor heterogeneity through allele analysis of single-cell RNA-seq data. Genome Res. gr.228080.117 (2018) doi:10.1101/gr.228080.117.
60. LeBlanc VG et al. Single-cell landscapes of primary glioblastomas and matched explants and cell lines show variable retention of inter- and intratumor heterogeneity. Cancer Cell 40, 379–392.e9 (2022). [PubMed: 35303420]
61. Andreatta M & Carmona SJ UCell: Robust and scalable single-cell gene signature scoring. Comput. Struct. Biotechnol. J. 19, 3796–3798 (2021). [PubMed: 34285779]
62. Korsunsky I et al. Fast, sensitive and accurate integration of single-cell data with Harmony. Nat. Methods 16, 1289–1296 (2019). [PubMed: 31740819]
63. Love MI, Huber W & Anders S Moderated estimation of fold change and dispersion for RNA-seq data with DESeq2. Genome Biol. 15, 550 (2014). [PubMed: 25516281]
64. Zhu A, Ibrahim JG & Love MI Heavy-tailed prior distributions for sequence count data: removing the noise and preserving large differences. Bioinformatics 35, 2084–2092 (2019). [PubMed: 30395178]
65. Thomas PD et al. PANTHER: Making genome-scale phylogenetics accessible to all. Protein Sci. 31, 8–22 (2022). [PubMed: 34717010]
66. Zhou Y et al. Molecular landscapes of human hippocampal immature neurons across lifespan. Nature 607, 527–533 (2022). [PubMed: 35794479]
67. Giandomenico SL et al. Cerebral organoids at the air–liquid interface generate diverse nerve tracts with functional output. Nat. Neurosci. 22, 669–679 (2019). [PubMed: 30886407]
68. Saleeba C, Dempsey B, Le S, Goodchild A & McMullan S A Student's Guide to Neural Circuit Tracing. Front. Neurosci. 13, (2019).
69. Wang Q et al. The Allen Mouse Brain Common Coordinate Framework: A 3D Reference Atlas. Cell 181, 936–953.e20 (2020). [PubMed: 32386544]
70. Chi J, Crane A, Wu Z & Cohen P Adipo-Clear: A Tissue Clearing Method for Three-Dimensional Imaging of Adipose Tissue. J. Vis. Exp. 58271 (2018) doi:10.3791/58271. [PubMed: 30102289]
71. Bhattarai JP, Schreck M, Moberly AH, Luo W & Ma M Aversive Learning Increases Release Probability of Olfactory Sensory Neurons. Curr. Biol. 30, 31–41.e3 (2020). [PubMed: 31839448]
72. Armbruster BN, Li X, Pausch MH, Herlitze S & Roth BL Evolving the lock to fit the key to create a family of G protein-coupled receptors potently activated by an inert ligand. Proc. Natl. Acad. Sci. 104, 5163–5168 (2007). [PubMed: 17360345]
73. Ullman-Culleré MH & Foltz CJ Body Condition Scoring: A Rapid and Accurate Method for Assessing Health Status in Mice. Lab. Anim. Sci. 49, (1999).
74. Bowman RL, Wang Q, Carro A, Verhaak RGW & Squatrito M GlioVis data portal for visualization and analysis of brain tumor expression datasets. Neuro-Oncol. 19, 139–141 (2017). [PubMed: 28031383]
75. McLendon R et al. Comprehensive genomic characterization defines human glioblastoma genes and core pathways. Nature 455, 1061–1068 (2008). [PubMed: 18772890]
76. Zhao Z et al. Chinese Glioma Genome Atlas (CGGA): A Comprehensive Resource with Functional Genomic Data from Chinese Glioma Patients. Genomics Proteomics Bioinformatics 19, 1–12 (2021). [PubMed: 33662628]
77. Hänzelmann S, Castelo R & Guinney J GSVA: gene set variation analysis for microarray and RNA-Seq data. BMC Bioinformatics 14, 7 (2013). [PubMed: 23323831]
78. Yu Z et al. Beyond t test and ANOVA: applications of mixed-effects models for more rigorous statistical analysis in neuroscience research. Neuron 110, 21–35 (2022). [PubMed: 34784504]
79. The Gene Ontology Consortium. The Gene Ontology resource: enriching a GOld mine. Nucleic Acids Res. 49, D325–D334 (2021). [PubMed: 33290552]

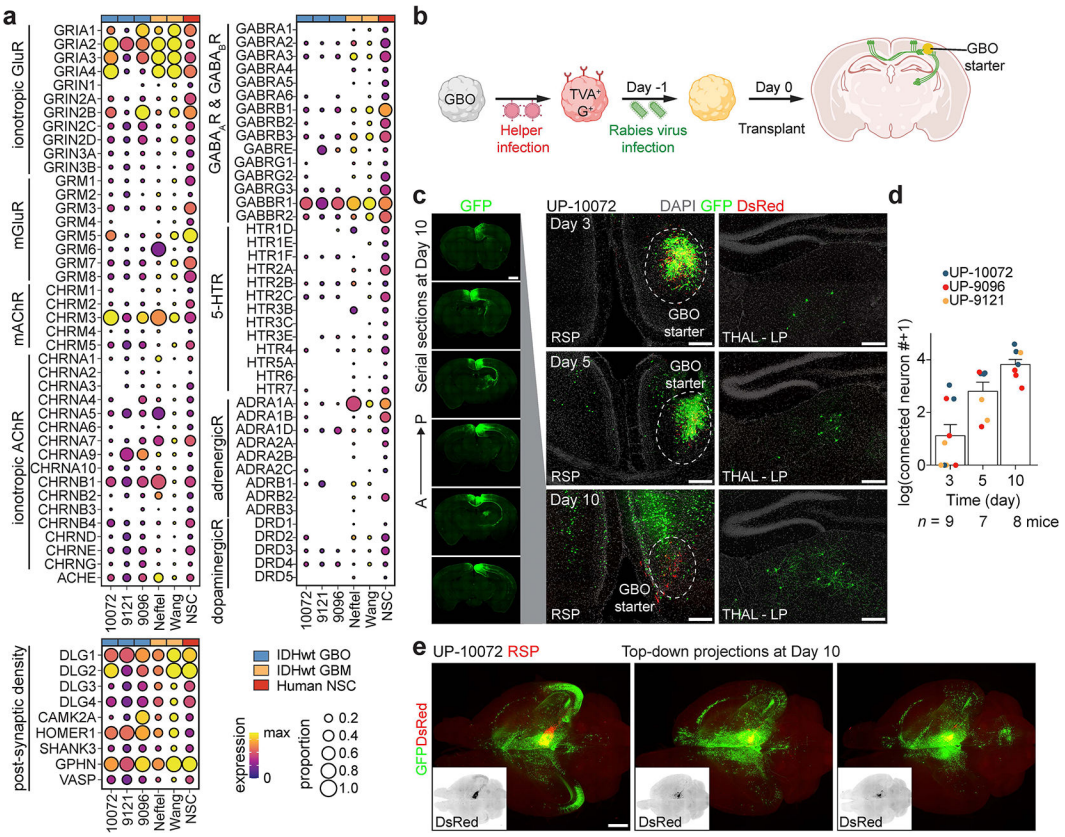


**Figure 1. Rapid neuronal circuit integration of transplanted human GBM cells in the adult mouse brain.**

**a**, Expression of neurotransmitter receptor and post-synaptic density genes across single-cell transcriptomes of adult GBM (blue: UP-10072, UP-9121, UP-9096, $n = 3$ patient-derived GBOs; orange: Neftel et al.[8], $n = 20$ patients, and Wang et al.[17], $n = 6$ patients) and NSCs in 100-day old SNOs (red: $n = 3$ organoids). Data are plotted as log-normalized counts, and the dot size represents the proportion of cells with the given gene detected. **b**, Schematic illustrations of the transplantation paradigm of rabies virus pre-infected GBOs into adult immunodeficient mice. **c**, Sample confocal images of local (retrosplenial cortex, RSP) and long-range (lateral posterior thalamus, TH - LP) regions at 3-, 5-, and 10-dpt of UP-10072 into the RSP. Scale bars, 200 μm. Left, representative serial sections from anterior to posterior at 10 dpt. Scale bar, 500 μm. See additional sample images in Extended Data Fig. 3a. **d**, Quantification of the number of labeled neurons at 3, 5, and 10 dpt. Each dot represents data from one mouse, and colors represent GBOs from different patients ($n = 3$ patients). **e**, Representative cleared whole-brain images of trans-monosynaptic tracing experiments with transplantation of UP-10072 into RSP at 10 dpt. Images are shown as top-down maximum intensity projections for 3 different mice. Scale bars, 1 mm. See Supplementary Video 1.

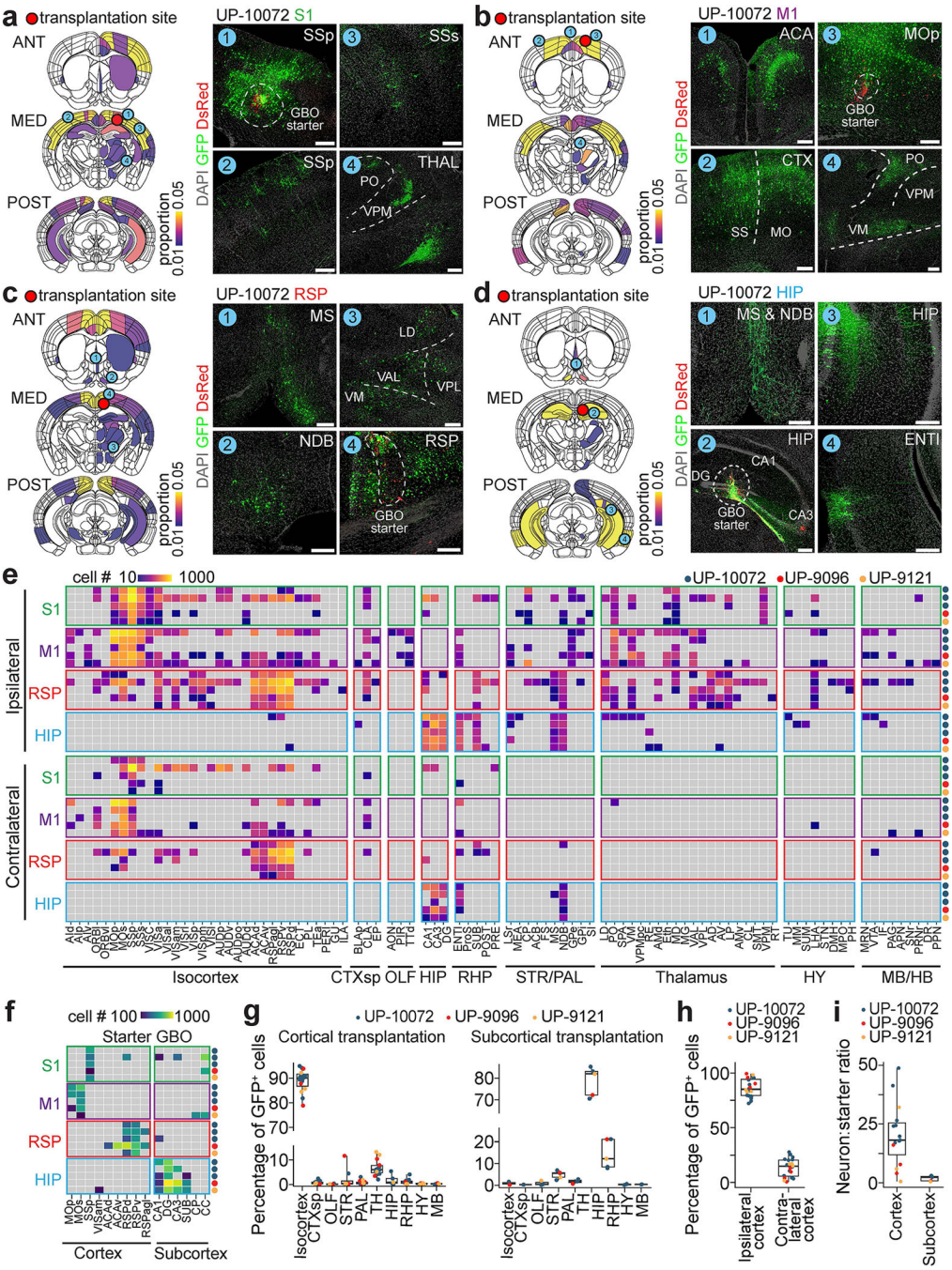


**Figure 2. GBM cell input connectome with diverse anatomical projections.**

**a**, Left shows representative coronal sections corresponding to anterior (ANT), medial (MED), and posterior (POST) areas for primary somatosensory cortex (S1) transplantations. Areas are colored by normalized proportion of GFP$^+$ neurons relative to total GFP$^+$ neuron number in each hemisphere at 10 dpt (summed across $n = 3$ mice per region). Right shows sample confocal images with locations indicated on the left. Scale bars, 200 μm. **b**, Same as **a** but for primary motor cortex (M1) transplantations. **c**, Same as **a** but for RSP transplantations. **d**, Same as **a** but for hippocampal (HIP) area transplantations. **e**,

Heatmap of input projections to GBM cells, colored by $GFP^+$ neuron number, grouped by transplantation location, and arranged by hemisphere. Each row represents an individual experiment at 10 dpt ($n$ = 20 mice from GBOs from $n$ = 3 patients). In this and subsequent figures, GBO transplantation locations and patient ID are color-coded as indicated. **f**, Heatmap of starter GBM cell distributions as in **e** for the same experiments, colored by GBO cell number and arranged by cortical versus subcortical regions. **g**, Proportions of input neurons across brain regions for subcortical (HIP, $n$ = 5 mice) and cortical (S1, M1, and RSP, $n$ = 15 mice) transplantation experiments at 10 dpt, colored by GBOs from different patients. Each dot represents data from one mouse. **h**, Proportion of input cortical neurons arising from either hemisphere for experiments in **g**. **i**, Quantification of input neuron to starter GBM cell ratio for subcortical and cortical transplantation experiments in **g**. Abbreviations for all brain regions are listed in Supplementary Table 6.

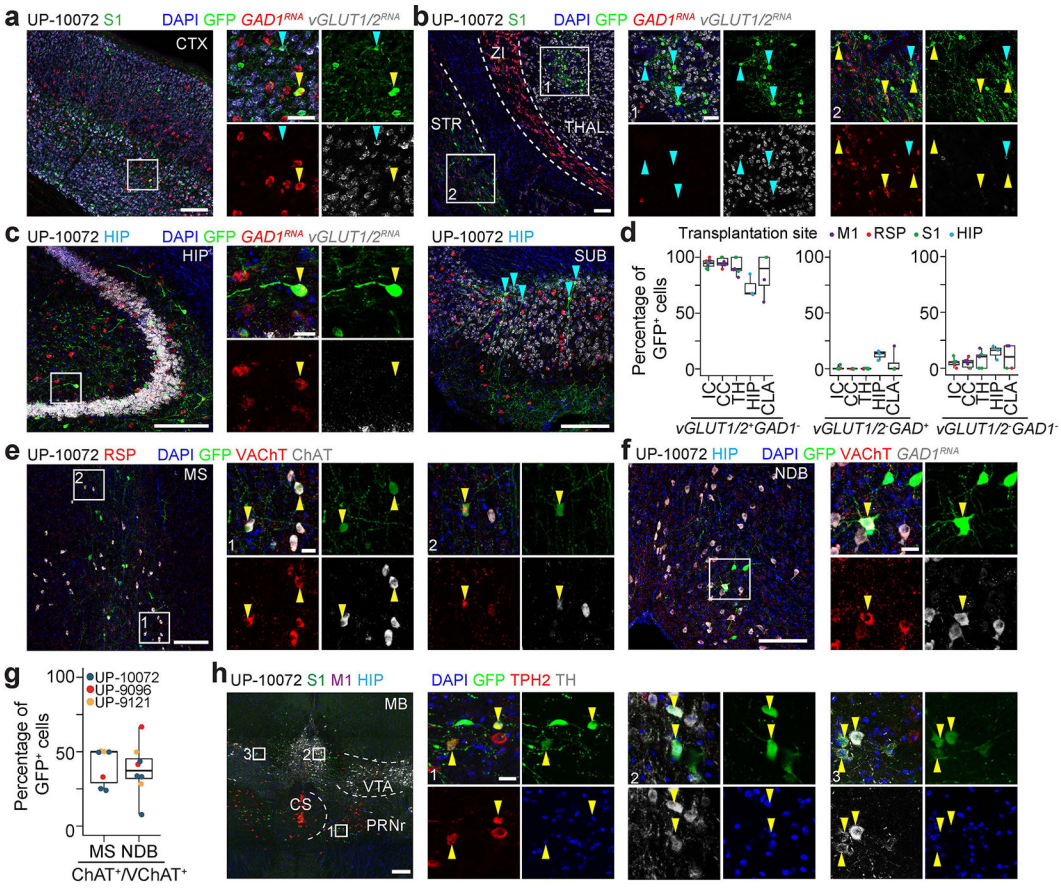


**Figure 3. Integration of GBM cells into neuronal circuits with diverse neurotransmitter systems.**

**a-c**, Sample confocal images of RNA *in situ* hybridization for *GAD1* (red) and *vGLUT1/vGLUT2* (white) and GFP immunostaining of rabies virus-labeled neurons in the ipsilateral CTX (**a**), ventral THAL (inset 1) (**b**), STR (inset 2) (**b**), and HIP/SUB (**c**). Orange arrowheads indicate GABAergic neuron cell bodies, and blue arrows indicate glutamatergic neuron cell bodies. **d**, Quantification of percentages of $GFP^+$ rabies virus-labeled neurons that were $vGLUT1/2^+GAD1^-$ (glutamatergic), $vGLUT1/2^-GAD1^+$ (GABAergic), or $vGLUT1/2^-GAD1^-$ (other) across brain regions. IC, ipsilateral CTX; CC, contralateral CTX. Dots are colored by transplantation site as indicated. Data are from $n = 28$ sections from $n = 4$ mice (from UP-10072 transplantations), with each dot representing one section. **e – f**, Sample immunostaining of $VAChT^+ChAT^+GFP^+$ cholinergic neurons in the MS (**e**) and NDB (**f**). Arrowheads indicate example cholinergic neurons. g, Quantification of percentages of $GFP^+VAChT^+$ or $GFP^+ChAT^+$ neurons in the MS or NDB. Data are from $n = 7$ mice ($n = 4$ RSP and $n = 3$ HIP transplantations) for MS and $n = 8$ mice ($n = 2$ HIP, $n = 4$ RSP, and $n = 2$ M1/S1/HIP transplantations) for NDB, with each dot representing one mouse, and color representing GBOs from different patients. h, Sample confocal images of $TPH2^+$ serotonergic (inset 1) or $TH^+$ dopaminergic (insets 2 and 3) $GFP^+$ neurons in the MB. Arrowheads indicate example neurons of interest. Results are representative of 3 experiments. Scale bars, 200 μm (low magnification) and 20 μm (high magnification). Abbreviations for additional relevant brain regions are listed in Supplementary Table 6.

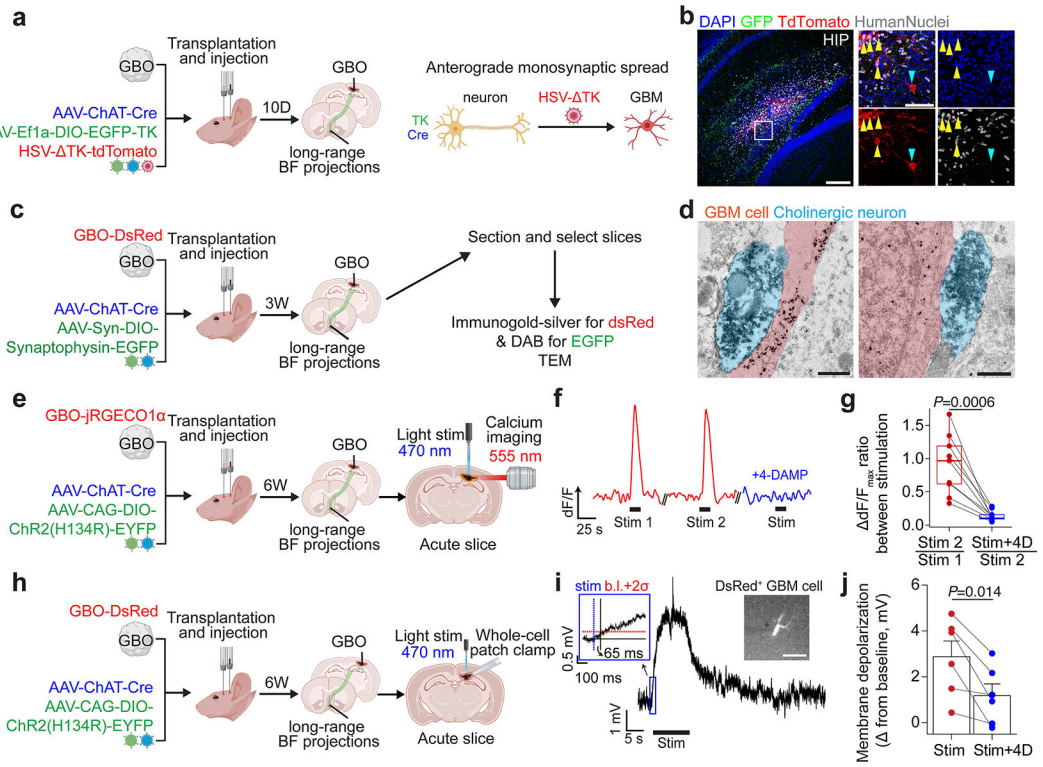


**Figure 4. Functional cholinergic inputs onto GBM cells mediated by metabotropic receptors.**

**a**, Schematic of HSV-mediated anterograde trans-monosynaptic tracing paradigm. BF, basal forebrain. **b**, Sample confocal images of TdTomato$^{+}$HuNu$^{+}$ (Human Nuclei) GBM cells (yellow arrowheads) in the HIP at 10 dpt (representative of $n = 3$ mice). Blue arrowhead indicates a traced mouse hippocampal neuron. Scale bars, 200 μm (low magnification) and 20 μm (high magnification). **c**, Schematic of ultrastructural characterization of transplanted GBM cells. **d**, Representative immuno-electron micrographs of direct contacts between presynaptic cholinergic axon terminals (pseudo-colored blue) and GBM cells (pseudo-colored red). Representative of 5 synapses from 12 ultrathin brain sections. Scale bars, 500 nm. **e**, Schematic of $Ca^{2+}$ imaging paradigm of GBM cells in the acute slice. **f**, Representative intensity trace of a GBM cell with three light stimulations. Red, stimulation in ACSF only; blue, stimulation in ACSF with 100 μM 4-DAMP. **g**, Quantification of maximal $Ca^{2+}$ response to stimulation normalized to baseline intensity. Data are plotted as the maximal $Ca^{2+}$ response ratio between the second and first stimulations and between the third and second stimulations ($n = 9$ cells from 3 mice). **h**, Schematic illustration of electrophysiology experiments of transplanted GBM cells in acute slice. **i**, Representative GBM cell membrane depolarization in current-clamp (I = 0 pA; resting $V_m$ = −69 mV) in response to light stimulation in the presence of 25 μM CNQX and 200 μM 4-AP. Inset shows response time after stimulation (blue dotted line). b.l., baseline. Image on right shows patched DsRed$^{+}$ GBM cell in the RSP. Scale bar, 100 μm. **j**, Quantification of maximum membrane depolarization from baseline in response to light stimulation ($n = 6$ cells from 4 mice). Two-tailed paired *t*-tests in **g**, **j**.

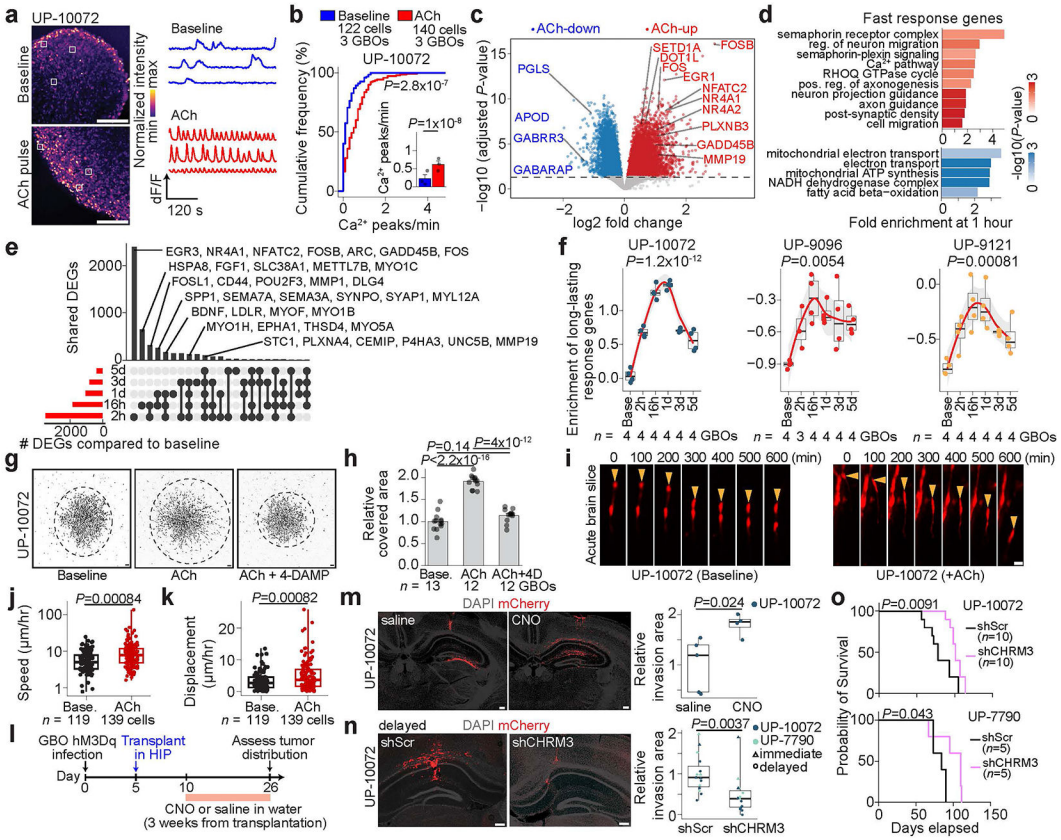

**Figure 5. Acute ACh-induced long-lasting $Ca^{2+}$ oscillations, transcriptional changes, and increased motility of GBM via CHRM3.**

**a – b**, Representative $Ca^{2+}$ imaging at baseline or 30-minutes after a 5-minute pulse of ACh (**a**; scale bars, 50 μm) and cumulative distribution plots of the number of $Ca^{2+}$ peaks/minute (**b**; Kolmogorov-Smirnov test). Inset, LMM (see Methods). **c**, Volcano plot of differentially expressed genes across GBOs following 1-hour ACh treatment. **d**, Representative GO terms for up/down-regulated fast-response genes. Fisher's exact test, FDR $P < 0.05$. Reg., regulation. **e**, UpSet plot showing co-occurrence of upregulated genes at various durations following ACh pulse. h, hours; d, days. **f**, Time-dependent changes in long-lasting gene enrichment (see Supplementary Table 4). Curve represents LOESS fit with s.e.m. One-way ANOVA. **g – h**, Representative images (**g**) and quantification (**h**) of migration assay. Scale bars, 200 μm. In **h**, y-axis represents covered area by GBO cells compared to baseline. One-way ANOVA with Tukey's post hoc test. **i**, Representative time-lapse images of UP-10072 cells (yellow arrowheads) within acute mouse brain slices. Scale bars, 20 μm. **j – k**, Quantification of cell speed (**j**) and displacement (**k**) at baseline and ACh-treated conditions (3 mice each). **l**, Schematic to chemogenetically activate GBM *in vivo*. **m**, Left, representative images under CNO or saline conditions. Scale bars, 200 μm. Right, quantification of relative area of distribution of hM3Dq-mCherry cells (CNO, 4 mice; saline, 5 mice). **n**, Left, representative confocal images of UP-10072 expressing shScramble or shCHRM3. Scale bars, 200 μm. Right, quantification. GBM cells were transplanted after overnight transduction (UP-10072, 3 mice, HIP; UP-7790, 2 mice, HIP) or 7 days post-transduction (UP-10072, 6 mice, HIP; UP-7790, 2 mice, striatum; 2 mice, HIP). Two-tailed

Student's *t*-tests in **j**, **k**, **m**, **n**. **o**, Kaplan-Meier plots of mice with shScramble versus shCHRM3 GBOs, log-rank tests.